Abstract

TOMBOKAN, XENIA CLARISSA. Ternary Phase Equilibria of the Sclareol-Ethyl Lactate-CO_2 System and its Application in the Extraction and Isolation of Sclareol from Clary Sage. (Under the direction of Dr. Ruben G. Carbonell and Dr. Peter K. Kilpatrick.)

The purpose of the research is to develop an environmentally responsible process to extract sclareol from *Salvia sclarea* L., more commonly known as Clary Sage. Sclareol is a highly water-insoluble plant natural product that is used as a fragrance in cosmetics and as a synthon for preparation of Ambrenolide odorants in perfumery. In addition, it is characterized as an antioxidant and has recently been studied for its cytotoxic and cytostatic effects against human leukemia cell lines. In these studies, sclareol was found to induce cancer cell cycle arrest and apoptosis. Moreover, sclareol is said to promote a calming effect on the nervous system and has been reported to relieve muscle spasms and menopausal symptoms.

In this work we studied the use of a GRAS solvent, ethyl lactate, as a solvent for sclareol, followed by the use of CO_2 as an antisolvent for precipitation. We also studied the use of mixtures of ethyl lactate and CO_2, followed by the use of water as a liquid antisolvent for sclareol precipitation. The solubility behavior of pure sclareol in ethyl lactate at various temperatures and in the mixture of ethyl lactate and CO_2 at various temperatures and pressures was investigated. The finding suggested that ethyl lactate was capable of dissolving high concentration of sclareol at ambient temperature. Moreover, the generated ternary phase behavior of the sclareol-ethyl-lactate CO_2 systems using a static synthetic method indicated the slight cybotactic effect. CO_2 acted as a co-solvent to ethyl lactate at lower pressure and/or

lower CO_2 concentrations and as an anti-solvent at higher pressure and/or higher CO_2 concentrations. The ability of the Peng-Robinson EOS with Vidal and Michelsen mixing rules model to predict the complex three-component phase behavior of this system is discussed, together with the implications of the thermodynamic behavior of the system on process design.

The generated ternary phase diagrams provided essential information for designing the extraction process. The extraction with ethyl lactate, followed by gas antisolvent (GAS) precipitation with CO_2 faced some challenges, such as the need for evaporating a large amount of organic solvents, low sclareol precipitation yield, and low sclareol selectivity. The extraction with a mixture of ethyl lactate and CO_2, on the other hand, is promising. By adjusting the ethyl lactate ratio in the extraction mixture, the extraction process could achieve high sclareol yield and relatively high sclareol purity. This process eliminated some problems encountered in the earlier process.

The liquid extract with the highest purity from CO_2-ethyl lactate extraction was subjected for the purification and recovery processes. Activated carbon was used to remove some contaminants, such as plant pigments, terpenes, polyphenols, waxes, wax esters, etc., in the liquid extract. Afterward, the sclareol in the purified extract was recovered via a liquid precipitation, i.e. using water as the antisolvent for sclareol. The effect of the extract purity on the phase behavior of the mixture upon addition of water is discussed. Overall, the purification with the activated carbon at varied concentrations, followed by recovery of sclareol via water antisolvent process obtained products with reasonably high sclareol purity, ranging from 78 to 97 % (w/w).

Ternary Phase Equilibria of the Sclareol-Ethyl Lactate-CO_2 System and its Application in the Extraction and Isolation of Sclareol from Clary Sage

by
Xenia C. Tombokan

A dissertation submitted to the Graduate Faculty of
North Carolina State University
in partial fulfillment of the
requirements for the Degree of
Doctor of Philosophy

Chemical and Biomolecular Engineering

Raleigh, North Carolina

2008

APPROVED BY:

_____	_____
Dr. Ruben G. Carbonell Chair of Advisory Committee	Dr. Peter K. Kilpatrick Co-chair of Advisory Committee
_____	_____
Dr. Ratna R. Sharma	Dr. Saad A. Khan

Dedication

I dedicate this dissertation

to my father (Santje), mother (Winanti), sister (Felicia), and brother (Raymond)

for their kind hearts, encouragements, and everlasting love

Biography

Xenia Tombokan was born and raised in Jakarta, the capital and largest city of Indonesia on the northwest coast of Java island. She is the middle child of three from Santje and Winanti Tombokan. Her family has always been her greatest source of education and inspirations. In July 1996, she attended Santa Ursula high school whose teaching system is built upon the motto “Serviam”, that literally means to serve God by serving a community.

After graduating from Santa Ursula high school in June 1999, she went to the University of Wisconsin Stevens Point for a year and transferred to the University of Wisconsin Madison to pursue her bachelor’s degree in chemical engineering. Besides the snowy winter, she enjoyed her experience of being independent, being far away from the family for the first time. During the study, she worked in Prof. Sean Palecek’s lab for 2 semesters to assist in a yeast cell biosensor research. This research experience piqued her interest in pursuing a research-related career.

She joined North Carolina State University in August 2003. In May 2004, she started working on the nutraceutical extraction project under the supervision of Prof. Ruben G. Carbonell and Prof. Peter K. Kilpatrick. She defended this dissertation and received a Doctorate of Philosophy in chemical & biomolecular engineering in October 2008. Following graduation, she will begin her professional career as an application scientist at Bruker Optics, Inc. in Woodlands, TX.

Acknowledgements

I would like to express my profound gratitude to my advisors, Dr. Ruben G. Carbonell and Dr. Peter K. Kilpatrick, for their invaluable support, continuous guidance, and useful suggestions throughout this research work. They helped me develop independent thinking and research skills, continually stimulated my analytical thinking, and greatly assisted me with scientific writing. I am also thankful for the various opportunities to attend and present at conferences.

I am extremely grateful for the assistance, generosity, and advice I received from Dr. David A. Danehower. He kindly allowed me to use his lab and gas chromatography (GC) equipments, and provided continuous support for the success of this research work. Many thanks go also to Dr. Matthew Finney and Tyler Steede for their efforts in helping me resolve problems with the GC and its data analysis software.

The members of my dissertation committee, Dr. Ratna R. Sharma and Dr. Saad A. Khan, have generously provided time and shared their expertise to improve my work. I thank them for their contribution and encouragement.

I owe a special note of gratitude to Remil Aguda for his help in the lab: setting up and improving the experimental setups, and for the useful feedback and discussions; to Dr. Erik Santiso and Dr. Ibrahim Ozkan for their great contribution in the thermodynamic modeling and computational part of the research work; and to Dana McDiffet for the guidance when I first joined the group.

Special thanks to CO_2 center members for the encouragements, friendship, and for sharing knowledge, skills, and experiences: Dr. Yazan Husain who especially helped me with

technical software issues. The wisdoms that he shared during lunchtime are the inspirations to do my best in facing some challenges; Dr. Shaun Tanner, Dr. Alan Chang, Dr. Tao Liu, Dr. Dawei Xu, Dr. Jaehoon Kim, Dr. Tamer Ahmed, Laura Beth Dong, and Nathan Cain for always trying their best to answer any research-related queries; Peggy Wilkins, Carol Carroll, and Jane Perry for the assistance with the administrative issues.

My thanks and appreciation to: Dr. David Frankowski and Chris Bonino for the DSC measurements; Dr. Vincent Verruto and Dr. Dhana Savithri for the help with UV-visible spectroscopy and centrifugation experiments; Sandra Bailey for always responding to my concerns regarding class registration, degree requirements, graduate school deadlines, school paper works, and many other issues.

I must acknowledge as well Hai Bui whom I came to for help whenever I had problems with the high pressure equipments. I also wish to thank Winnell Newman and Dr. Yan Solihin for the advice and encouragements during the job searching, Dr. Shalini Gupta, Dr. Xiaoyu Sun, Dr. Sachin Talwar, and Dr. Chun-Chao Wang for the care and friendship during my first few years in Raleigh. I will always remember both the happy and difficult times we spent together.

The graduate school has truly been a journey. I could not have completed this dissertation without the moral support of my family and friends. To papa and mama, thank you for your unconditional love and support. You taught me to never give up on obstacles. You always say that failing is better than never trying. To Raymond, thank you for playing your role as a great big brother. To Ica, I wish someday I don’t need to fly to meet you. We grow by learning from each other’s life experiences. You’ve seen me at my worst and best

and love me anyway. To Yenny Malikasim, thank you for being such a wonderful friend, the best friend to share laughter and tears with. Your sincere heart makes me believe that true friendship still exists. We still have a long journey ahead and I hope that our path will always cross. To my childhood friends, Yolanda Harten and Myra Koesdjojo, thank you for inspiring me to purse an advanced degree. It is unquestionably worth my time and efforts. To Julita Malikasim and Hwai-Yeng Chan, thank you for your advice, guidance, help, and encouragements during my study here. Your hospitality makes Raleigh feels like home. To Jack Ngui, Yufanni Ngui, Myrna Bawono, and many others whose names I did not mention, thank you for making my stay fun and lively.

Finally, this dissertation would not have been possible without the hands of God the Almighty. Without Him we are nothing…with Him all things are possible.

Table of Contents

List of Tables

List of Figures

1. Introduction

1.1. Research Motivation and Objectives

The huge wave of health consciousness that started during the 1990s in the United States has drastically changed people's behavior towards diet regimens. People have begun to use dietary supplements merely as foods that will prevent diseases and enhance performance rather than consuming them to meet the recommended dietary allowance. They are taking fewer synthetic ingredients and opting for natural and organic foods, functional beverages, and natural supplements. These supplements deliver nutraceuticals, small molecule bioactive components found in natural sources and typically in low concentrations, that have associated health benefits [1-5].

Nutraceuticals develop means to maintain the body's delicate balance between environmental stressors (oxidants) and our antioxidant defense system [1, 2]. Regular oxygen metabolism inside the body due to contact with environmental pollutants, radiation, sunlight, drugs, cigarette smoke, dietary fats, certain chemicals, bacteria, viruses, and parasites, produce free radicals. Free radicals are essentially oxygen molecules with a missing or unpaired electron that travels throughout the body causing damage until oxidized by a component in the body. They are the cause of cell membrane destruction, collagen damage, and mutations within the DNA of cells, and thus they play a part in diseases, such as heart disease, arthritis, cancer, hardening of the arteries, Alzheimer's disease, and cataracts [6]. The strong antioxidant powers of nutraceuticals play an important role in the human body, i.e. to quench these damaging free radicals.

The media has drawn people's attention to scientific developments in the health and nutrition field and the nutraceutical market has benefited immensely from this greater consumer awareness. The nutraceuticals market had global sales of 77 billion dollars in 2004, and projected sales reaching 103 billion dollars by 2009 [7, 8]. The fast-growing market for nutraceuticals has motivated us to design an efficient extraction and separation process to recover these high-value products, specifically sclareol.

Sclareol is a highly water-insoluble plant natural product, and is used as a fragrance in cosmetics and as a synthon for preparation of Ambrenolide odorants in perfumery [9]. In addition, it is characterized as an antioxidant and has recently been studied for its cytotoxic and cytostatic effects against human leukemia cell lines [10-12]. In these studies, sclareol was found to induce cell cycle arrest and apoptosis. Moreover, it is said to promote a calming effect to the nervous system and has been reported to relieve muscle spasms and menopausal symptoms [13]. The molecular structure of sclareol is provided in Figure 1-1.

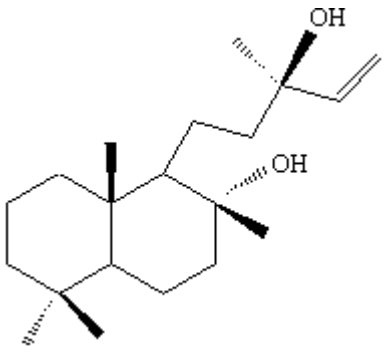

Figure 1-1. Molecular structure of sclareol [13].

Manufacturers isolate crude sclareol from the flowers and leaves of *Salvia Sclarea* Lamiacea, more commonly known as Clary Sage, using hexane extraction followed by partial solvent evaporation. Typically this is done using a falling film evaporator, after which the solution is filtered to remove any debris and precipitated waxes. This concentrated extract is then subjected to liquid-liquid countercurrent extraction using a polar solvent such as methanol-water, to selectively remove sclareol from the mixed extract. Sclareol is then re-crystallized from hexane to yield a 98 % pure natural product. Other toxic organic solvents used to extract sclareol are petroleum ether [14], ethylene glycol [15], ethanol, methanol, isopropanol, acetone, and diethyl ether [16].

The goal of our study is to develop an environmentally friendly technology to recover sclareol with high purity from the Clary Sage plant materials. We are using two different approaches of liquid/supercritical carbon dioxide technology. The first approach is to extract sclareol from the plant materials using a GRAS (generally recognized as safe) solvent, followed by sclareol isolation from the liquid extracts via a gas antisolvent precipitation (GAS) process. The second approach is to apply mixtures of carbon dioxide and cosolvent (GRAS solvent) for extracting sclareol from the plant materials, followed by recovery of sclareol via a liquid antisolvent process. For both processes, ethyl lactate was chosen as the GRAS solvent.

We generated the phase behavior of the system of interest: sclareol-ethyl lactate-CO_2 as a basis for selecting the experimental conditions for the extraction process. In parallel to the experimental work, we also developed Matlab codes based on a hybrid thermodynamic model, Peng-Robinson equation of state (PR EOS) with a linear combination of Vidal and

Michelsen (LCVM) mixing rules, to predict the binary and ternary phase behavior of the systems of interest.

1.2. Outlines of Dissertation

This dissertation consists of 6 chapters. The rest of chapter 1 focuses on the principles and applications of some extraction processes of natural compounds. Chapter 2 presents the thermodynamic study of the sclareol-ethyl lactate-CO_2 system. PR EOS with LCVM mixing rules was used to generate the vapor-liquid, solid-liquid, and solid-vapor-liquid equilibrium of the binary and ternary system of interest. Chapter 3 describes the experimental technique to generate the ternary phase behavior of sclareol-ethyl lactate-CO_2. The generated data were used as a guide for the extraction process of sclareol from the real plant materials. The cybotactic effect on the system is introduced and the ability of the PR-LCVM model to qualitatively but not quantitatively predict the experimental data is presented. Chapter 4 discusses the extraction techniques to recover sclareol from Clary Sage. The extraction with ethyl lactate followed by GAS process faced some challenges. The CO_2 and cosolvent (ethyl lactate) extraction, on the other hand, is promising. Chapter 5 focuses on the purification and isolation of sclareol from the CO_2 + ethyl lactate extracts. Chapter 6 presents the general conclusion of the research work and some recommendations for future work.

1.3. Extraction Processes of Natural Compounds

There are several different processes to extract valuable compounds from plant materials or natural sources. This section will review these processes and the applications with which they are normally associated.

1.3.1. Organic Solvent Extraction

In the 18th century, scientific research regarding the extraction of valuable compounds from plant materials focused on the isolation of odors from flowers. When extracting odors from plant matrix in the technique called enfleurage, fat was brought into direct contact with the plant materials [17]. More recently, liquid extraction is used to isolate valuable compounds from the plant materials or other natural sources for use in the cosmetic, pharmaceutical, and food industries, such as for use in the functional foods, beverages, and dietary supplements. In general, this extraction process involves the use of organic solvent to dissolve and remove a soluble fraction, which is the desired solute, from an insoluble permeable solid.

The general industrial extraction methods used for extracting raw materials are dispersed solids extraction and percolation extraction [18]. The equipments used for dispersed solids extraction consist of one or more tanks for mixing the solids with liquid, and a solid-liquid separation step, such as screening, filtration, or centrifuging, to collect the extract from the extracted biomass, as shown in Figure 1-2. This extraction process is more suitable for finely ground raw materials.

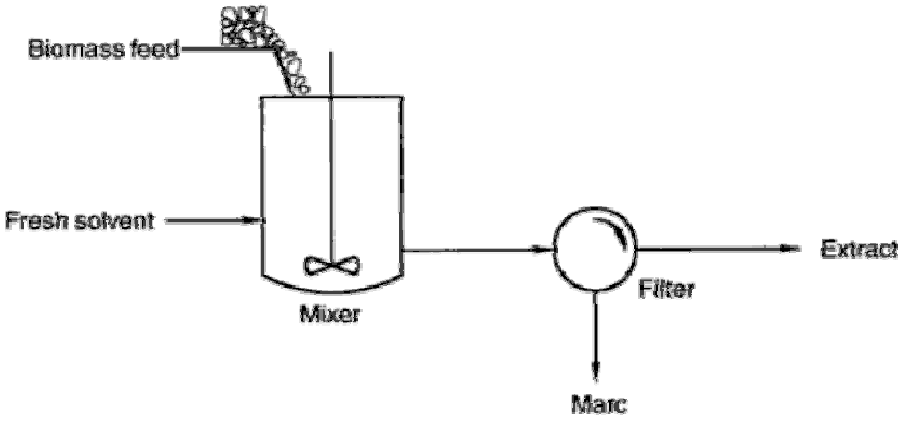

Figure 1-2. Dispersed solids extraction with filtration to separate the extracted plant material (marc) [18].

In the typical percolation extraction, a tank is filled with the ground raw material, and the solvent is then passed through the bed of solids, as described in Figure 1-3. The flow of the liquid past the particles carries the extract away from the particle surfaces. In this process, additional equipment to separate the extract from the extracted biomass is not generally needed, and the raw material grinding costs are reduced due to the use of a coarser grind size.

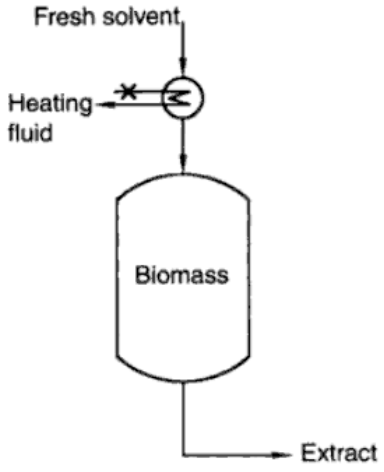

Figure 1-3. Percolation extraction [18].

Both dispersed solid and percolation extraction processes can be operated in a batch or a continuous mode. In the batch operation, solids are contacted with the liquid for sufficient time to allow an equilibrium concentration to be reached, and the extract is then collected. In continuous operation, solids and solvent are continuously fed to the extraction equipment, while the extract and the extracted plant are removed. For more efficient results, countercurrent extraction is applied to either batch or continuous equipment, as illustrated in Figure 1-4. The fresh solvent is contacted with the most extracted solid fraction and the fresh solid is contacted with the most concentrated solvent in a series of steps.

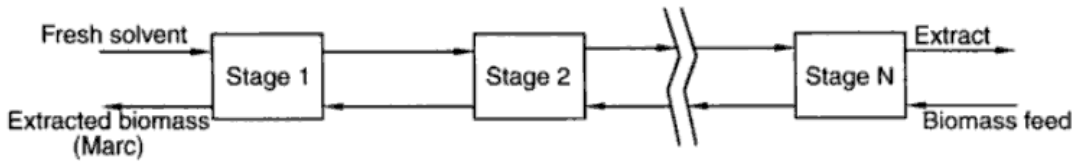

Figure 1-4. Countercurrent operation [18].

In solvent extraction process, it is essential to understand the fundamentals of equilibrium and mass transfer in order to successfully choose and operate the proper equipment for producing the desired product yield and purity. The choice of solvent or solvent mixture composition, operating temperature, particle size of raw materials, and liquid to solid ratio are important factors that affect the efficiency of an extraction process. The choice of solvent can significantly change both the amount of desired compound that extracts into the liquid and the rate at which the compound is extracted. It can also greatly affect the purity of the extract. Moreover, it is necessary that the solvents are thermally and chemically stable, are compatible with the solutes, have low viscosity to increase the diffusion

coefficient and the rate of extraction, have low flammability and low toxicity for safety reason, and have low cost for economic reason [17-21].

Generally, a higher temperature results in a higher solubility of compounds into the solvent and an increase in the extraction rate due to an increase in the solvent diffusivity. However, elevated temperatures may cause degradation of the compounds of interest. The balancing act is thus needed to keep the temperature as high as required for fast extraction rate and high solubility while not destroying the valuable compounds. In addition, change in temperature may change the selectivity of one compound over the other compounds [17-21].

The rate of extraction is also governed by the particle size of the materials or sources. For smaller particles, the path of migration of the solute through the pores of the particles to the particle surface is shorter and thus equates to a faster extraction rate. Furthermore, a higher liquid to solids ratio dilutes the concentration of dissolved compounds at the surface of particles. This will create a higher concentration gradient between the concentration inside and at the surface of the particles, and thus results in a faster extraction rate. A more dilute extract, however, requires a much more extensive downstream processing. So, once again, a balancing act is needed in selecting the appropriate liquid to solids ratio [18].

Numerous studies have been done on the extraction of nutraceuticals from natural sources using a variety of extraction solvents and procedures. In a study by Cu et al. [22], the effect of various extraction solvents on the chemical composition of essential oils from carrot seeds were investigated. They used several extraction solvents, such as ethanol, dichloromethane, methylfuran, and 1,1,2-trichloro-1,2,2-trifluoroethane (TTE). Following the evaporation of solvent was steam distillation to separate the volatile components from the

residues. Fernandez de Simon et al. [23] investigated the antioxidant activity of low molecular weight phenols extracted from oak wood using ethyl acetate and diethyl ether. They reported a strong antioxidant activity of polyphenols extracted with ethyl acetate. A similar study by Tsuda et al. [24] concluded that less polar solvents, such as ethyl acetate, provided slightly more active extracts than mixtures with ethanol or methanol, or methanol alone, for tamarind (Tamarindus indica L.) seeds. Santos-Buelga et al. [25] described an extraction process of polyphenols from grape seeds. The ground seeds were continuously homogenized in a mixture of methanol and 0.5 g/L ascorbic acid. Water was added to the solution and the mixture was vacuum dried until methanol was completely removed. N-hexane was then used on the aqueous extract for the removal of liposoluble material, and the remaining solvent was evaporated. Another study focused on the extraction of anthocyanins from black currants with sulfured water [26]. The study suggested that an increase in the extraction temperature from 293.15 to 333.15 K resulted in a much faster equilibrium time but a decrease in the amount of anthocyanins recovered.

Goncalves et al. [27] performed study on the influence of deacidification of palm oil by solvent extraction on the partition coefficients of carotenoids and tocopherols. The traditional physical refining usually provided a refined palm oil with approximately 0.03 % (w/w) of tocopherols and exempt of carotenoids. Using aqueous ethanol as the solvent, on the other hand, produced a refined palm oil with 80 % (w/w) of tocopherols and 99 % (w/w) of carotenoids. Handayani et al. [28] investigated the effect of temperatures and particle sizes on the extraction of carotenoids from dried shrimp waste using palm oil as the extraction solvent. In this study, mass transfer kinetic and reaction kinetic models were proposed to

correlate the experimental data, and the results suggested that both temperature and particle sizes controlled the extraction efficiency. The focus on a similar study by Sachindra et al. [29] was to investigate the different organic solvent or solvent mixtures and various ratios of solvents to waste for maximum extraction yield of carotenoids from shrimp waste. The use of 60 % (w/w) of hexane in a mixture with isopropyl alcohol, and a solvent-to-waste ratio of 5, produced the highest extraction yield.

1.3.2. Steam Distillation

Steam distillation is commonly used to extract essential oils from plant materials. Essential oil plants include a broad range of plant species that are used for their aromatic value as flavorings in foods and beverages and as fragrances in pharmaceutical and industrial products. Steam distillation employs a type of vapor-phase extraction technique. In general, steam is introduced into the plant materials and the volatile organic compounds are taken up by the vapor phase because of their low partial vapor pressure. By lowering the temperature of the vapor stream, condensation occurs and results in static separation of the oil phase from the water phase. Comparing to liquid extraction, the vapor can penetrate coarsely pretreated material better due to its low viscosity, and thus results in a larger effective contact area. Moreover, the diffusion of small compounds in a vapor phase is much higher than in a liquid phase. These advantages will balance with the much lower dissolving capability of the vapor phase compared to liquid phase. A schematic representation of a steam distillation apparatus is shown in Figure 1-5

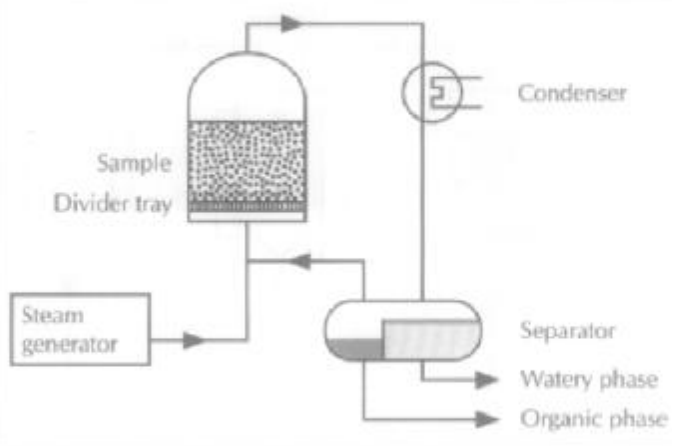

Figure 1-5. Steam distillation setup [17].

A number of studies have been done on the extraction of essential oils using steam distillation. Some research has been focused on determining the content and composition of the extracted essential oils from various plants, such as *Salvia anatolica* L. [30], *Piper* species [31], *Hypericum* L. species [32], and several shrubs belonging to the genus *Santolina* A. [33]. Besides their composition, the activities of the oil are of research interests. For example, the antibacterial effects of volatile components from *Pinus densiflora* S. and *Pinus densiflora* Z. were examined on six foodborne bacteria [34], the activities of clove (*Syzygium aromaticum* L.), basil (*Ocimum basilicum* L.), and yarrow (*Achillea millefolium* L.) were investigated on trypanosomiasis or Chagas' disease [35], and the antimicrobial activities of oils from Brazilian genus *Cunila* M. were investigated on several bacterial species [36].

Vapor-phase extraction can also be applied to liquid samples. Vistzthum et al. [37] performed extraction of black tea aroma using supercritical CO_2. The extracts were then fractionated into basic and neutral components by steam distillation. A similar study was performed on the isolation of essential oils, which have antioxidant activity, from caraway,

clove, cumin, rosemary, sage, and thyme [38]. Some scientists explored the effect of distillation methods on the content, composition, and activity of the extracts. For instance, the essential oils of *Satureja rechingeri* J. were extracted by steam, water, and water-steam distillation [39]. In the manufacture of essential oils using the method of water distillation, the plant material is completely immersed in water and the mixture is brought to a boil. The condensed material is cooled, and the water and oil are then separated. In the water-steam distillation process, the plant material is immersed in water in a still with heating source and steam is then introduced into the mixture. For the case of *S. rechingeri* oil, the highest oil yield was obtained by water distillation respectively followed by water-steam and steam distillation.

1.3.3. Supercritical Carbon Dioxide Extraction

In the last few decades, supercritical fluid technology has been reemerged as an alternative to traditional solvent extraction for the extraction and fractionation of active ingredients. This is mainly due to the increased preference for natural products over synthetic ones and new regulations related to nutritional and toxicity levels of the active ingredients in the nutraceutical, pharmaceutical, and food industry. Supercritical fluids (SCFs) and near-critical fluids when used as the extraction solvents leave no residue in the extract and are gaseous at ambient temperature. In addition, the density of SCFs can be tuned according to the process needs by changing the operating temperature, pressure, and/or composition. Other important properties of SCFs are their low surface tension, low viscosities, and moderately high diffusion coefficients [40-42]. These properties enable SCFs to easily penetrate the natural sources from which the active component is to be extracted. In addition

to its dissolving property, it can also selectively extract target compounds from a complex mixture. The target compounds can be the active ingredient of interest or an undesirable component, which needs to be removed from the final product [42].

Many supercritical fluids are used as in supercritical extraction processes, such as carbon dioxide, ethane, propane, butane, pentane, ethylene, ammonia, sulfur dioxide, water, chlorodifluoromethane, etc. Supercritical carbon dioxide is most attractive for extracting natural products for foods and medicinal uses. Its characteristic traits are inert, nonflammable, non-corrosive, inexpensive, easily available, odorless, tasteless, environmentally friendly, and it's a GRAS (generally recognized as safe) solvent. In addition, its near ambient critical temperature (304.25 K) makes it suitable for thermally sensitive natural products. Due to its low latent heat of vaporization, low energy input is required for the extract separation system, which delivers the most natural smelling and tasting extracts. Furthermore, the energy required for attaining the supercritical state of CO_2 is often less than the energy associated with distillation of conventional organic solvents. In general, the extractability of the compounds with supercritical CO_2 depends on the presence of the individual functional groups in these compounds, their molecular weights, and polarity. Table 1-1 presents a classification of natural ingredients solubility in supercritical CO_2 [40-42].

Table 1-1. Solubility of natural ingredients in liquid and supercritical CO_2 [42].

Very Soluble	Sparingly Soluble	Almost Insoluble
Nonpolar and slightly polar low M.W. (<250) Organics, e.g., mono and sesquiterpenes, e.g., thiols, pyrazines, and thiazoles, acetic acid, benzaldehyde hexanol, glycerol, acetates	Higher M.W. organics,(<400), e.g., substituted terpenes and sesquiterpenes, water, oleic acid, glycerol, decanol, saturated lipids up to C_{12}	Organics with M.W. above 400, e.g., sugars, proteins, tannins, waxes, inorganic salts, chlorophyll, carotenoids, citric, malic acids, amino acids, nitrates, pesticides, insecticides, glycine, etc.

The schematic diagram of the supercritical CO_2 extraction process is described in Figure 1-6. In this process, generally ground solid is fed into the extractor. CO_2 is then charged to the extractor through a high-pressure pump (10-35 MPa). Subsequently, the extract is sent to a separator (5-12 MPa) via a pressure reduction valve. By reducing the temperature and pressure of the system, the extract precipitates in the separator and CO_2 is either released or recycled to the extractor. In the commercial scale process, separation is often carried out in stages by maintaining different conditions in two or three separators for fractionation of extract, depending on the solubility of the components and the desired specifications of the products. Similarly, the solvent power of CO_2 or the polarity of the solvent can be altered by varying the extraction pressure. Therefore, a production plant can have flexible operating conditions for multiple natural products and it is also possible to obtain various product profiles from a single source by merely using CO_2.

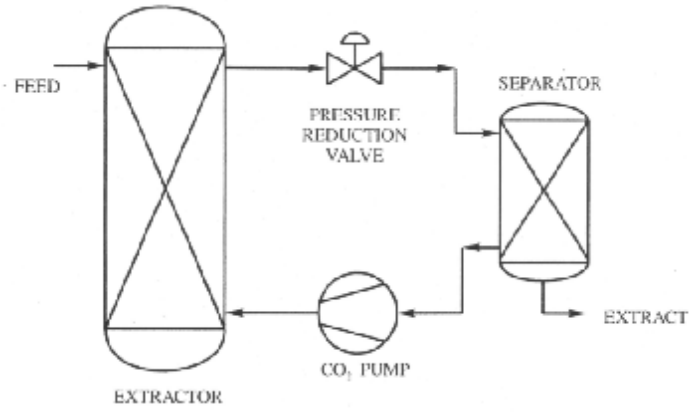

Figure 1-6. Supercritical CO_2 extraction setup [42].

Supercritical CO_2 technology has been widely applied to the extraction of natural compounds and processing of food and biomaterials. It has been largely used for the extraction of essential oils, flavors, fragrances, and aromas from plants [43-51]. Other processes including extraction of antioxidants, herbal medicines, and food colors from botanicals [52-65], extraction of pharmaceuticals from various matrices (human, animal, and plant tissues) [66-71], stabilization of fruit juices [72], decaffeination of coffee and tea [73-75], denicotinization of tobacco [42, 76], and reduction of fat and cholesterol levels in consumed meals [77, 78].

Process parameters, such as solvent flow rate, resident time, moisture content, particle sizes, and particle size distribution in conjunction with supercritical pressures and temperatures play important roles in achieving an optimum extraction yield [79]. Most of these parameters have individual or combined effects on the extraction process. If pressure is increased, fluid density as well as solvency power will increase. On the other hand, the

diffusion coefficient or the interaction between the fluid and matrix will decrease. Excessive pressure tends to cause the matrix to be more compact, thus reducing the pore sizes and mass transport, which eventually results in lower yields. Temperature does not normally have an individual effect on the extraction results. The effect of temperature is strongly related to the pressure. For instance, Tonthubthimthong et al. [80] reported the optimum yield for the extraction of nimbin from neem seeds at a pressure of 23 MPa and a temperature of 328.15 K. Chao et al. [81] studied the combined effects of pressure and temperature on the yield and selectivity of cholesterol extraction from beef tallow. The results demonstrated that higher selectivity could be achieved at lower pressures and higher temperatures.

Pretreatment of sample before being subjected into supercritical CO_2 extraction also has essential effects on the process optimization. For example, the higher moisture contents, the higher the probability for the formation of a thin film of water between the sample matrix and the fluid. This interaction will inhibit the flow of fluid and thus reduce the mass transport intensity. In addition, the particle sizes of the sample matrix may significantly impact the extraction yield. Papimichail et al. [50] experienced increased essential oil yield as the particle sizes of the celery seeds were reduced. Ge et al. [64], however, observed an optimum particle size for the wheat germ to obtain the maximum yield of natural vitamin E. They found that very fine and big particles produced lower yield probably because of higher resistances to mass transfer. The compact tendency reflecting the reduced pore sizes for finer particles and the less interaction between the sample matrix and the fluid for the latter case contribute to the higher resistances to mass transfer, and thus result in lower extraction yields.

Fluid flow rate and extraction time also have influences on the yield and selectivity. A study by Coelho et al. [45] concluded that at given temperature and pressure, the highest applied flow rate produced the highest extraction yield. Similar trends were also observed by Ge et al. [64]. For the case of supercritical CO_2 extraction of lycopene and β-carotene, an optimum flow rate was identified for the highest extraction yield [65]. In most cases, yield was also dependent on the extraction time. For instance, in the extraction of caffeine from coffee beans, long extraction time was necessary for conditions when a low flow rate was used [75]. Chierchi et al. [51] performed a detailed analysis on the flavor compounds in the essential oil extracted from *Santolina insularis* by supercritical CO_2. They reported a significant increase in sesquiterpenes concentration and a constant monoterpenes concentration with an increase in the extraction time. Hence, longer extraction time produced higher overall yield but lower selectivity for monoterpenes.

Supercritical carbon dioxide has been shown to be a viable alternative to the conventional solvent extraction technique for application in the nutraceutical, pharmaceutical, and food industry. Some drawbacks of this technique are the difficulties in extracting polar compounds and its susceptibility of extracting compounds from a complex matrix where the phase interaction with the intrinsic properties of the product inhibits its effectiveness. Moreover, this technique can only be cost effective under a large-scale production. Even though the process requires high capital and moderate operating costs, it is still more economical than the conventional solvent extraction and steam distillation at high production scales [40].

1.3.4. Supercritical Carbon Dioxide Extraction with Cosolvent

The role of cosolvents in supercritical CO_2 extraction is to enhance the extraction efficiency and the cost effectiveness of the process. Addition of a small amount of cosolvent can significantly change the overall characteristic of the extraction fluid, such as polarity, solvent strength, and specific interactions. Additionally, cosolvents can improve the extraction selectivity because it can preferentially interact with one or more desired components and facilitate selective fractional separation [40, 42].

A number of studies on the solubility of polar compounds in mixtures of supercritical CO_2 and cosolvent have appeared in the literature and demonstrated the enhancement in solubility due to the addition of a small amount of polar cosolvents [82, 83]. Chafer et al. [84] studied the solubility of antioxidant gallic acid in supercritical CO_2 and ethanol as a cosolvent with different ethanol content ranging from 0.7 to 6 mol %. Ethanol was chosen because it is a polar solvent, its use is allowed in the food industry, and it can be easily removed from the extract by evaporation at relatively low temperature. The experiments showed that the solubility of gallic acid decreased with temperature and increased with pressure and ethanol content. Salgin [85] investigated the solubility of jojoba seed oil in supercritical CO_2 as a function of temperature and pressure. The maximum extraction yield was obtained as 50.6 % (w/w) at 363.15 K and 60 MPa. The use of hexane as the co-solvent at a concentration of 5 vol. % improved the yield to 52.2 % (w/w) at relatively lower pressure and temperature (333.15 K and 30 MPa).

A study by Machmudah et al. [86] showed that the amount of astaxanthin extracted from *Haematococcus pluvialis* was more than twice enhanced with the use of ethanol as an

entrainer and effective extraction could be achieved at a more moderate pressure. As a representative study of biomass extraction, okara was chosen by Quitan et al. [87]. Okara is the residue left in the manufacture of soymilk and tofu from ground soybeans by water extraction. Dry okara contains about 26.8 % proteins, 52.9 % fibers/carbohydrates and 12.3 % fats and oils by weight. Other components include isoflavones, lignans, phytosterols, coumestans, saponins, and phytates. In supercritical CO_2 extraction, the presence of 10 mol % ethanol increased the recovery of the oil components by a factor of three. As a result of the increase in solvent power, co-extraction of some polyphenols and isoflavones also occurred. The drawback of this technique is that subsequent processing for solvent elimination is required since the cosolvent is a liquid at atmospheric pressure and is collected in the separator together with the extracted compounds [88].

1.4. Gas Antisolvent Precipitation Process to Recover Natural Compounds

The recovery of one or more solid compounds from a liquid mixture can be performed using a gas antisolvent (GAS) precipitation process. The GAS process utilizes dense gas, such as CO_2 to precipitate solid compounds from a batch solution. In order for the process to work, the CO_2 must be appreciably miscible with the solvent while the solid compounds need to be insoluble in CO_2 at operating temperature and pressure [88-96]. The dissolution of CO_2 into the solution at a given concentration causes a decrease in the solvating power of the solution, resulting in the solute precipitation at near-ambient temperature. The fact that GAS processes work at relatively low temperatures and moderate pressures can result in high active product yields since there is typically little degradation of target molecules. This process also offers the potential to fractionate a complex mixture into its various constituents

by applying CO_2 over a broad pressure range [88, 97-99]. The schematic diagram of a GAS process is illustrated in Figure 1-7.

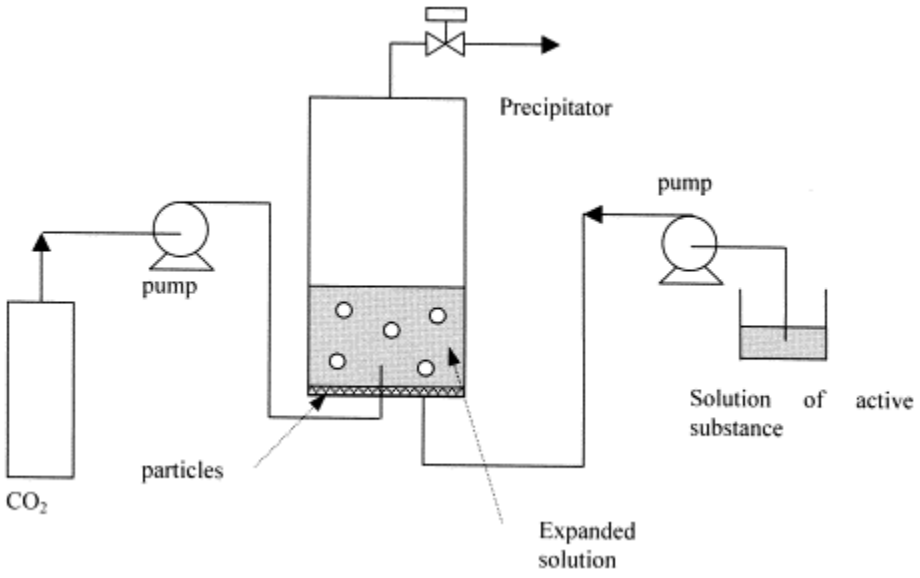

Figure 1-7. Gas antisolvent precipitation setup [93].

GAS precipitation has been widely applied in the process to isolate and/or fractionate natural compounds from liquid mixtures. For instance, it is used to isolate lecithin from crude extracts containing a high percentage of oils [42, 100]. The seed oils are highly soluble in supercritical CO_2 while lecithin is completely insoluble in the medium. A similar study was performed by Mukhopadhyay and Singh [101]. They dissolved crude lecithin in hexane and the mixture was contacted with dense CO_2 to precipitate lecithin. Catchpole et al. [97] performed GAS process to separate the high molecular weight compounds from flavonoids and the essential oil fractions in propolis tincture. Other examples include the recovery of

proteins from tobacco extracts in ethanol [88], triacylglycerols from oat bran extracts in acetone [102], and curcuminoid from triglyceride oil [103].

In addition, the GAS process was initially employed to produce ultra-fine particles of superconductor precursors, pigments, explosives, and a variety of pharmaceuticals for controlled drug release applications [92, 93, 104]. The rapid mass transfer of compressed CO_2 into the solvent causes a very fast mixing of the two fluids, leading to smaller and more uniform particles as compared to conventional liquid antisolvent processes. Moreover, it is possible to control the particle size distribution and morphology by changing the operating conditions.

The operating conditions for precipitation of particular solutes are different even with the same solvent-antisolvent pair. Several researchers performed theoretical studies on the phase behavior of the solute, the solvent, and the antisolvent of interests as a basis to select the operating conditions to fractionate or precipitate the desired compounds from a complex mixture. For example, Dixon and Johnston [105] measured the phase equilibrium of naphthalene (solid 1), phenanthrene (solid 2), toluene, and CO_2. They studied the possibility of separating naphthalene from phenanthrene using a GAS technique from a theoretical point of view. They used a hybrid model of Peng-Robinson equation of state (EOS) and regular solution theory to predict the experimental data. A related study was done by Kikic et al. [98] using Peng-Robinson EOS with classical mixing rules. The same thermodynamic approach was applied by de la Fuente et al. [90] to investigate the phase behavior of several systems including salicylic acid-propanol-CO_2, benzoic acid-acetone-CO_2, and benzoic acid-acetone-

C_2H_4. The theoretical calculations for these systems were compared with the available experimental data in literature.

1.5. Summary

This chapter presents the research motivation and objectives as well as literature review on the extraction processes of natural compounds. Following this chapter is the discussion on the thermodynamic modeling of the system of interest, sclareol-ethyl lactate-CO_2, using Peng-Robinson equation of state with a linear combination of Vidal and Michelsen mixing rules. Subsequently, the experimental works to generate the phase behavior of the sclareol-ethyl lactate-CO_2 system are discussed in chapter 3. The generated ternary phase diagrams provided essential information for the extraction process of sclareol from Clary Sage plant materials. The detailed experimental procedure and results on the extraction process of sclareol from Clary Sage plants are presented in chapter 4. The extraction with ethyl lactate followed by GAS process faced some challenges. The CO_2 and cosolvent (ethyl lactate) extraction, on the other hand, is promising. Following chapter 4 is the discussion on the processes to purify and recover sclareol from the CO_2 + ethyl lactate extracts. Finally, chapter 6 presents the summary of the research work and provides some recommendations for future work.

1.6. References

1. Watson, R., *Vegetables, fruits, and herbs in health promotion.* 2001: CRC Press.

2. Seim, H., K. Eichler, and H. Kleber, *Nutraceuticals in health and disease prevention*. 2001, New York, Marcel Dekker, Inc.

3. Biesalski, H., *Nutraceuticals: The link between nutrition and medicine.* Nutraceuticals in Health and Disease Prevention, 2001.

4. Ho, C. and Q. Zheng, *Quality management of nutraceuticals*. 2002: American Chemical Society.

5. Hurst, W., *Methods of analysis for functional foods and nutraceuticals.* 2002: CRC Press.

6. Shi, J., et al., *Extraction of polyphenolics from plant material for functional foods—engineering and technology.* Food Reviews International, 2005. **21**(1): p. 139-166.

7. De Guzman, D., *Nutraceuticals still healthy.* Chemical Market Reporter, 2006. **269**(17): p. 25.

8. Nutraceuticals in the united states., in Nutraceuticals Industry Profile: United States. 2004, Datamonitor Plc. p. 1.

9. Kyrikou, I., et al., *A comparative study of the effects of cholesterol and sclareol, a bioactive labdane type diterpene, on phospholipid bilayers.* Chemistry and Physics of Lipids, 2005. **133**(2): p. 125-134.

10. Hatziantoniou, S., et al., *Cytotoxic and antitumor activity of liposome-incorporated sclareol against cancer cell lines and human colon cancer xenografts.* Pharmacological Research, 2006. **53**(1): p. 80-87.

11. Dimas, K., et al., *The effect of sclareol on growth and cell cycle progression of human leukemic cell lines.* Leukemia Research, 1999. **23**(3): p. 217-234.

12. Oktay, M., *Evaluation of the antioxidant and antimicrobial activities of clary sage (Salvia sclarea L.).* Turk J Agric For, 2004. **28**: p. 25-33.

13. www.dweckdata.co.uk/Published_papers/Salvia.pdf [November, 2005]

14. Balinova-Tsvetkova, A., P. Tsankova, *On the extraction of Salvia sclarea L.* Flavour and fragrance journal, 1992. **7**(3): p. 151-154.

15. Kiseleva, E.N., V.A. Belyaeva, and T.N. Voitsekhovich, *Separation of sclareol.* Maslozhirovaya Promyshlennost, 1966. **32**(2): p. 23-24.

16. Belevich, E.R., et al., *Method for isolation of sclareol from clary sage concrete obtained from plant wastes.* 1996.

17. Starmans, D.A.J. and H.H. Nijhuis, *Extraction of secondary metabolites from plant material: A review.* Trends in Food Science & Technology, 1996. **7**: p. 191-197.

18. Mazza, G., J. Shi, and M. Le Maguer, *Functional foods: Biochemical and processing aspects.* 2002: CRC Press.

19. Lo, T., M. Baird, and C. Hanson, *Handbook of solvent extraction.* John Wiley & Sons, 1983: p. 980.

20. Wang, L. and C. Weller, *Recent advances in extraction of nutraceuticals from plants.* Trends in Food Science & Technology, 2006. **17**(6): p. 300-312.

21. Moure, A., *Natural antioxidants from residual sources*, in Food chemistry. 2001. p. 145.

22. Cu, J., et al., *Comparison of the chemical composition of carrot seed essential oil extracted by different solvents.* Flavour and fragrance journal, 1989. **4**(4): p. 225-231.

23. Fernandez De Simon, B., et al., *Low molecular weight phenolic compounds in spanish oak woods.* J. Agric. Food Chem., 1996. **44**(6): p. 1507-1511.

24. Tsuda, T., et al., *Antioxidative components isolated from the seed of tamarind (Tamarindus indica L.).* J. Agric. Food Chem., 1994. **42**(12): p. 2671-2674.

25. Santos-Buelga, C. and G. Williamson, *Methods in polyphenol analysis.* 2003: Royal Society of Chemistry Cambridge.

26. Cacace, J. and G. Mazza, *Extraction of anthocyanins and other phenolics from black currants with sulfured water.* J. Agric. Food Chem, 2002. **50**(21): p. 5939-5946.

27. Goncalves, C.B., P.A. Pessoa Filho, and A.J.A. Meirelles, *Partition of nutraceutical compounds in deacidification of palm oil by solvent extraction.* Journal of Food Engineering, 2007. **81**(1): p. 21-26.

28. Handayani, A.D., et al., *Extraction of astaxanthin from giant tiger (Panaeus monodon) shrimp waste using palm oil: Studies of extraction kinetics and thermodynamic.* Bioresource Technology, 2008. **99**(10): p. 4414-4419.

29. Sachindra, N.M., N. Bhaskar, and N.S. Mahendrakar, *Recovery of carotenoids from shrimp waste in organic solvents.* Waste Management, 2006. **26**(10): p. 1092-1098.

30. Ozek, G., et al., *Composition of essential oils from Salvia anatolica, a new species endemic from turkey.* Chemistry of Natural Compounds, 2007. **43**(6): p. 667-671.

31. De Morais, S., et al., *Chemical composition and larvicidal activity of essential oils from piper species.* Biochemical Systematics and Ecology, 2007. **35**(10): p. 670-675.

32. Schwob, I., J. Bessière, and J. Viano, *Composition of the essential oils of Hypericum perforatum L. From southeastern france.* Comptes rendus-Biologies, 2002. **325**(7): p. 781-785.

33. Poli, F., et al., *Comparison between the essential oils of Santolina insularis (genn. Ex fiori) Arrigoni and Santolina corsica Jord. Et fourr. From the island of sardinia (italy).* Journal of Ethnopharmacology, 1997. **56**(3): p. 201-208.

34. Kim, Y. and D. Shin, *Volatile components and antibacterial effects of pine needle (Pinus densiflora S. And Z.) extracts.* Food Microbiology, 2005. **22**(1): p. 37-45.

35. Santoro, G., et al., *Trypanosoma cruzi: Activity of essential oils from Achillea millefolium L., Syzygium aromaticum L and Ocimum basilicum L. On epimastigotes and trypomastigotes.* Experimental Parasitology, 2007. **116**(3): p. 283-290.

36. Sandri, I., et al., *Antimicrobial activity of the essential oils of brazilian species of the genus cunila against foodborne pathogens and spoiling bacteria.* Food Chemistry, 2007. **103**(3): p. 823-828.

37. Vitzthum, O., P. Werkhoff, and P. Hubert, *New volatile constituents of black tea aroma.* Journal of Agricultural and Food Chemistry, 1975. **23**(5): p. 999-1003.

38. Farag, R., et al., *Antioxidant activity of some spice essential oils on linoleic acid oxidation in aqueous media.* Journal of the American Oil Chemists' Society, 1989. **66**(6): p. 792-799.

39. Sefidkon, F., et al., T*he effect of distillation methods and stage of plant growth on the essential oil content and composition of Satureja rechingeri Jamzad.* Food Chemistry, 2007. **100**(3): p. 1054-1058.

40. Functional food ingredients and nutraceuticals: Processing technologies, ed. J. Shi. 2007, Boca Raton: CRC Press.

41. Supercritical fluid extraction of nutraceuticals and bioactive compounds, ed. J.L. Martinez. 2008, Boca Raton: CRC Press. 424.

42. Mukhopadhyay, M., *Natural extracts using supercritical carbon dioxide.* 2000: CRC Press.

43. Sass-Kiss, A., et al., *Study on the pilot-scale extraction of onion oleoresin using supercritical CO_2.* Journal of the Science of Food and Agriculture, 1998. **76**(3): p. 320-326.

44. Reverchon, E. and F. Senatore, *Supercritical carbon dioxide extraction of chamomile essential oil and its analysis by gas chromatography-mass spectrometry.* Journal of Agricultural and Food Chemistry, 1994. **42**(1): p. 154-158.

45. Coelho, J., et al., *Supercritical carbon dioxide extraction of Foeniculum vulgare volatile oil.* Flavour and Fragrance Journal, 2003. **18**: p. 316–319.

46. Reverchon, E., G. Porta, and F. Senatore, *Supercritical CO_2 extraction and fractionation of lavender essential oil and waxes.* Journal of Agricultural and Food Chemistry, 1995. **43**(6): p. 1654-1658.

47. Povh, N., M. Marques, and M. Meireles, *Supercritical CO_2 extraction of essential oil and oleoresin from chamomile (Chamomilla Recutita).* The Journal of Supercritical Fluids, 2001. **21**(3): p. 245-256.

48. Mira, B., et al., *Supercritical CO_2 extraction of essential oils from orange peel.* The Journal of Supercritical Fluids, 1996. **9**(4): p. 238-243.

49. Giannuzzo, A., et al., *Supercritical fluid extraction of naringin from the peel of citrus paradisi.* Phytochemical Analysis, 2003. **14**(4): p. 221-223.

50. Papamichail, I., V. Louli, and K. Magoulas, *Supercritical fluid extraction of celery seed oil.* The Journal of Supercritical Fluids, 2000. **18**(3): p. 213-226.

51. Cherchi, G., et al., E*xtraction of santolina insularis essential oil by supercritical carbon dioxide: Influence of some process parameters and biological activity.* Flavour Fragrance J, 2001. **16**: p. 35-43.

52. Tsuda, T., et al., *Supercritical carbon dioxide extraction of antioxidative components from tamarind (Tamarindus indica L.) seed coat.* Journal of Agricultural and Food Chemistry, 1995. **43**(11): p. 2803-2806.

53. Lim, G., et al., *Separation of astaxanthin from red yeast phaffia rhodozyma by supercritical carbon dioxide extraction.* Biochemical Engineering Journal, 2002. **11**(2-3): p. 181-187.

54. Chang, C., et al., *Separation of catechins from green tea using carbon dioxide extraction.* Food Chemistry, 2000. **68**(1): p. 109-113.

55. Ollanketo, M., et al., *Supercritical carbon dioxide extraction of lycopene in tomato skins.* European Food Research and Technology, 2001. **212**(5): p. 561-565.

56. Bauman, D., et al., *Supercritical fluid extraction of rosemary and sage antioxidants.* Acta alimentaria(Budapest), 1999. **28**(1): p. 15-28.

57. Murga, R., et al., *Extraction of natural complex phenols and tannins from grape seeds by using supercritical mixtures of carbon dioxide and alcohol.* J. Agric. Food Chem, 2000. **48**(8): p. 3408-3412.

58. Catchpole, O., et al., *Supercritical extraction of herbs i: Saw palmetto, stjohn's wort, kava root, and echinacea.* The Journal of Supercritical Fluids, 2002. **22**(2): p. 129-138.

59. Zizovic, I., et al., *Supercritical carbon dioxide extraction of sesquiterpenes from valerian root.* The Journal of Supercritical Fluids, 2007. **43**(2): p. 249-258.

60. Dean, J., B. Liu, and R. Price, *Extraction of magnolol from magnolia officinalis using supercritical fluid extraction and phytosol solvent extraction.* Phytochemical Analysis, 1998. **9**(5): p. 248-252.

61. Grigonis, D., et al., *Comparison of different extraction techniques for isolation of antioxidants from sweet grass (Hierochloë odorata).* Journal of Supercritical Fluids, 2005. **33**(3): p. 223-233.

62. Schonemann, H., et al., *Method for extraction and concentration of carotenoids using supercritical fluids.* 2008, US Patent 7,329,789.

63. Fluids, E. and K. Bartle, *Sub-and supercritical extraction of hops and other botanicals.*

64. Ge, Y., et al., *Extraction of natural vitamin e from wheat germ by supercritical carbon dioxide.* Journal of Agricultural and Food Chemistry, 2002. **50**(4): p. 685-689.

65. Baysal, T., S. Ersus, and D. Starmans, *Supercritical CO_2 extraction of-carotene and lycopene from tomato paste waste.* J. Agric. Food Chem, 2000. **48**(11): p. 5507-5511.

66. Ramsey, E., et al., *Analysis of drug residues in tissue by combined supercritical-fluid extraction-supercritical-fluid chromatography-mass spectrometry-mass spectrometry.* J Chromatogr, 1989. **464**(2): p. 353-64.

67. Danaher, M., M. O'Keeffe, and J. Glennon, *Development and optimisation of a method for the extraction of benzimidazoles from animal liver using supercritical carbon dioxide.* Analytica Chimica Acta, 2003. **483**(1-2): p. 313-324.

68. Dean, J. and S. Khundker, *Extraction of pharmaceuticals using pressurised carbon dioxide.* Journal of Pharmaceutical and Biomedical Analysis, 1997. **15**(7): p. 875-886.

69. Brewer, W., et al., A*nalysis of cocaine, benzoylecgonine, codeine, and morphine in hair by supercritical fluid extraction with carbon dioxide modified with methanol.* Anal. Chem, 2001. **73**(11): p. 2371-2376.

70. Kohler, M., et al., *Extraction of artemisinin and artemisinic acid from Artemisia annua L. using supercritical carbon dioxide.* Journal of Chromatography A, 1997. **785**(1-2): p. 353-360.

71. Heaton, D., et al., *Application of supercritical fluid extraction and supercritical fluid chromatography to the production of taxanes as anti-cancer drugs.* Journal of High Resolution Chromatography, 1993. **16**: p. 667.

72. Summerland, B., V. Iu, and H. Ltd, *Supercritical carbon dioxide percolation of sea buckthorn press juice'.* Journal of Food Quality, 2004. **27**: p. 41-54.

73. Zosel, K., *Process for the decaffeination of coffee.* 1981, Google Patents.

74. Gehrig, M. and A. Forster, *Process for the production of decaffeinated tea*. 1990, Google Patents.

75. Peker, H., et al., *Caffeine extraction rates from coffee beans with supercritical carbon dioxide.* AIChE journal, 1992. **38**(5): p. 761-770.

76. Fiori, L., D. Calcagno, and P. Costa, *Sensitivity analysis and operative conditions of a supercritical fluid extractor.* The Journal of Supercritical Fluids, 2007. **41**(1): p. 31-42.

77. Froning, G., et al., *Extraction of cholesterol and other lipids from dried egg yolk using supercritical carbon dioxide.* J. Food Sci, 1990. **55**(1): p. 95-98.

78. Froning, G., et al., *Supercritical carbon dioxide extraction of lipids and cholesterol from dehydrated chicken meat.* Poult Sci, 1994. **73**(4): p. 571-5.

79. Shi, J., L. Kassama, and Y. Kakuda, *Supercritical fluid technology for extraction of bioactive components.* Functional Food Ingredients and Nutraceuticals: Processing Technologies, 2006.

80. Tonthubthimthong, P., et al., *Supercritical CO_2 extraction of nimbin from neem seeds–an experimental study.* Journal of Food Engineering, 2001. **47**(4): p. 289-293.

81. Chao, R., S. Mulvaney, and H. Huang, *Effects of extraction and fractionation pressures on supercritical extraction of cholesterol from beef tallow.* Journal of the American Oil Chemists' Society, 1993. **70**(2): p. 139-143.

82. Cháfer, A., et al., *Solubility of solid carnosic acid in supercritical CO_2 with ethanol as a co-solvent.* The Journal of Supercritical Fluids, 2005. **34**(3): p. 323-329.

83. Huang, Z., S. Kawi, and Y. Chiew, *Solubility of cholesterol and its esters in supercritical carbon dioxide with and without cosolvents.* J. Supercrit. Fluids, 2004. **30**: p. 25.

84. Cháfer, A., et al., *Solubility of the natural antioxidant gallic acid in supercritical CO_2 + ethanol as a cosolvent.* J. Chem. Eng. Data, 2007. **52**(1): p. 116-121.

85. Salgin, U., *Extraction of jojoba seed oil using supercritical CO_2 + ethanol mixture in green and high-tech separation process.* The Journal of Supercritical Fluids, 2007. **39**(3): p. 330-337.

86. Machmudah, S., et al., E*xtraction of astaxanthin from Haematococcus pluvialis using supercritical CO_2 and ethanol as entrainer.* Ind. Eng. Chem. Res., 2006. **45**(10): p. 3652-3657.

87. Quitain, A., et al., R*ecovery of oil components of okara by ethanol-modified supercritical carbon dioxide extraction.* Bioresource Technology, 2006. **97**(13): p. 1509-1514.

88. Reverchon, E. and I. De Marco, *Supercritical fluid extraction and fractionation of natural matter.* The Journal of supercritical fluids, 2006. **38**(2): p. 146-166.

89. Miguel, F., A. Martin, and T. Gamseb, *Supercritical anti solvent precipitation of lycopene effect of the operating parameters.* J of Supercritical Fluids, 2006. **36**: p. 225-235.

90. De La Fuente, J., A. Shariati, and C. Peters, *On the selection of optimum thermodynamic conditions for the gas process.* J. Supercrit. Fluids, 2004. **32**(1-3): p. 55.

91. Cocero, M. and S. Ferrero, *Crystallization of ß-carotene by a gas process in batch effect of operating conditions.* The Journal of Supercritical Fluids, 2002. **22**(3): p. 237-245.

92. Reverchon, E., *Supercritical antisolvent precipitation of micro-and nano-particles.* The Journal of Supercritical Fluids, 1999. **15**(1): p. 1-21.

93. Jung, J. and M. Perrut, *Particle design using supercritical fluids: Literature and patent survey.* The Journal of Supercritical Fluids, 2001. **20**(3): p. 179-219.

94. Shariati, A. and C. Peters, *Recent developments in particle design using supercritical fluids.* Current Opinion in Solid State & Materials Science, 2003. **7**(4-5): p. 371-383.

95. Liu, Z., et al., *Solubility of hydroxybenzoic acid isomers in ethyl acetate expanded with CO_2.* The Journal of Supercritical Fluids, 2000. **18**(2): p. 111-119.

96. Liu, Z., et al., *Study on the phase behavior of cholesterol–acetone– CO_2 system and recrystallization of cholesterol by antisolvent CO_2.* The Journal of Supercritical Fluids, 2002. **24**(1): p. 1-6.

97. Catchpole, O., et al., *Supercritical antisolvent fractionation of propolis tincture.* Journal of Supercritical Fluids, 2004. **29**: p. 97-106.

98. Bertucco, A., M. Lora, and I. Kikic, *Fractional crystallization by gas antisolvent technique: Theory and experiments.* AIChE Journal, 1998. **44**(10): p. 2149-2158.

99. Catchpole, O., S. Hochmann, and S. Anderson, *Gas anti-solvent fractionation of natural products.* High Pressure Chemical Engineering", R. von Rohr et C. Trepp éditeurs, Elsevier, Amsterdam, Netherlands, 1996: p. 309–314.

100. Montanari, L., et al., *Selective extraction of phospholipids from soybeans with supercritical carbon dioxide and ethanol.* The Journal of Supercritical Fluids, 1999. **14**(2): p. 87-93.

101. Mukhopadhyay, M. and S. Singh, *Refining of crude lecithin using dense carbon dioxide as anti-solvent.* The Journal of Supercritical Fluids, 2004. **30**(2): p. 201-211.

102. Andersson, M., M. Demirbüker, and L. Blomberg, *Semi-continuous extraction/purification of lipids by means of supercritical fluids.* Journal of Chromatography A, 1997. **785**(1-2): p. 337-343.

103. Catchpole, O. and C. Bergmann, *Continuous gas anti-solvent fractionation of natural products.* Proceedings of the Fifth Meeting on Supercritical Fluids, Nice, Tome. **1**: p. 23–25.

104. Bothun, G., K. White, and B. Knutson, *Gas antisolvent fractionation of semicrystalline and amorphous poly (lactic acid) using compressed CO_2.* Polymer, 2002. **43**(16): p. 4445-4452.

105. Dixon, D. and K. Johnston, *Molecular thermodynamics of solubilities in gas antisolvent crystallization.* AIChE Journal, 1991. **37**(10): p. 1441-1449.

2. Thermodynamic Modeling of the Ternary System of Sclareol-Ethyl lactate-CO_2

This chapter was published as a part of article in Journal of Supercritical Fluids 45 (2008), page 146-155.

2.1. Introduction

For effective implementation of the extraction process, it is essential to first understand the phase behavior of the system of interest as a function of temperature and pressure. In the extraction process of sclareol from Clary Sage plant materials, the important factor is the capability of the ethyl lactate and/or carbon dioxide for dissolving sclareol whereas the driving force in the GAS precipitation process is the degree of sclareol super-saturation induced by the presence of CO_2 in solution. The PR-EOS has been commonly used to model systems involving CO_2. It is used to calculate the fugacity of the fluid and the vapor phases while a separate fugacity expression based on the solute physical properties (heat of fusion, triple point temperature and pressure, differential heat capacity, and solid molar volume) is used to calculate the fugacity of the solid phase (precipitate). Applying this model to our sclareol system has become more of a challenge due to the scarcity of parameter values. For that reason, we were motivated to examine a predictive model by incorporating a group contribution approach through a UNIFAC activity coefficient model into a PR EOS.

The so-called LCVM (Linear Combination of Vidal-Michelsen mixing rule), was first developed by Boukouvalas et al [1]. In this model, the Vidal-Michelsen mixing rule is used for the calculation of parameter a in the attractive term of the PR EOS while a linear mixing

rule is used for the calculation of parameter *b*. The range of applicability of the UNIFAC group-contribution method is dependent on the availability of group volumes (R_k), group surface areas (Q_k), and group interaction parameters (a_{mn} and a_{nm}) [1-6]. Fortunately, tables of these interaction parameters have been largely extended to correspond to a number of systems with supercritical CO_2 and organic compounds, like alkenes, ethers, alcohols, esters, and acids [1].

The PR-LCVM model had been applied to the description of VLE in polar systems at high pressures as well as systems containing gases (CO_2, CH_4 and C_2H_6) with n-alkanes [7]. Coutsikos et al. [8] examined the ability of the LCVM model to predict the solubility behavior of solid - supercritical fluid binary systems. They obtained adequate predictions of the solubilities of aromatic hydrocarbons, aliphatic acids, and some alcohols along with complex solids in CO_2. Also, Gerszt et al. [9] studied the phase behavior of sterols and vitamins in CO_2 and obtained comparable results with the available experimental data. Due to these promising results presented in the literature, we apply the PR-LCVM model to our system of interest: sclareol-ethyl lactate-CO_2.

2.2. Peng-Robinson Equation of State with Linear Combination of Vidal and Michelsen Mixing Rules

The Gibbs Phase Rule states that for an equilibrium system the number of degrees of freedom, *F*, or independent intensive variables, which must be set to completely specify an equilibrium system with *C* components and *p* phases is given by Equation (1).

$$F = C - p + 2 \tag{1}$$

Thus, for a two-component vapor - liquid equilibrium (VLE), solid - liquid equilibrium (SLE), or solid - vapor equilibrium (SVE) system, or a three-component solid - vapor - liquid equilibrium (SVLE) system, only the temperature and pressure need to be specified for the compositions of the fluid phase(s) to be set in each case [10]. On the other hand, for a three-component VLE, SLE, and SVE, the mole fraction of one species needs to be specified in addition to the temperature and pressure. By definition, at equilibrium the temperature and pressure are constant in all phases, and the chemical potential, m_i, of each component is equal in all phases that the component appears.

$$T^1 = T^2 = \ldots = T^p \tag{2}$$

$$P^1 = P^2 = \ldots = P^p \tag{3}$$

$$\begin{aligned} & m_1^1 = m_1^2 = \ldots = m_1^p \\ & \text{M} \\ & m_1^1 = m_C^2 = \ldots = m_C^p \end{aligned} \tag{4}$$

It is convenient to use iso-fugacity relationships to represent this chemical equilibrium for mixtures. Using the $\Phi - \Phi$ approach, the fugacity of species *i* in both liquid and vapor phases can be calculated as:

$$f_i^L = P \cdot x_i \cdot \Phi_i^L \tag{5}$$

$$f_i^V = P \cdot y_i \cdot \Phi_i^V \tag{6}$$

where Φ_i^L and Φ_i^V are the fugacity coefficient of species *i* in the liquid and the vapor phase, respectively. When a solid phase is present, as in the case of SLE, SVE, and SVLE, the fugacity of the fluid phases can be represented using an equation of state, but a separate relationship is required for the pure solid. Prausnitz [11] derived Equation (7) that relates the fugacity of the solute in the solid phase (f_3^s) to that in the sub-cooled liquid phase ($f_3^L(T, P_{tp})$), at temperature T and pressure P. DH_{fus} is the heat of fusion of the solute at the melting temperature, T_{tp} is the triple point temperature, P_{tp} is the triple point pressure, DC_p is the differential heat capacity, and v_3^S is the molar volume of the solid. Equation of state can be used to calculate $f_3^L(T, P_{tp})$.

$$f_3^S = f_3^L(T, P_{tp}) \exp\left[\frac{\Delta H_{fus}}{R}\left(\frac{1}{T_{tp}} - \frac{1}{T}\right) + \frac{v_3^S(P - P_{tp})}{RT} - \frac{\Delta C_P}{R}\left(\ln\left(\frac{T_{tp}}{T}\right) - \frac{T_{tp}}{T} + 1\right)\right] \quad (7)$$

The differential heat capacity is the difference between the heat capacity of the liquid and the solid solute at the melting temperature. Often this last term in the exponential is neglected, since at high pressure the first and second terms dominate. The triple point temperature is usually approximated as the melting temperature.

In order to calculate the fugacity coefficients required for the calculations, an equation of state is used to solve for a fugacity coefficient for each of the fluid phases to try to represent their non-ideality. The pressure-explicit PR EOS, given in Equation (8), is considered to

calculate the fugacity coefficients [9]. The PR EOS is semi-empirical with two parameters: *a*, a temperature-dependent energy parameter which provides a measure of the intermolecular attractive force, and *b*, a volume parameter related to the size of the molecules. The expressions for the fugacity coefficients using the PR EOS are given in Equations (9) and (10).

$$P = \frac{RT}{v-b} - \frac{a(T)}{v(v+b)+b(v-b)} \tag{8}$$

$$\ln(f_i) = \frac{b_m}{b}\left(Z^V - 1\right) - \ln\left(Z^V - B\right) - \frac{A}{2\sqrt{2}B}\left[\frac{2\sum_{k=1}^{N} x_k a_{ki}}{a} - \frac{b_i}{b}\right]\ln\left[\frac{Z^V + 2.414B}{Z^V - 0.414B}\right] \tag{9}$$

$$\ln(f_i) = \frac{b_m}{b}\left(Z^L - 1\right) - \ln\left(Z^L - B\right) - \frac{A}{2\sqrt{2}B}\left[\frac{2\sum_{k=1}^{N} x_k a_{ki}}{a} - \frac{b_i}{b}\right]\ln\left[\frac{Z^L + 2.414B}{Z^L - 0.414B}\right] \tag{10}$$

First, the pure component parameters can be calculated using the critical temperatures, T_{ci}, the critical pressures, P_{ci}, and the acentric factors, w_i, for each component in the mixture, as derived in Equation (11) and (12). *R* represents the ideal gas constant.

$$a_i(T) = 0.45724\frac{R^2\left(T_{ci}\right)^2}{P_{ci}}\left[1 + \left(0.37464 + 1.54226w_i - 0.26992w_i^2\right)\cdot\left(1 - \sqrt{\frac{T}{T_{ci}}}\right)\right]^2 \tag{11}$$

$$b_i = 0.07780\frac{RT_{ci}}{P_{ci}} \tag{12}$$

Traditionally, quadratic mixing rules are employed to solve for the mixture parameters in terms of the equilibrium composition of the mixture, as described in Equation (13) and (14). Two binary interaction parameters, k_{ij} and l_{ij}, are fit from the experimental data, and can allow for much better predictions of equilibrium compositions. Often l_{ij} is set to zero and only a single binary interaction parameter is used [12].

$$a = \sum_{i=1}^{N}\sum_{j=1}^{N} x_i x_j \cdot \sqrt{a_i(T)\cdot a_j(T)} \cdot (1-k_{ij}) \tag{13}$$

$$b = \sum_{i=1}^{N}\sum_{j=1}^{N} x_i x_j \cdot \left(\frac{b_i + b_j}{2}\right) \cdot (1-l_{ij}) \tag{14}$$

Subsequently, A and B are calculated using Equation (15) and (16).

$$A = \frac{aP}{RT} \tag{15}$$

$$B = \frac{bP}{RT} \tag{16}$$

It is necessary to solve the cubic equations for the compressibility factor of the vapor phase, Z^V, and the liquid phase, Z^L.

$$\left(Z^V\right)^3 - (1-B)\left(Z^V\right)^2 + (A - 3B^2 - 2B)Z^V - (AB - B^2 - B^3) = 0 \tag{17}$$

$$\left(Z^L\right)^3 - (1-B)\left(Z^L\right)^2 + (A - 3B^2 - 2B)Z^L - (AB - B^2 - B^3) = 0 \quad (18)$$

The largest root of Equation (17) represents the solution for the vapor phase, and the smallest root of Equation (18) represents the correct solution for the liquid phase, as the compressibility factor is proportional to the molar volume of each phase, as represented in Equation (19).

$$Z^a = \frac{Pv^a}{RT} \quad (19)$$

The compressibility factors can be substituted into Equations (9) and (10) to solve for the fugacity coefficients. These equations are used along with the necessary conditions that the equilibrium composition values sum to unity for each phase to solve for the mole fractions of each component in the vapor and liquid phases. Because calculation of the fugacity coefficients requires knowing the compositions of each phase, an iterative process must be employed using an appropriate initial guess for the equilibrium mole fractions.

The use of PR EOS for high pressure systems is a reliable method to do the phase equilibrium calculations, however experimental data is required to fit the binary interaction parameters. In cases where there is no or scarce amount of information about the nutraceutical solute, the use of the model with conventional mixing rules is not possible. Therefore, we applied PR-LCVM model for the phase behavior calculation involving nutraceutical solute (sclareol). In this model, the linear mixing rule is used for the mixture

covolume parameter b of PR EOS, while the mixing rule for the attractive-term parameter a (in terms of the dimensionless parameter a) is a linear combination of Huron-Vidal [13] and Michelsen [14] mixing rules, as shown in equation (20).

$$a = \frac{a}{bRT} = \left(\frac{l}{A_V} + \frac{1-l}{A_M} \right) \cdot \frac{G^E}{RT} + \frac{1-l}{A_M} \cdot \sum x_i \ln\left(\frac{b}{b_i} \right) + \sum x_i a_i \tag{20}$$

where $A_M = -0.52$, $A_V = -0.623$ for the PR- EOS and $l = 0.36$.

The advantage of using this mixing rule as compared to conventional mixing rules alone is that it does not require binary interaction parameters regressed from experimental data. It employs the UNIFAC model [2-6] for the calculation of excess Gibbs free energy, G^E. In addition, this hybrid model is essential for pressurized systems in which one of the components does not have well defined critical properties and has very low vapor pressure, which in this case is sclareol. The fugacity coefficient of species i in a mixture, for the PR EOS coupled with LCVM model, can be expressed as:

$$\Phi_i = \exp\left[\frac{b_i}{b} \cdot (Z-1) - \ln(Z-b) - \frac{\bar{a}_i}{2\sqrt{2}} \ln\left(\frac{Z + 2.414B}{Z + 0.414B} \right) \right] \tag{21}$$

$$\bar{a}_i = \left(\frac{l}{A_V} + \frac{1-l}{A_M} \right) \cdot \ln g_i + \frac{1-l}{A_M} \cdot \left(\ln \frac{b}{b_i} + \frac{b_i}{b} - 1 \right) + a_i \tag{22}$$

where γ_i represents the activity coefficient of species i from the UNIFAC G^E model and Z represents the compressibility factor, which is a real root of cubic PR EOS. More details on LCVM mixing rules and UNIFAC activity coefficient calculations are described in Appendix A.1.

2.3. Equilibrium Data Generated from PR-LCVM

2.3.1. Critical Values and Interaction Parameters for PR-LCVM Model

The critical properties of sclareol, ethyl lactate, and carbon dioxide and physical properties of sclareol used in the PR-LCVM model are summarized in Table 2-1.

Table 2-1. Sclareol, ethyl lactate, and CO_2 critical constants and sclareol physical properties. The data are obtained from DIPPR database or elsewhere as noted.

	CO_2	Ethyl Lactate	Sclareol
Tc (K)	304.2	588	845.5[a]
Pc (MPa)	7.38	3.86	1.58[a]
ω	0.225	0.6[d]	1.023[a]
ΔH_{fusion} (KJ/mol)	-	-	26.225[b]
Tm (K)	-	-	376.45[b]
υ_s (m^3/mol)	-	-	0.0003[c]

[a] Joback method [15], [b] Differential Scanning Calorimetry (DSC), [c] Experimental measurement using helium pycnometer, [d] Adjusted to fit the experimental binary data of CO_2-ethyl lactate system from literature [16].

The value of ΔH_{fusion} of sclareol was measured using differential scanning calorimetry (TA Instruments, Q100). The experiments were performed using a ramp rate of 10 ^oC/min under a nitrogen atmosphere. The area under the DSC curve of heat flow versus temperature was integrated to determine the ΔH_{fusion} value at the melting temperature of sclareol. The

density of sclareol was determined experimentally using a helium-displacement pycnometer (Micrometrics Accu Pyc 1330). This instrument measures the volume occupied by the solid sample of known mass. For the binary CO_2-ethyl lactate system, the values of critical temperature and pressure used in PR-LCVM model were obtained from DIPPR and the acentric factor of ethyl lactate was adjusted to fit the experimental solubility data from the literature [16]. The PR-LCVM model agrees with the experimental data when the ethyl lactate acentric factor, *w*, is adjusted to 0.6 at 311.15 and 318.15 K. The percentage error between the experimental and the predicted solubility data was calculated to be < 10%.

The functional groups that represent the sclareol and ethyl lactate molecules for UNIFAC calculations are described as follows: sclareol is represented by the following functional groups: 5 CH_3, 7 CH_2, 2 CH, 4 C, 1 CH_2=CH_2, 2 OH whereas ethyl lactate is represented by the following functional groups: 2 CH_3, 1 CH, 1 OH, 1 CH_2COO. The functional group structural parameters and the interaction parameters between functional groups employed in the activity coefficient calculations using UNIFAC are summarized in Table 2-2 and Table 2-3, respectively.

Table 2-2. Functional group structural parameters for UNIFAC [2, 17, 18].

	r_i	q_i
CH_3	0.9011	0.848
CH_2	0.6744	0.54
CH	0.4469	0.228
C	0.2195	0
CH_2=CH_2	1.3454	1.176
OH	1	1.2
CH_2COO	1.6764	1.42
CO_2	1.296	1.261

Table 2-3. Interaction parameters between functional groups for UNIFAC [2, 17, 18].

a_{mn}	CH_3	CH_2	CH	C	CH_2=CH_2	OH	CH_2COO	CO_2
CH_3	0	0	0	0	-200	986.5	232.1	116.7
CH_2	0	0	0	0	-200	986.5	232.1	116.7
CH	0	0	0	0	-200	986.5	232.1	116.7
C	0	0	0	0	-200	986.5	232.1	116.7
CH_2=CH_2	2520	2520	2520	2520	0	639.9	71.23	48.57
OH	156.4	156.4	156.4	156.4	8694	0	101.1	471.83
CH_2COO	114.8	114.8	114.8	114.8	269.3	245.4	0	102.75
CO_2	110.6	110.6	110.6	110.6	55.74	87.1	-126.9	0

2.3.2. Two-Component System: Ethyl Lactate-CO_2

The success of the extraction and precipitation processes depends on how well the CO_2 is mixed with the solvent, which is ethyl lactate in this case. The miscibility between these fluids is essential in determining the necessary operating conditions, such as temperature, pressure, and composition. Figure 2-1 describes the vapor liquid equilibrium of ethyl lactate and CO_2 as a function of temperature and pressure. It is observed that the miscibility of ethyl lactate and CO_2 increases with pressure but decreases with temperature. When the temperature is increased, the CO_2 weight fraction in the liquid phase decreases. At relatively low pressure (< 0.75 MPa), more ethyl lactate is dissolved in the vapor phase (CO_2-rich phase) as temperature increases whereas at pressure > 0.75 MPa, CO_2-rich phase contains negligible amount of ethyl lactate. The matlab code for the vapor liquid equilibrium of ethyl lactate and CO_2 is described in Appendix A.2.2.

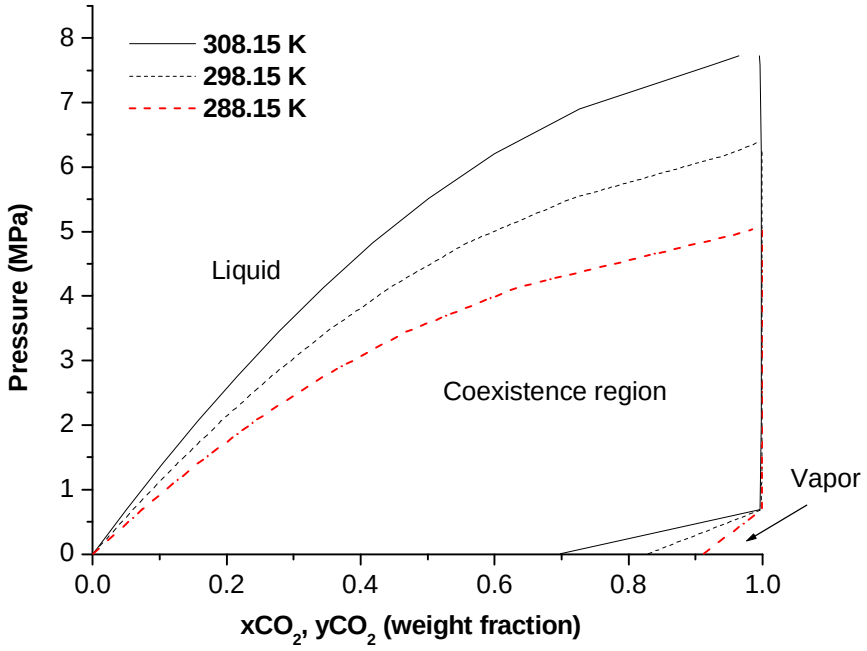

Figure 2-1. Prediction of VLE for ethyl lactate-CO_2 system at various temperatures and pressures.

In order to test the validity of the binary VLE code, the generated data from PR-LCVM were compared to some available systems in the literature. The physical property values used in the validation studies are given in Appendix A.4. Figure 2-2 shows the predicted and experimental high pressure VLE data for CO_2 (1) – propane (2) system [19] at 344.4 K and the model correctly captures the solubility behavior in both liquid and vapor phases, indicating that the model is able to predict VLE phase behavior at high pressures. Taking into account that propane system data have not been utilized to develop UNIFAC parameter tables, surprisingly good results are obtained. Along with validating the model with other available high pressure VLE data, systems containing alcohol and ester systems have been

investigated. In this measured system of butyl propanoate (1) with ethanol (2) [20], the model is able to get very close results to the published experimental data, illustrated in Figure 2-3.

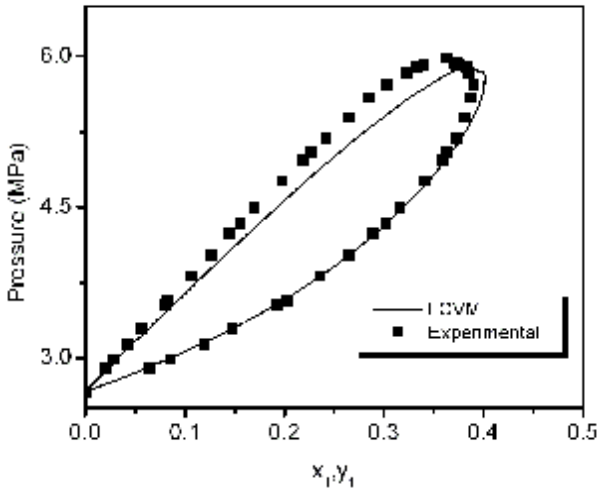

Figure 2-2. Experimental and predicted VLE of propane-CO_2 system at 344.4 K.

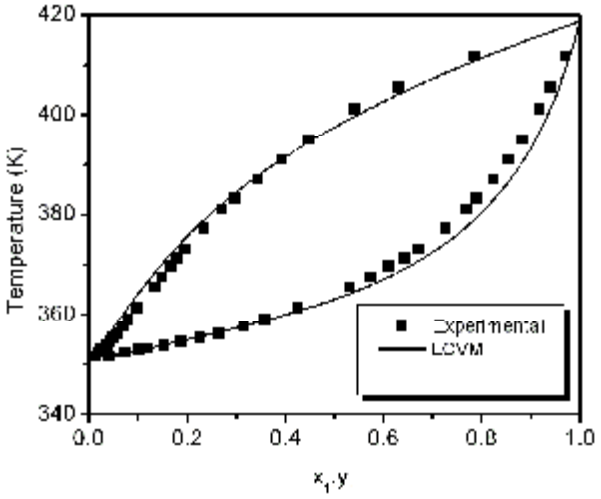

Figure 2-3. Experimental and predicted VLE of butyl propanoate-ethanol system at 101.32 KPa.

The more similar systems to our work are ethyl acetate-CO_2 [21] and ethyl hexanoate-CO_2 [22], presented in Figure 2-4 and Figure 2-5. At the conditions investigated, both esters have relatively low solubility in CO_2-rich phase, as also the case for ethyl lactate. It is observed from these systems that the PR-LCVM model agrees well with the published experimental data.

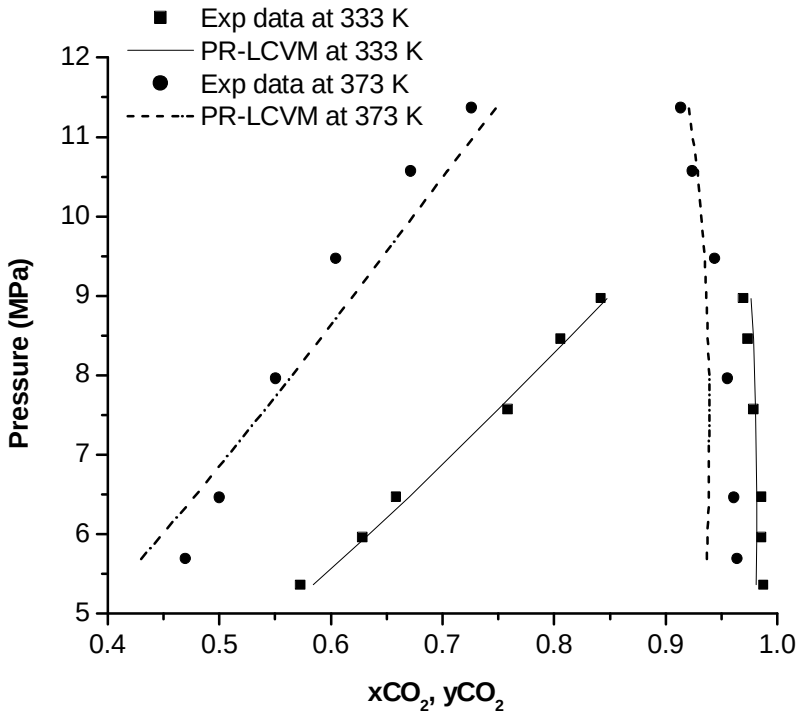

Figure 2-4. Experimental and predicted VLE of ethyl acetate-CO_2 system at 333 and 373 K.

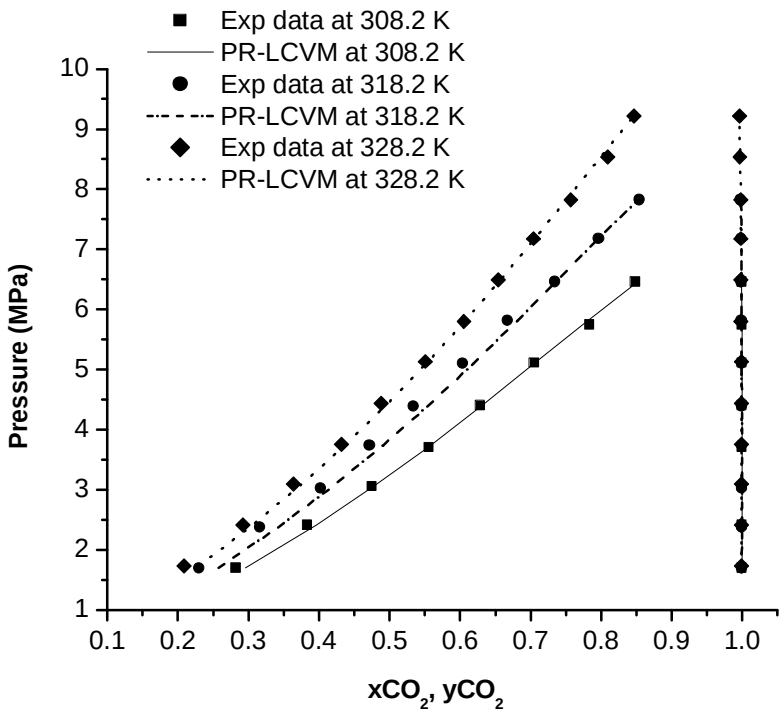

Figure 2-5. Experimental and predicted VLE of ethyl hexanoate-CO_2 system at 308.2, 318.2 and 328.2 K.

2.3.3. Three-Component System: Sclareol-Ethyl Lactate-CO_2

In constructing the ternary phase diagrams of sclareol-ethyl lactate-CO_2 system at certain temperature and pressure, three algorithms (ternary vapor-liquid, ternary solid liquid, and ternary solid-vapor-liquid equilibrium codes) based on PR-LCVM model are required. In this case, it is assumed that the solubility of ethyl lactate and sclareol in CO_2-rich phase (vapor phase) is negligible. The generated vapor liquid equilibrium of ethyl lactate-CO_2 system (shown in Figure 2-1) confirmed the low solubility of ethyl lactate in CO_2-rich phase. In addition, Chylinski and Gregorowicz [16] reported that the ethyl lactate solubility in CO_2-rich phase in terms of weight fraction at T = 311-323 K and P = 1-8 MPa was fairly small, in

the order of 10^{-3}. Figure 2-6 describes the ternary phase behavior in terms of weight fraction at 298.15 K and 4.14 MPa.

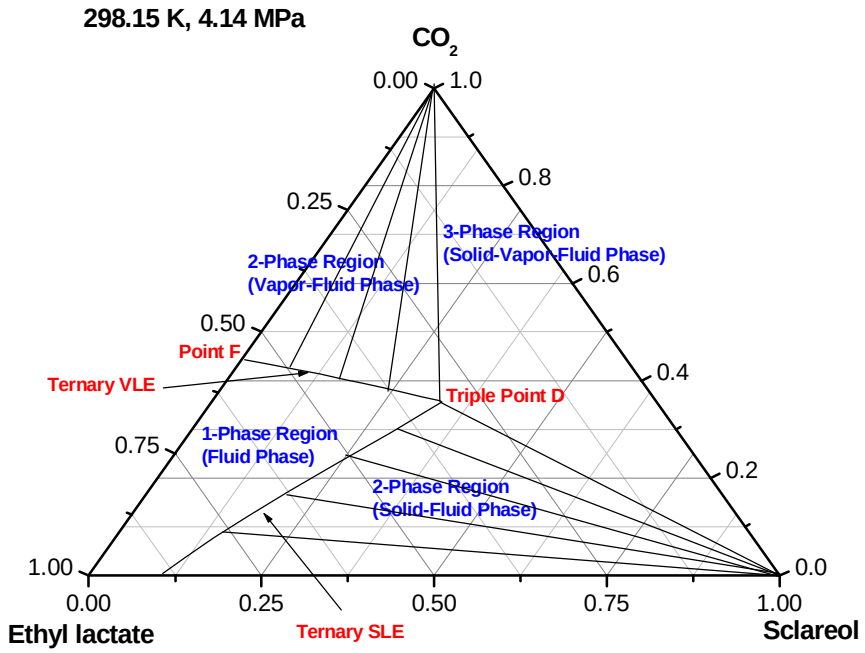

Figure 2-6. Computed ternary phase diagram of sclareol-ethyl lactate-CO_2 at 298.15 K and 4.14 MPa using PR-LCVM.

Tripe point D represents the point where all the phases, which are the fluid phase, solid-fluid, vapor-fluid, and solid-vapor-fluid phase, coexist. Point D is calculated from the ternary SVLE code as shown in Appendix A.3.4. Point F, on the other hand, represents the equilibrium composition of ethyl lactate-CO_2 when there is no sclareol present. The line from sclareol corner to point D indicates the transition from a two-phase (solid-fluid) to a three-phase (solid-vapor-fluid) region, assuming that the solid phase consists of only sclareol. The line from CO_2 corner to point D indicates the transition from a three-phase to a two-phase

(vapor-fluid) region by assuming that the sclareol solubility in CO_2-rich phase is very small. The F-D equilibrium line is obtained from the ternary VLE code whereas the line indicating the transition from a two-phase (solid-fluid) to a one-phase (fluid) region is generated from the ternary SLE code, as shown in Appendix A.3.2 and A.3.3, respectively.

The validity of the phase equilibrium codes for the ternary system was tested using available systems in the literature. For the systems involving the precipitation of solute, the reported data is usually on the equilibrium solubility of solute in the mixture of solvent and carbon dioxide (fluid phase) as a function of temperature and/or pressure. This solubility value is the point D of the ternary phase diagram (Figure 2-6), which is generated from the ternary SVLE code described in Appendix A.3.4. Liu et al. [23] measured the liquid phase composition of the three-component SVLE system CO_2 (1) – acetone (2) – cholesterol (3) at 318.15 K as a function of pressure. It is shown in Figure 2-7 that the model is able to get a good confirmation of the published data when the critical temperature of solute is adjusted to fit the ternary data. Strong dependency on critical values can be also seen in Figure 2-8 where the model is used to correlate the liquid phase solid solubility data for CO_2 (1) - ethyl acetate (2) - tetradecanoic acid (3) SVLE system at 318.15 K reported by Liu et al. [24]. The data illustrate clearly that as pressure increases, more CO_2 is dissolved in the liquid solvent resulting in the precipitation of the solute. At approximately 7 MPa, it is calculated that more than 90 % of the solute is already dropped out of the expanded liquid solution. This phenomenon is well captured by the model when the adjustment for the solid solute critical temperature is made. The physical property values used in the validation studies are given in Appendix A.4.

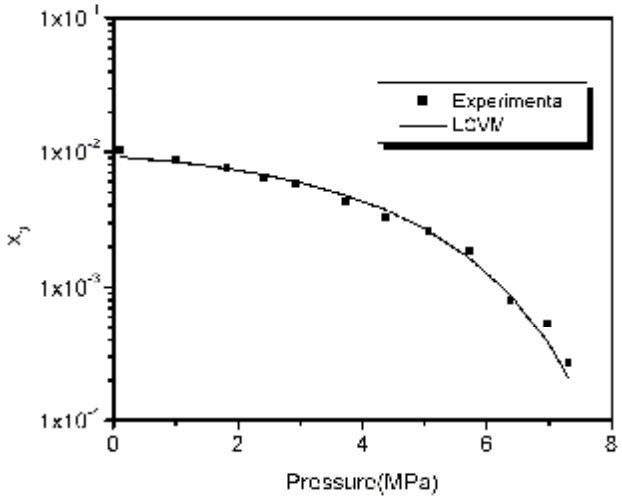

Figure 2-7. Prediction for expanded liquid phase mole fraction of cholesterol with respect to pressure at 318.15 K in CO_2 (1) - acetone (2) - cholesterol (3) system using PR -LCVM model. Adjusted cholesterol T_c is 1189.16 K.

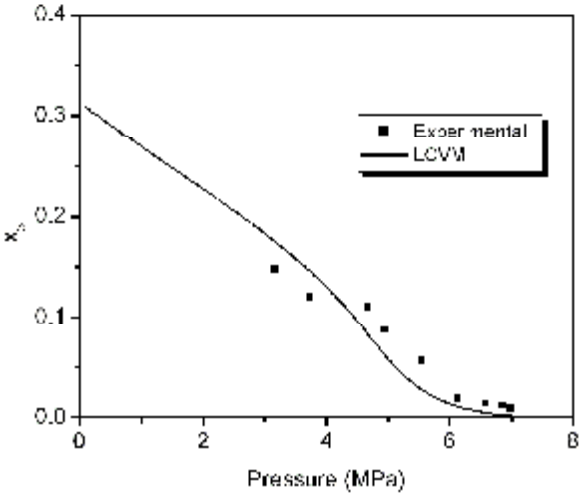

Figure 2-8. Prediction for expanded liquid phase mole fraction of tetradecanoic acid with respect to pressure at 318.15 K in CO_2 (1) - ethyl acetate (2) - tetradecanoic acid (3) system using PR - LCVM model. Adjusted tetradecanoic acid T_c is 902.7 K.

The critical properties of complex solids or natural compounds often cannot be measured due to the fact that they decompose before reaching critical conditions, and therefore values for these compounds are usually predicted using group contribution techniques. These techniques are usually used to estimate the normal boiling point of the solid first to calculate the critical point. Different estimation methods can yield quite different values [25]. Due to the uncertainty in critical point values, the adjustment made on the solute critical temperature in order to get a good confirmation with the literature data is reasonable. The adjustments made on the other critical constants (critical pressure and acentric factor) were not as significant as the critical temperature.

The sensitivity of the model to the solute critical temperature is also observed in our system of interest involving sclareol. Figure 2-9 presents the ternary phase diagrams generated with two different sclareol critical temperature values. The summary of sclareol boiling point and critical temperature values obtained from several group contribution methods is presented in Appendix A.5.

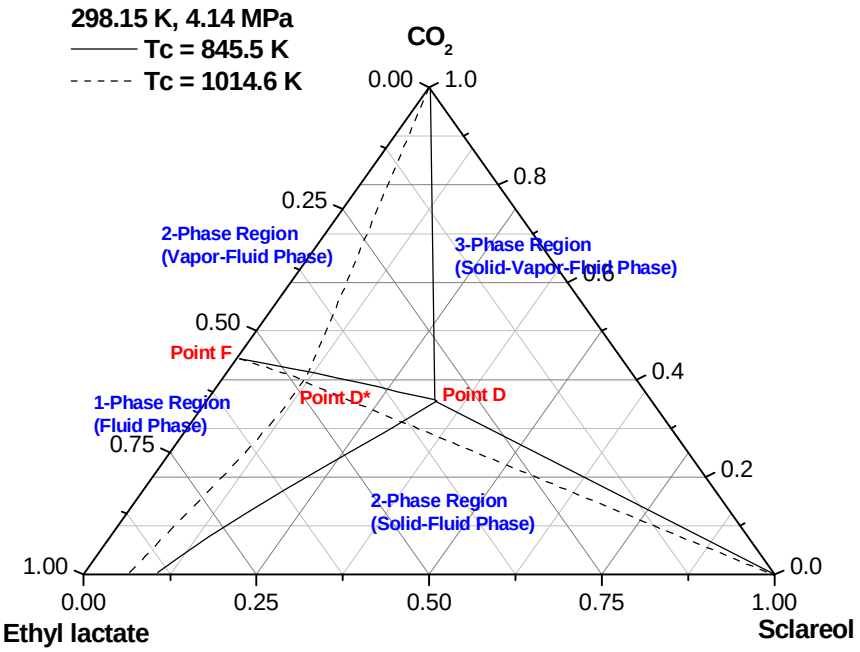

Figure 2-9. Ternary phase diagrams of sclareol-ethyl lactate-CO_2 at at 298.15 K and 4.14 MPa calculated from PR-LCVM using different sclareol critical temperature values.

Figure 2-9 illustrates that the calculated phase behavior is greatly affected by the change in sclareol critical temperature. When the critical temperature is increased from 845.5 K to 1014.6 K, the solubility of sclareol in the fluid phase (point D) is notably decreased. This results in a shrinking of the 2-phase (vapor-fluid) and 1-phase (fluid) regions. The fact that the model is very sensitive to the solute critical temperature makes the model incapable of predicting the solubility of solute with undefined critical properties in high-pressure systems. Experimental data at given temperatures and pressures is necessary for accurate solubility prediction at other conditions.

The following figures describe the effect of pressure and temperature on the sclareol solubility in the mixture of ethyl lactate and CO_2.

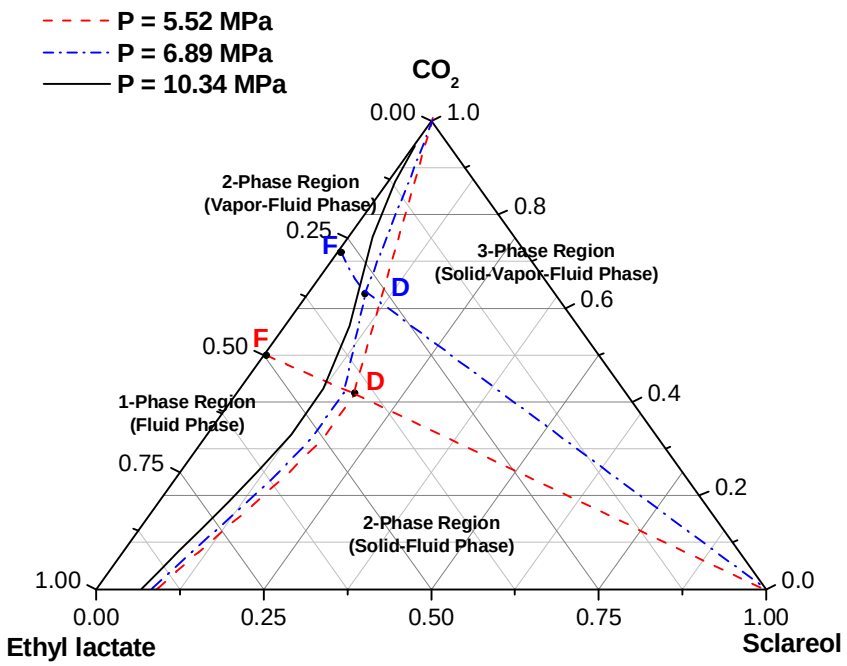

Figure 2-10. Computed ternary phase diagrams of sclareol-ethyl lactate-CO_2 at 308.15 K and various pressures (5.52, 6.89, and 10.34 MPa) using PR-LCVM. Tc of sclareol used in the calculation is 1014.6 K.

For pressures from 5.52 to 6.89 MPa, the sclareol-D line indicates the transition from a 2-phase (solid-fluid) to a 3-phase (solid-vapor-fluid) region, assuming that the solid phase consists of only sclareol. The CO_2-D line indicates the transition from a 3-phase (fluid-solid-vapor) to a 2-phase (fluid-vapor) region by assuming that sclareol solubility in the CO_2-rich phase is negligible. As pressure increases from 5.52 to 6.89 MPa, point F and the F-D line move towards the CO_2 rich corner. This also means that more CO_2 is dissolved in the fluid phase at varied sclareol concentrations and causes the 3-phase and 2-phase (vapor-fluid) regions to shrink. As pressure is further increased to 10.34 MPa, these regions disappear. In this case, CO_2 and ethyl lactate form a one-phase region. If the sclareol solubility in the fluid phase or the CO_2-ethyl lactate mixture (point D) is plotted as a function of pressure, as

illustrated in Figure 2-11, it is clearly observed that sclareol solubility slightly increases with pressure up to about 5 MPa at 308.15 K and then gradually decreases.

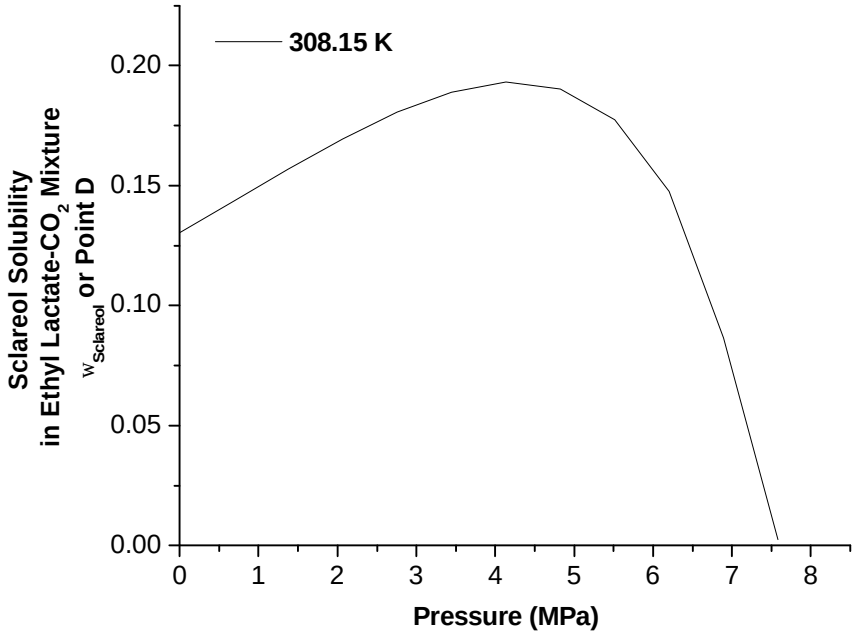

Figure 2-11. Calculated sclareol solubility in ethyl lactate-CO_2 mixture as a function of pressure using PR-LCVM. Tc of sclareol used in the calculation is 1014.6 K.

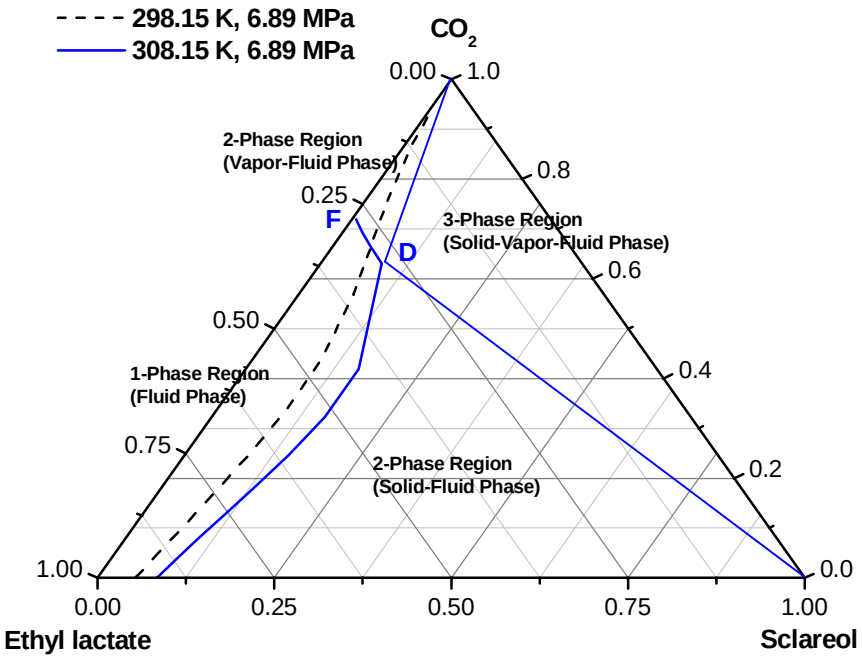

Figure 2-12. Computed ternary phase diagrams of sclareol-ethyl lactate-CO_2 at 6.89 MPa and 298.15, 308.15 K using PR-LCVM. Tc of sclareol used in the calculation is 1014.6 K.

As shown in Figure 2-12, the sclareol solubility in the fluid phase increases with temperature, and this moves the solubility value towards the sclareol-rich corner. The plot of point D as a function of pressure shown in Figure 2-13 also confirms the increase in sclareol solubility with temperature. In addition, as the temperature increases from 298.15 to 308.15 K and the pressure is fixed at 6.89 MPa, the two-phase region (vapor-fluid) and the three-phase region (solid-vapor fluid) appear. The phase separation is a result of a decrease in CO_2 solubility in the fluid phase. This phenomenon can also be observed from the vapor liquid equilibrium of the ethyl lactate-CO_2 system in Figure 2-1.

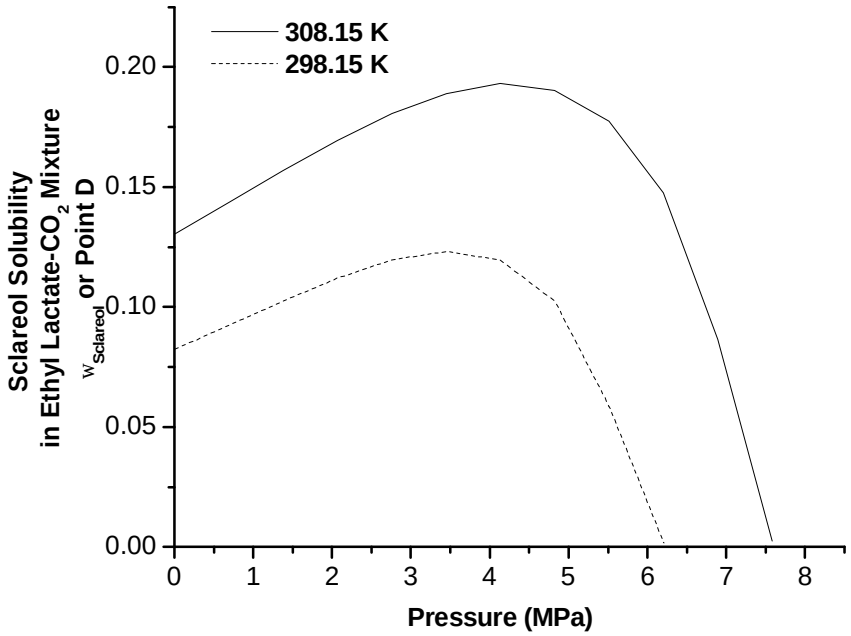

Figure 2-13. Calculated sclareol solubility in ethyl lactate-CO_2 mixture as a function of pressure and temperature using PR-LCVM. Tc of sclareol used in the calculation is 1014.6 K.

2.3.4. Cybotactic Effect

The phase diagrams developed here indicated that the solubility of sclareol in ethyl lactate was enhanced as CO_2 was added at low concentrations up to about 35-45 % (w/w). Addition of CO_2 beyond this concentration resulted in a decrease in sclareol solubility. This phenomenon of enhancement of solubility is related to the increase in mixture density with addition of CO_2 up to a certain concentration. This is called the cybotactic effect, which was also observed in some other applications of the GAS process [26, 27].

Studies by Sala et al. [28, 29] suggest that the nature of the organic solvent and CO_2 mixture has a strong influence on the solute solubility. When investigating the solubility of acetaminophen in CO_2-ethanol and CO_2-acetone mixtures, they found that the increase in the

CO_2 mole fraction caused a more pronounced solubility decrease for acetaminophen in CO_2-acetone than in CO_2-ethanol mixtures. As explained from the IR spectroscopic data, this occurrence is due to the fact that the dipole-dipole interactions between the carbonyl group of acetaminophen and acetone is more sensitive towards CO_2 solvent content changes than the hydrogen bonding type interactions between the carbonyl group of acetaminophen and ethanol.

Another study by Sala et al. [30] suggests that solubility enhancements observed in binary systems involving CO_2 and polar solvents with respect to pure CO_2 were attributed to local density augmentation and local composition enhancements of the polar solvent around the dissolved solute molecules. In the ternary hexamethylenetetramine/ethanol/CO_2 system the IR vibration bands signals indicate the presence of two solvating shells surrounding the hexamethylenetetramine molecules. The first solvating shell is populated by ethanol molecules interacting specifically with the solute molecules, while the second solvating shell is a region of exchange between ethanol and CO_2 molecules that is observed with an increase in CO_2 content. The cooperation between the hydrogen bonding interactions of hexamethylenetetramine-ethanol and Lewis acid-base type interactions of ethanol-CO_2 explain at the molecular level the synergistic enhancement of hexamethylenetetramine in CO_2-ethanol mixture. This means that introduction of CO_2 into a mixture of hexamethylenetetramine in ethanol provides an enthalpy contribution that favors significant solubility enhancement instead of producing a perturbation on the solute cybotactic region.

These studies help explain the cybotactic phenomenon observed in the sclareol-ethyl lactate-CO_2 mixture. In the cybotactic region, CO_2 molecules likely do not interact directly

with sclareol, but form Lewis acid-base interactions with ethyl lactate molecules. Ethyl lactate molecules can form strong hydrogen bonds to the hydroxyl group of sclareol, leading to a stronger Lewis acid-base interaction with CO_2 molecules. The cooperativity between hydrogen bonding and Lewis acid-base interactions can result in the initial enhancement of sclareol solubility in CO_2-ethyl lactate mixture.

2.4. Conclusions

In this chapter, we discuss about the ability of the PR-LCVM model to predict the phase behavior of several systems at high pressures. It is shown that the model correctly captures the experimental VLE of two-component systems involving CO_2, esters, and alcohols. For systems involving a solute, the model shows a strong dependency of a solute solubility on its critical temperature. This fact makes the model incapable of predicting the solubility behavior of a solute with undefined critical properties in high-pressure systems. This chapter also presents the effect of varying the temperature, pressure, and sclareol critical temperature on the sclareol solubility in CO_2-ethyl lactate mixture. We also observed in this study a cybotactic region, i.e. an enhancement of sclareol solubility at low pressure or low CO_2 concentration in the solvent mixture. In the next chapter, we present the experimental method to develop the ternary phase diagrams of the sclareol-ethyl lactate-CO_2 system at various pressures. The ability of the PR-LCVM model to accurately capture this ternary phase behavior is also discussed.

2.5. References

1. Boukouvalas, C., et al., *Prediction of vapor-liquid equilibrium with the LCVM model: A linear combination of the Vidal and Michelsen mixing rules coupled with the original UNIFAC and the t-mPR equation of state.* Fluid Phase Equilibria, 1994. **92**: p. 75-106.

2. Tiegs, D., et al., *Vapor-liquid equilibria by unifac group contribution. 4. Revision and extension.* Industrial & Engineering Chemistry Research, 1987. **26**(1): p. 159-161.

3. Hansen, H., et al., *Vapor-liquid equilibria by unifac group contribution. 5. Revision and extension.* Industrial & Engineering Chemistry Research, 1991. **30**(10): p. 2352-2355.

4. Yakoumis, I., et al., *Application of the LCVM model to systems containing organic compounds and supercritical carbon dioxide.* The Journal of Supercritical Fluids, 1996. **9**(2): p. 88-98.

5. Boukouvalas, C., et al., *Prediction of vapor-liquid equilibria with the LCVM model: Systems containing light gases with medium and high molecular weight compounds.* Ind. Eng. Chem. Res, 1997. **36**(12): p. 5454-5460.

6. Zhong, C. and H. Masuoka, *An EOS/G^E type mixing rule for perturbed hard-sphere equation of state and its application to the calculation of solid solubility in supercritical carbon dioxide.* Fluid Phase Equilibria, 1997. **141**(1-2): p. 13-23.

7. Spiliotis, N., K. Magoulas, and D. Tassios, *Prediction of the solubility of aromatic hydrocarbons in supercritical CO_2 with EOS/G^E models.* Fluid Phase Equilibria, 1994. **102**(2): p. 121-141.

8. Coutsikos, P., K. Magoulas, and G. Kontogeorgis, *Prediction of solid–gas equilibria with the Peng–Robinson equation of state.* The Journal of Supercritical Fluids, 2003. **25**(3): p. 197-212.

9. Gerszt, R., F. Pessoa, and M. Mendes, *Phase behaviour of sterols and vitamins in supercritical CO_2.* Brazilian Journal of Chemical Engineering, 2000. **17**: p. 261-270.

10. Stanley, I., *Chemical and engineering thermodynamics*: Wiley.

11. Prausnitz, J., *Molecular thermodynamics of fluid-phase equilibria.* 1969: Prentice Hall.

12. Orbey, H. and S. Sandler, *Modeling vapor-liquid equilibria*. 1998: Cambridge University Press New York.

13. Huron, M. and J. Vidal, *New mixing rules in simple equations of state for representing vapor-liquid equilibria of strongly nonideal mixtures.* Fluid Phase Equilibria, 1979. **3**(4): p. 255-271.

14. Michelsen, M., *A modified Huron-Vidal mixing rule for cubic equations of state.* Fluid Phase Equilibria, 1990. **60**: p. 213-219.

15. Joback, K. and R. Reid, *Estimation of pure-component properties from group-contributions.* Chemical Engineering Communications, 1987. **57**(1): p. 233-243.

16. Chylinski, K. and J. Gregorowicz, *Solubilities of (1-hexanol, or 1, 2-hexanediol, or 2-hydroxypropanoic acid ethyl ester, or 2-hydroxyhexanoic acid ethyl ester) in supercritical CO_2.* The Journal of Chemical Thermodynamics, 1998. **30**(9): p. 1131-1140.

17. Voutsas, E., et al., *The performance of EOS/G^E models in the prediction of vapor-liquid equilibria in asymmetric systems.* Fluid Phase Equilibria, 1996. **116**(1-2): p. 480-487.

18. Larsen, B., P. Rasmussen, and A. Fredenslund, *A modified UNIFAC group-contribution model for prediction of phase equilibria and heats of mixing.* Industrial & Engineering Chemistry Research, 1987. **26**(11): p. 2274-2286.

19. Niesen, V.G. and J.C. Rainwater, *Critical locus, (vapor + liquid) equilibria, and coexisting densities of (carbon-dioxide + propane) at temperatures from 311 K to 361 K.* Journal of Chemical Thermodynamics, 1990. **22**(8): p. 777-795.

20. Gonzalez, E. and J. Ortega, *Densities and isobaric vapor-liquid equilibria of butyl esters (methanoate to butanoate) with ethanol at 101.32 KPa.* Journal of Chemical and Engineering Data, 1995. **40**(6): p. 1178-1183.

21. Tian, Y., et al., *Vapor–liquid equilibria of the carbon dioxide + ethyl propanoate and carbon dioxide + ethyl acetate systems at pressure from 2.96 MPa to 11.79 MPa and temperature from 313 K to 393 K.* J. Chem. Eng. Data, 2004. **49**(6): p. 1554-1559.

22. Hwu, W., et al., *Vapor-liquid equilibrium of carbon dioxide with ethyl caproate, ethyl caprylate and ethyl caprate at elevated pressures.* The Journal of Supercritical Fluids, 2004. **28**(1): p. 1-9.

23. Liu, Z., et al., *Solubility of organic acids in ethyl acetate expanded with CO_2.* Fluid Phase Equilibria, 2000. **167**(1): p. 123-130.

24. Liu, Z., et al., S*tudy on the phase behavior of cholesterol–acetone– CO_2 system and recrystallization of cholesterol by antisolvent CO_2.* The Journal of Supercritical Fluids, 2002. **24**(1): p. 1-6.

25. Macnaughton, S., et al., *Solubility of anti-inflammatory drugs in supercritical carbon dioxide.* J. Chem. Eng. Data, 1996. **41**: p. 1083–1086.

26. Shariati, A. and C. Peters, *Measurements and modeling of the phase behavior of ternary systems of interest for the GAS process: I. The system carbon dioxide + 1-propanol + salicylic acid.* The Journal of Supercritical Fluids, 2002. **23**(3): p. 195-208.

27. De La Fuente, J.C., S.B. Bottini, and C.J. Peters, *Measurement of the phase behavior of the ternary system carbon dioxide plus acetone plus phenanthrene.* Journal of Chemical and Engineering Data, 2006. **51**(1): p. 2-6.

28. Santiago Sala, T.T., Nora Ventosa, Yann Danten, Marcel Besnard, Jaume Veciana, *Molecular insight, through IR spectroscopy, on solvating phenomena occurring in CO_2-expanded solutions.* ChemPhysChem, 2004. **5**(2): p. 243-245.

29. Sala, S., et al., *Solute-solvent interactions governing preferential solvation phenomena of acetaminophen in CO_2-expanded organic solutions: A spectroscopic and theoretical study.* The Journal of Supercritical Fluids, 2006. **38**(3): p. 295-305.

30. Santiago Sala, N.V., Thierry Tassaing, Mary Cano, Yann Danten, Marcel Besnard, Jaume Veciana,, *Synergistic enhancement of the solubility of hexamethylenetetramine in subcritical CO_2-ethanol mixtures studied by infrared spectroscopy.* ChemPhysChem, 2005. **6**(4): p. 587-590.

3. Experimental Ternary Phase Behavior of the Sclareol-Ethyl Lactate-CO_2 System

This chapter was published as a part of an article in Journal of Supercritical Fluids 45 (2008), page 146-155.

In designing an extraction process for sclareol, it is crucial to first study the behavior of sclareol in the solvents of interest, i.e. ethyl lactate and mixtures of CO_2 and ethyl lactate. This chapter presents the solubility of sclareol in ethyl lactate at various temperatures. It also presents the experimental procedure of the static synthetic method for estimating the ternary phase behavior of the sclareol-ethyl lactate-CO_2 system at 308.15 K and various pressures. The ability of the PR-LCVM model to capture the behavior of the binary CO_2-ethyl lactate and ternary sclareol-ethyl lactate-CO_2 system is also discussed.

3.1. Experimental Procedure

3.1.1. Materials and Analysis

Sclareol (CAS number 515-03-7; > 95 % purity) and ethyl lactate (CAS number 687-47-8; 98 % purity) were supplied by Sigma-Aldrich. Carbon dioxide (CAS number 124-38-9; > 99.99 % purity) was supplied by National Welders. These chemicals were used without further purification. The concentration of sclareol in ethyl lactate was determined by gas chromatography (GC) using heptadecanol (CAS number 1454-85-9; 98 % purity) from Sigma-Aldrich as an internal standard. Gas chromatographic analyses [1] were performed using an HP 6890N with conditions of analysis as follows: Column: 30 meter DB-5 (methyl-phenyl bonded phase, J & W Scientific) with a 0.53 mm I.D. and a 0.25 μm phase thickness;

Carrier gas: UHP helium (National Welders) at a linear gas velocity of approximately 28 cm/sec; Injector temperature: 275 ^{o}C; FID detector temperature: 310 ^{o}C; Temperature program: 160 to 310 ^{o}C at 4 degrees/minute. Data was collected using the Perkin-Elmer Total Chrom 6.2 chromatographic analysis system.

3.1.2. Experimental Techniques

Solubility of sclareol in ethyl lactate

The solubility of sclareol in ethyl lactate was determined at a temperature range of 298.15 to 318.15 K. An excess amount of sclareol was added to a 20 mL vial containing a known amount of solvent, which was kept in an oven (VWR Scientific, model 1330 FM) maintained at a fixed temperature. The solution was stirred to allow the system to rapidly reach equilibrium. After a day, the solution was quickly transferred into a 20 mL vial through a syringeless filter (Whatman Autovial, Teflon® membrane with 0.45 μm pore diameter) to trap any undissolved sclareol. The concentration of the remaining solution was then determined by gas chromatography and the solubility value for sclareol under the conditions of the experiment calculated.

Sclareol-ethyl lactate-CO_2 phase behavior

A static synthetic GAS precipitation experiment was used to examine the phase behavior of the sclareol-ethyl lactate-CO_2 system at 308.15 K as a function of pressure (1.38-13.79 MPa). A schematic diagram of the apparatus is shown in Figure 3-1. The equipment consists of a 24.1 $\pm$ 0.1 mL high-pressure view cell, fabricated from stainless steel (316 SS) and equipped with two sapphire windows (pressure range: 0-69 MPa), a stirring plate (Fisher

Scientific) underneath the view cell, a temperature controller (Barnant Company, R/S) with heating tapes (Omega Inc.) to regulate the system temperature with a precision of $\pm$ 0.5 K, a syringe pump (ISCO, model 500D) to control the system pressure set point to within $\pm$ 0.1 MPa, a heating bath/circulator (Neslab, model ex-111) to maintain the syringe pump at a constant temperature, a pressure transducer (Omega Engineering Inc., model PX302, pressure range: 0-69 MPa), a portable lamp as a light source located at the back of the view cell (Underwriters Laboratories, Inc.), and a video camera to capture the image of the view cell (Pulnix, model TM-7CN). The apparatus is connected with 1/16" OD stainless steel tubing (HIP), with two-way valves (V1 and V3, HIP) and one three-way valve (V2, HIP).

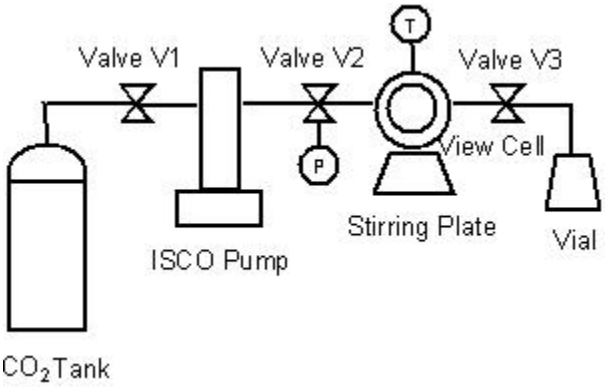

Figure 3-1. Static synthetic phase observation equipment. A light source at the back of the view cell and a video camera were used to capture the image of the view cell.

A solution of sclareol in ethyl lactate with known concentration was prepared. The prepared solution was transferred into a beaker and weighed using an analytical balance (Ohaus Explorer Pro, model EP214DC). A given amount of solution was withdrawn using a pre-heated syringe (Hamilton, model 1005TLL) and placed into the view cell. The syringe was pre-heated to prevent any precipitation of sclareol during the transfer. The beaker was

then re-weighed to calculate the mass of solution transferred into the cell. The solution in the cell was heated to 308.15 K using the temperature controller. Once the temperature stabilized, CO_2 was delivered into the cell using a syringe pump through 3-way valve V2 until the desired pressure was achieved. The mixture was then stirred for 45-60 minutes using a 0.2 mL magnetic stir bar (Fisher Scientific). The temperature and pressure were recorded every 15 minutes. The formation of phases was also observed every 15 minutes with the aid of soft white light source at the back of the cell. A laser pointer was used to assist in detecting the clarity of the solution.

The camera was used to capture the image of the view cell and Scion image software (Scion Corporation) was used to calculate the liquid level in the view cell [2]. Subsequently, the fluid phase volume after addition of CO_2 could be determined from the calibration curve of volume as a function of liquid level, as shown in Figure 3. The experiments were repeated for different solution concentrations, volumes, and pressures. Figure 3 compares the average experimental values of liquid levels and volumes from six trials with the volumes calculated according to Equation (3.1). This equation was derived from the dimensions of the high-pressure cell, and the detailed derivation of the equation is given in Appendix B.1.

$$V = 2L\left[\frac{(x-r)\sqrt{r^2-(x-r)^2}}{2}+\frac{r^2}{2}\sin^{-1}\left(\frac{(x-r)}{r}\right)+\frac{p.r^2}{4}\right] \tag{3.1}$$

In this expression: L = cell length (3.427$\pm$0.003 cm), r = cell radius (1.496$\pm$0.003 cm), and x = liquid level inside the cell.

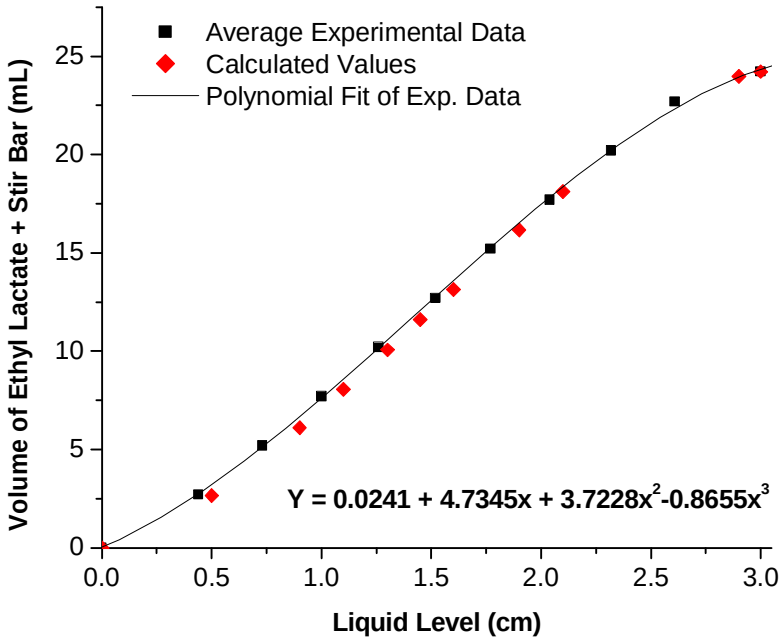

Figure 3-2. Correlation between ethyl lactate volume and liquid level, obtained from experiments and calculation.

Using the static synthetic method, the total mass of CO_2 introduced into the cell could be monitored; however, the fraction of CO_2 that was dissolved in the ethyl lactate-rich phase could not be directly measured. By knowing the ethyl lactate-rich phase volume after addition of CO_2, we calculated the CO_2-rich phase volume and subsequently the mass of CO_2 in the light phase, assuming that the phase consists of pure CO_2. The mass of CO_2 dissolved in ethyl lactate-rich phase was then calculated by subtracting the mass of CO_2 in the light phase from the total mass of CO_2 charged into the cell.

With the assumptions that sclareol solubility in CO_2 was negligible, the solid phase consisted only of pure sclareol, and the CO_2-rich phase was considered to be pure CO_2, the

solubility boundary of sclareol in the mixture of CO_2 and ethyl lactate at a given temperature and pressure could be estimated by observing the phases that formed during the experiments. The assumption that CO_2-rich phase consisted of pure CO_2 was confirmed by the low solubility of ethyl lactate in CO_2-rich phase predicted from PR-LCVM. The solubility of ethyl lactate in CO_2-rich phase in terms of weight fraction at 308.15 K and P = 1.38 – 6.89 MPa was calculated to be in the order of 10^{-4} to 10^{-3}, as indicated in Figure 2-1. Chylinski and Gregorowicz [3] also reported that the ethyl lactate solubility in the CO_2-rich phase in terms of weight fraction at T = 311-323 K and P = 1-8 MPa was in the order of 10^{-3}.

Moreover, the solubility of sclareol in CO_2 at 308.15 K and 5.52 to 10.34 MPa were determined to be fairly small, in the order of 10^{-6} to 10^{-4}. The experiments were performed using the setup in Figure 3-1. An amount of sclareol (1-2 g) was loaded into the view cell. CO_2 was then delivered into the cell using a syringe pump through a 3-way valve V2 until achieving the desired pressure. Sclareol and CO_2 were mixed in the cell at constant temperature and pressure for 3 days. At low sampling flow rate (0.05-0.1 mL/min) and constant temperature and pressure, the mixture of CO_2 and sclareol was sampled into a vial containing ethyl lactate. The amount of sclareol sampled was determined from GC analysis of the ethyl lactate solution whereas the amount of CO_2 sampled was determined from the difference in syringe volume before and after sampling. By knowing the CO_2 density at the experimental condition, the solubility of sclareol could then be calculated. The assumption that sclareol solubility in CO_2 was neglected contributed to an average percentage error of < 1 % in the 3-component phase equilibrium calculation. The plot of sclareol solubility in CO_2

at various pressures, obtained from experiment and predicted from PR-LCVM, is presented in Appendix B.2.

3.2. Experimental Ternary Phase Diagrams

Solubility of sclareol in ethyl lactate

The plot of sclareol solubility in ethyl lactate at various temperatures shown in Figure 3-3 illustrates the dependence of the solubility value on the temperature. As also the case with other solute-solvent pair, the solute solubility in a liquid generally increases with temperature [4].

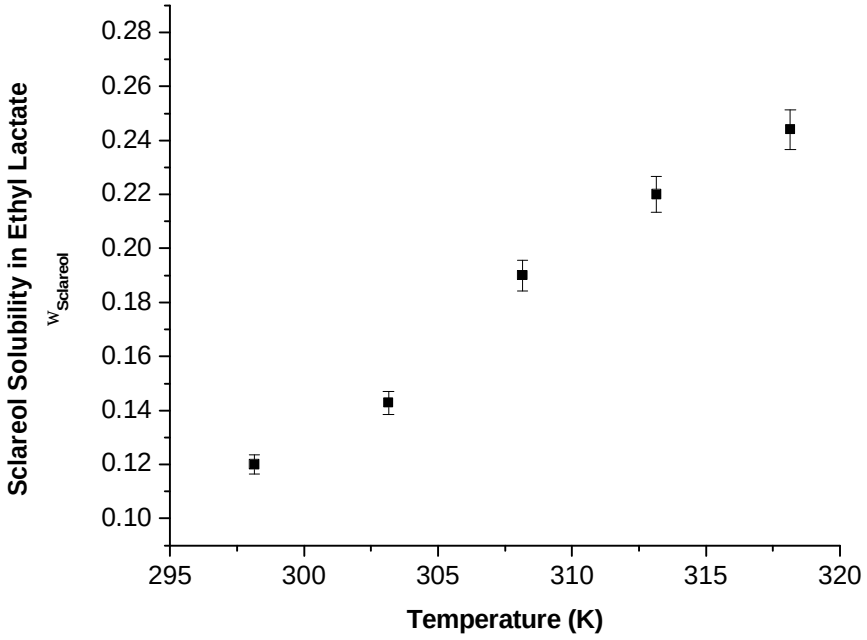

Figure 3-3. Solubility of sclareol in ethyl lactate at temperatures ranging from 298.15 to 318.15 K.

Sclareol-ethyl lactate-CO_2 phase behavior

The experimental solubility behavior of sclareol in ethyl lactate-CO_2 mixture from the phase observation experiments at various pressures and a temperature of 308.15 K were described in terms of weight fraction in Figure 3-4 to 3-11. In these figures, squares represent the one-phase region (fluid), circles represent the two-phase region (solid-fluid), dark/red triangles represent the two-phase region (vapor-fluid), and orange/light-colored triangles represent the three-phase region (solid-vapor-fluid). For experimental pressures of 1.38 to 6.89 MPa (Figures 3-4 to 3-9), Point D represents the point where all the phases (the fluid phase, solid-fluid phase, vapor-fluid phase, and solid-vapor-fluid phase) co-exist whereas point F describes the equilibrium composition of CO_2-ethyl lactate in the ethyl lactate-rich phase when there is no sclareol present. Point F was not experimentally determined from the binary system of ethyl lactate and CO_2, but was estimated from the ternary phase diagrams.

The Gibbs Phase Rule dictates the number of phases that may be present at equilibrium. At a fixed temperature and pressure, two phases may exist over a range of compositions in equilibrium whereas three phases have unique compositions. A range of composition is possible when either temperature or pressure is specified. For pressures of 1.38 to 6.89 MPa (Figure 3-4 to 3-9), the sclareol-D line indicates the transition from a 2-phase (solid-fluid) to a 3-phase (solid-vapor-fluid) region, assuming that the solid phase consists of pure sclareol. The CO_2-D line indicates the transition from a 3-phase (solid-vapor-fluid) to a 2-phase (vapor-fluid) region by assuming that the sclareol solubility in the CO_2-rich phase was negligible. As pressure increases at a fixed temperature, more CO_2 is dissolved in the ethyl lactate-rich phase with the result that the boundary between the 2-phase (vapor-fluid) and

one-phase (fluid) region moves toward the CO_2-rich corner. As pressure increases further to 10.34 MPa (Figure 3-10), the 3-phase region and 2-phase (vapor-fluid) region shrink and disappear into a critical endpoint tie line. In other words, the CO_2 and ethyl lactate become completely miscible with each other at 308.15 K and 10.34 MPa, forming a one-phase region.

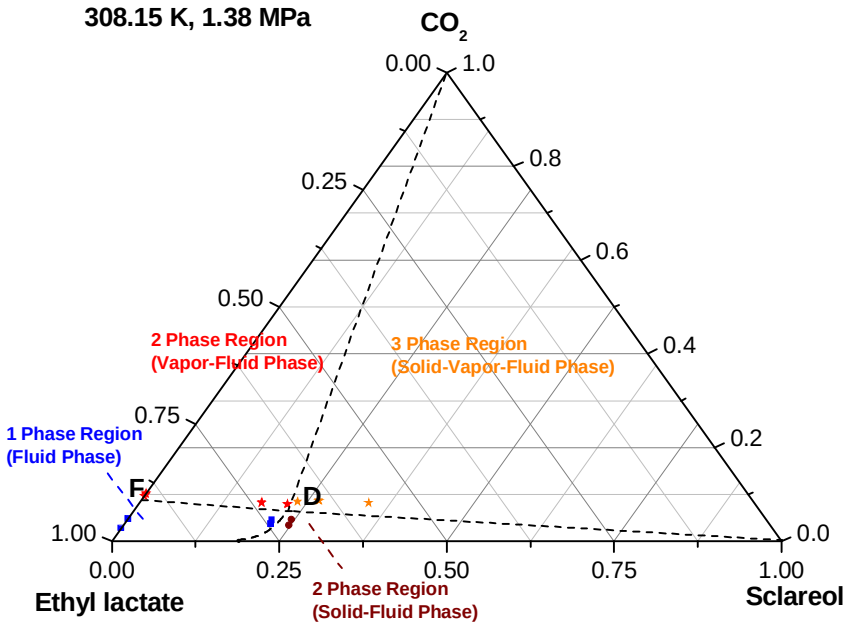

Figure 3-4. Experimental ternary-phase diagram at 308.15 K and 1.38 MPa obtained from static synthetic observations.

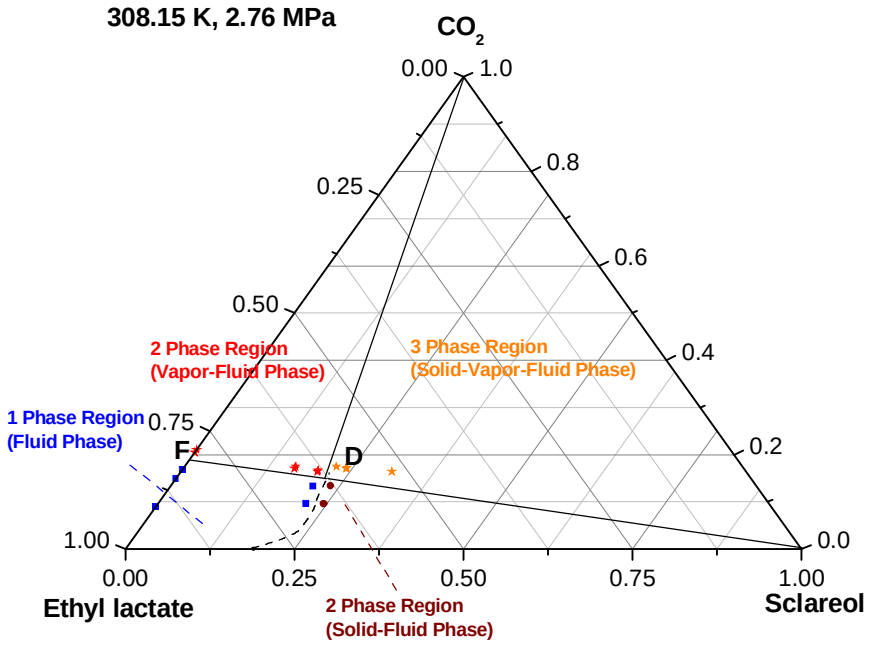

Figure 3-5. Experimental ternary-phase diagram at 308.15 K and 2.76 MPa obtained from static synthetic observations.

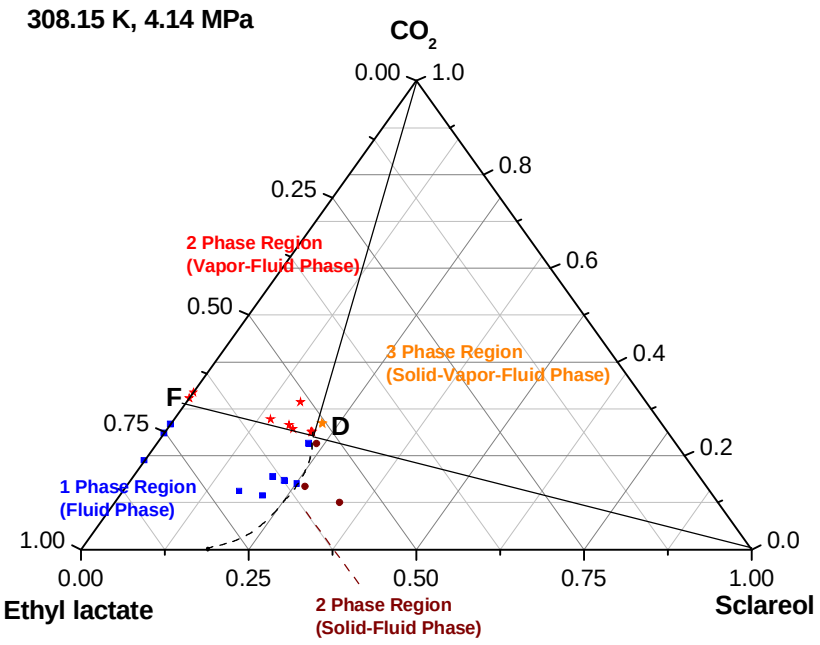

Figure 3-6. Experimental ternary-phase diagram at 308.15 K and 4.14 MPa obtained from static synthetic observations.

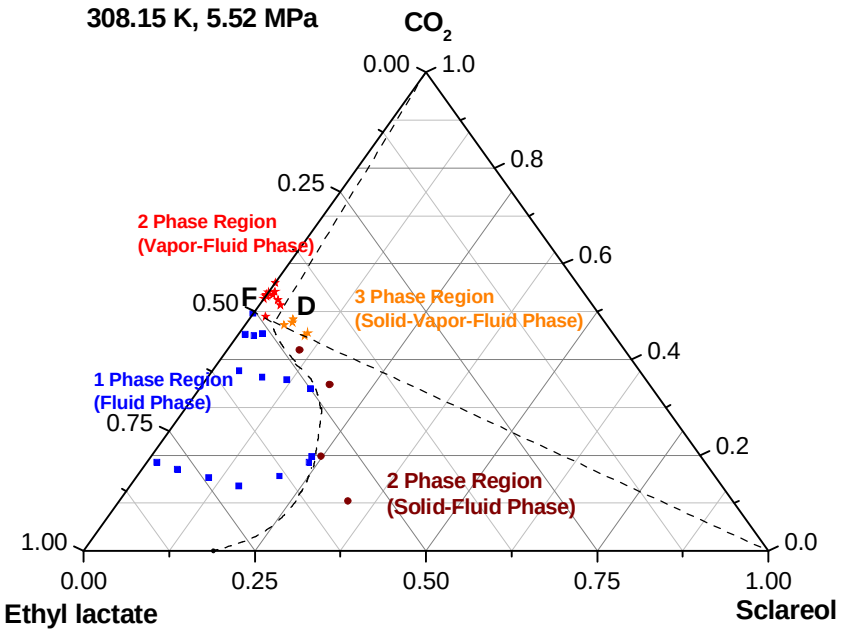

Figure 3-7. Experimental ternary-phase diagram at 308.15 K and 5.52 MPa obtained from static synthetic observations.

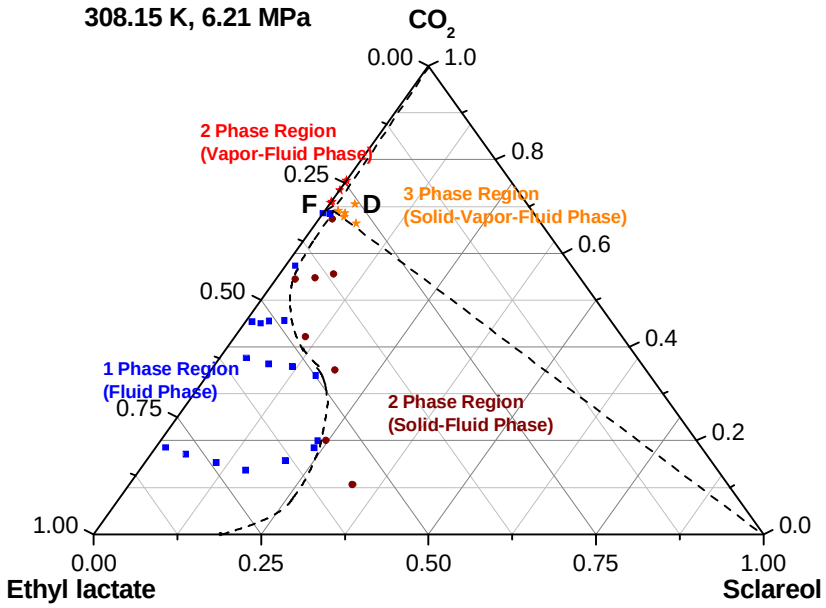

Figure 3-8. Experimental ternary-phase diagram at 308.15 K and 6.21 MPa obtained from static synthetic observations.

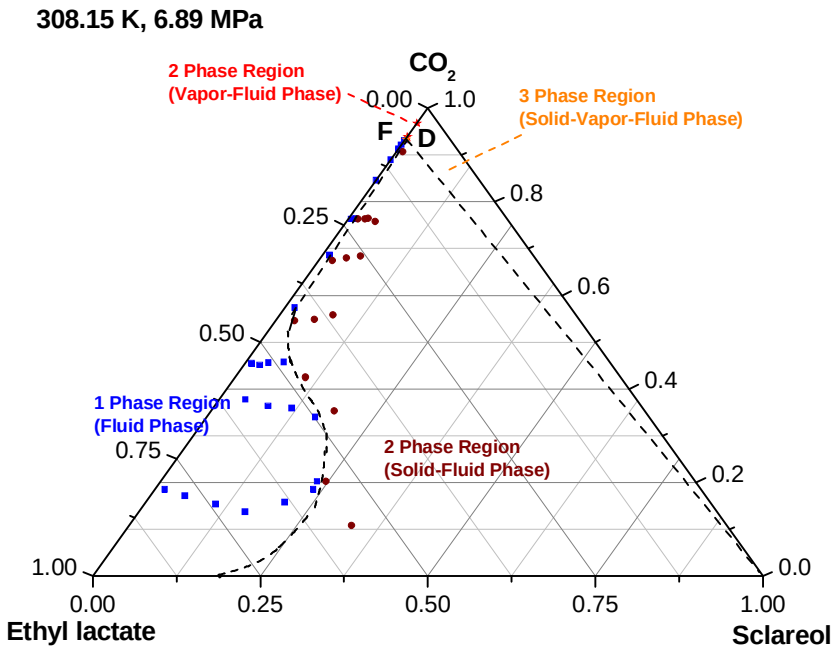

Figure 3-9. Experimental ternary-phase diagram at 308.15 K and 6.89 MPa obtained from static synthetic observations.

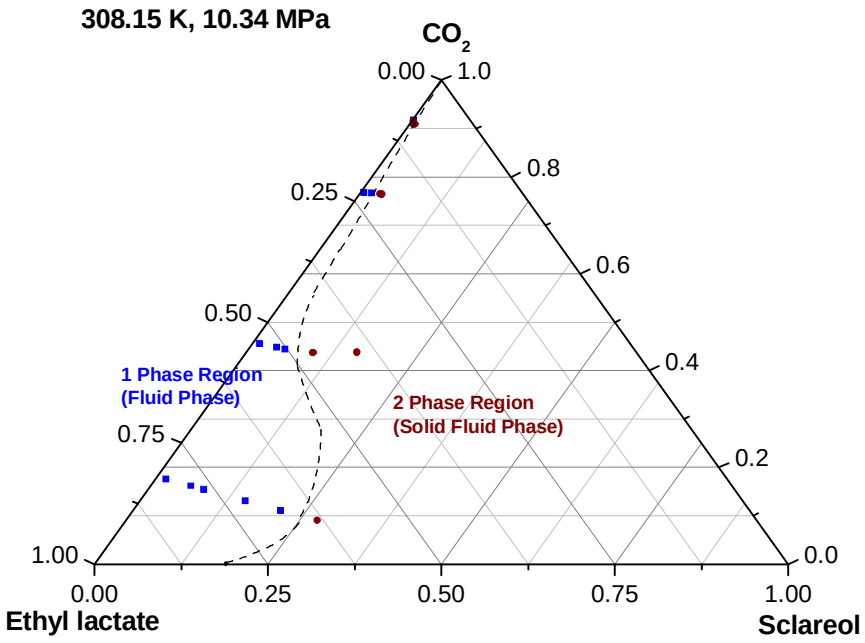

Figure 3-10. Experimental ternary-phase diagram at 308.15 K and 10.34 MPa obtained from static synthetic observations.

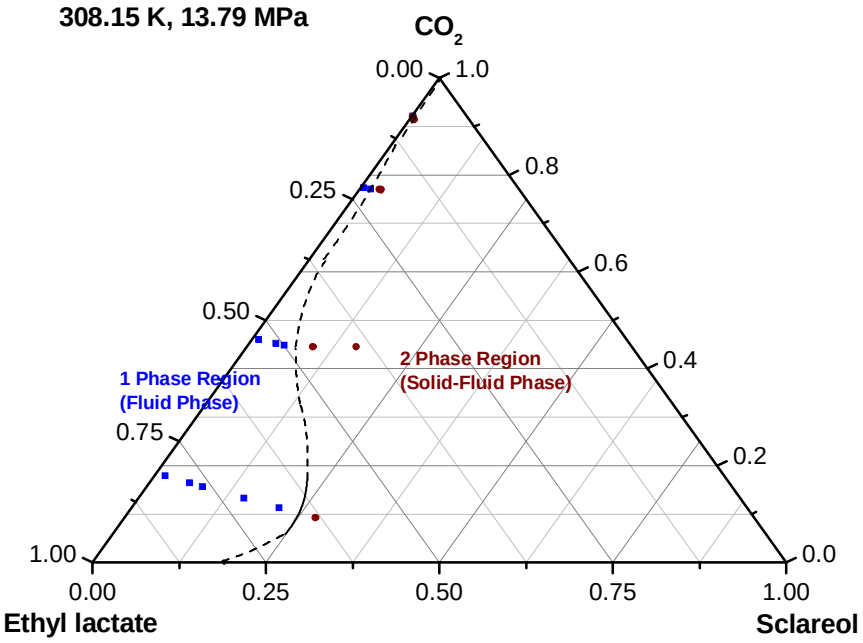

Figure 3-11. Experimental ternary-phase diagram at 308.15 K and 13.79 MPa obtained from static synthetic observations.

From these diagrams, it is also noted that the addition of CO_2 into the sclareol-ethyl lactate mixture up to about 20-30 % (w/w) results in an increase in sclareol solubility. Peters et al. observed a similar phenomenon in their studies of the phase behavior of the salicylic acid-propanol-CO_2 system [5] and the phenanthrene-acetone-CO_2 system [6]. They observed that at lower concentrations CO_2 had a co-solvency effect, while it acted as an anti-solvent at higher concentrations.

The sclareol solubility in the fluid phase (point D), i.e. the fluid phase in a 3-phases solid-vapor-fluid tie triangle, was plotted as a function of pressure in Figure 3-12. The solubility of sclareol in ethyl lactate at ambient pressure was determined experimentally as 19 $\pm$ 1 % (w/w) at 308.15 K. Figure 3-12 shows a slight increase in sclareol solubility as CO_2

is added (low pressure). A dramatic decrease in sclareol solubility is observed when pressure is increased from 4.14 to 6.89 MPa. This phenomenon of enhancement of solubility is related to the increase in mixture density with addition of CO_2 up to a certain concentration. This is called the cybotactic effect, which was also observed in some other applications of the GAS process [7, 8]. In the cybotactic region, CO_2 molecules likely do not interact directly with sclareol, but form Lewis acid-base interactions with ethyl lactate molecules. Ethyl lactate molecules can form strong hydrogen bonds to the hydroxyl group of sclareol, leading to a stronger Lewis acid-base interaction with CO_2 molecules. The cooperativity between hydrogen bonding and Lewis acid-base interactions results in the initial enhancement of sclareol solubility in CO_2-ethyl lactate mixture.

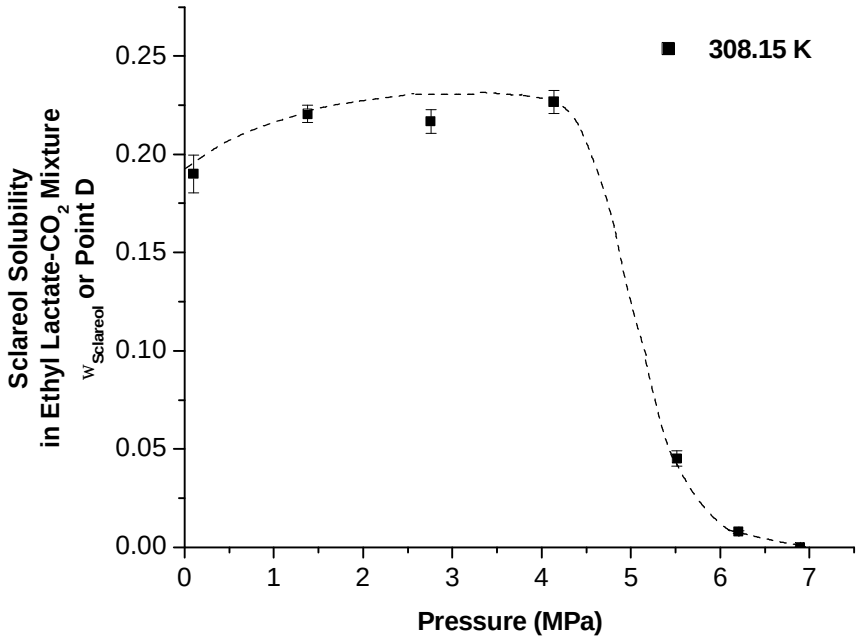

Figure 3-12. The solubility of sclareol in ethyl lactate-CO_2 mixture as a function of pressure.

3.3. Comparison between Experimental and Thermodynamic Equilibrium Data

The experimental composition of sclareol in the fluid phase (point D in the ternary phase diagram) as a function of pressure is compared with PR-LCVM data generated from two different values of sclareol critical temperature, shown in Figure 3-13. It is illustrated that PR-LCVM model does not capture the behavior of sclareol in the fluid phase well. As also explained in chapter 2, the model is very sensitive to the solute critical temperature. A decrease in Tc of < 4 % results in an increase solubility value of about 20 %.

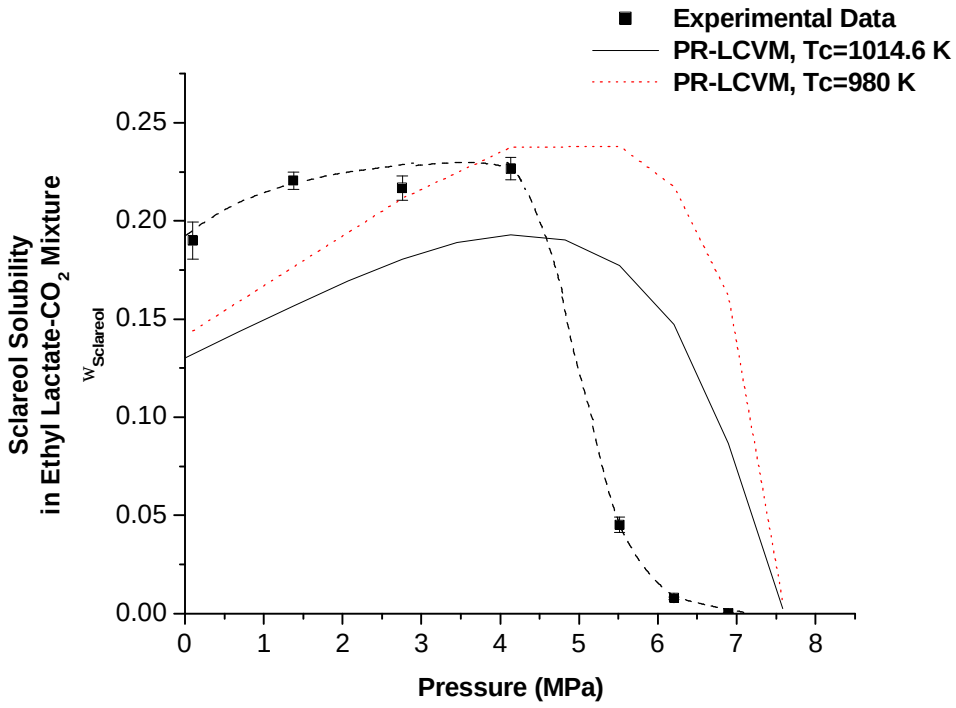

Figure 3-13. The solubility of sclareol in ethyl lactate-CO_2 mixture as a function of pressure obtained from the ternary phase diagrams (point D) and predicted from PR-LCVM.

Figure 3-14 compares the experimental ternary phase diagram with the one calculated from PR-LCVM at 308.15 K and 5.52 MPa. It is also shown here that the model fails to give a quantitative prediction for the ternary solid-fluid and the ternary vapor-fluid behavior of the sclareol-ethyl lactate-CO_2 system. Figure 3-15 shows the plot of the binary vapor-liquid equilibrium of the ethyl lactate-CO_2 system. The experimental data is obtained from the ternary phase diagrams, which is point F from the ethyl lactate-CO_2 edge. It is illustrated that the model captures the behavior of the binary system pretty well.

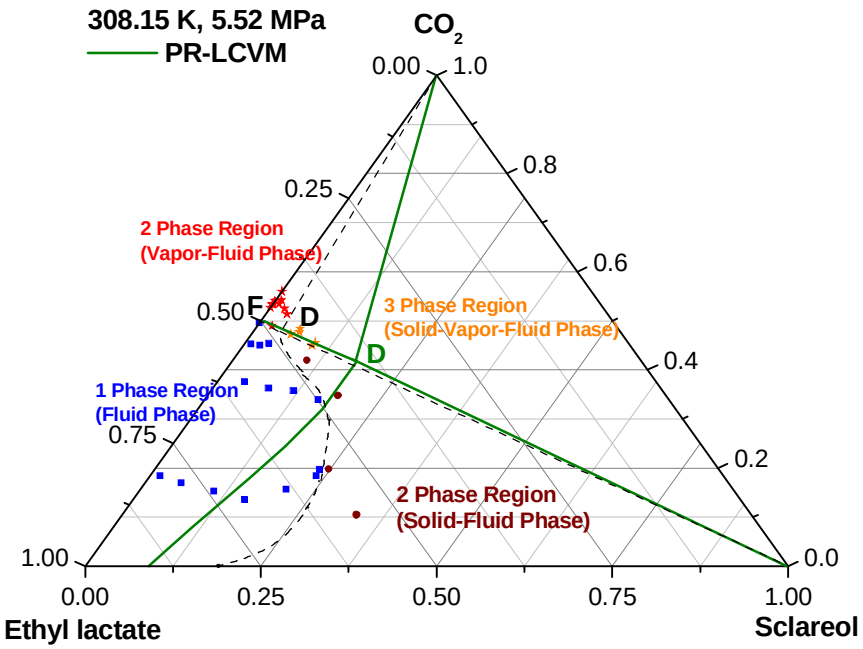

Figure 3-14. Ternary-phase diagrams at 308.15 K and 5.52 MPa obtained from static synthetic observations and predicted from PR-LCVM. Tc of sclareol used in the calculation is 1014.6 K.

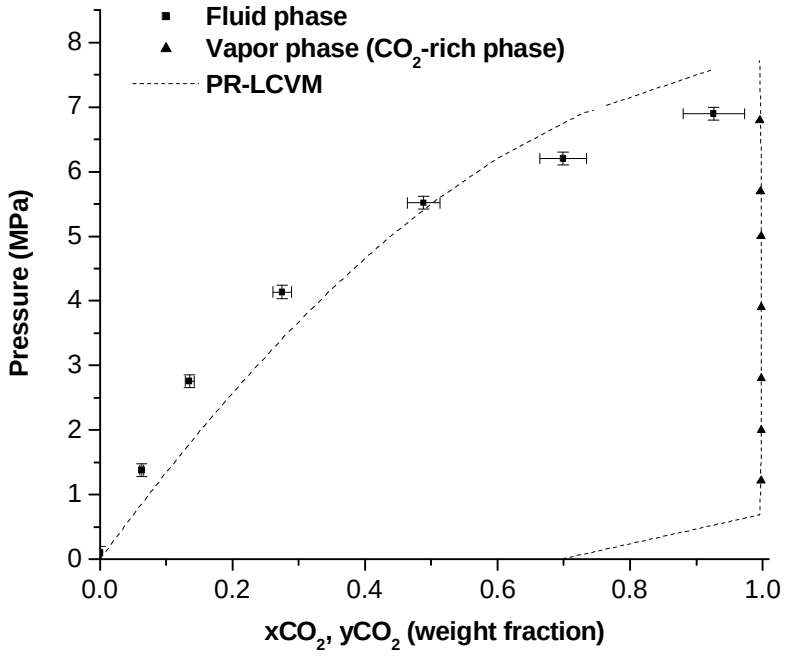

Figure 3-15. VLE of ethyl lactate-CO_2 system at 308.15 K. The solubility weight fraction of CO_2 in fluid phase (ethyl lactate-rich phase) is obtained from the solubility point (CO_2-ethyl lactate edge) in experimental ternary-phase diagram (point F) whereas that in CO_2-rich phase is obtained from literature at 311.15 K [3].

Mendes et al. [9] also observed that PR-LCVM could not represent the experimental solubility of α-tocopherol well, but it was in agreement with the vapor liquid equilibrium data for the binary CO_2-squalene system. The % error between the calculated and the experimental solubility data of the α-tocopherol-CO_2 system at 313.15-353.15 K was > 100 %. This might be due to the critical property calculation and sublimation pressure of α-tocopherol and the fact that its structure could not be well represented using the UNIFAC method. In addition, the model did not take into account a contribution to the activity coefficient due to hydrogen bonding interactions. They showed that the choice of a group contribution method was very important in obtaining good phase equilibrium results [9, 10].

For sclareol-ethyl lactate-CO_2 system, further study is necessary for understanding the inability of PR-LCVM to quantitatively predict the experimental ternary phase equilibrium.

3.4. Conclusions

In summary, the static synthetic approach is a reliable method to estimate the ternary phase behavior of the sclareol-ethyl lactate-CO_2 system. The generated phase diagrams could be used as a basis for choosing the proper operating pressure to obtain a high recovery of sclareol from the extraction process. Moreover, the phase diagrams show a cybotactic region of sclareol in CO_2-ethyl lactate mixture. CO_2 acted as a co-solvent to ethyl lactate at lower pressures and/or lower CO_2 concentrations and as an anti-solvent at higher pressures and/or higher CO_2 concentrations. In addition, the PR-LCVM model gives a reasonable quantitative prediction of CO_2 solubility in the fluid phase for the two-component system. This model is unsuccessful in giving a quantitative agreement with the experimental solubility data of the three-component system. In the next chapter, the extraction process of sclareol from Clary Sage plant materials using ethyl lactate followed by CO_2 antisolvent precipitation and using mixtures of ethyl lactate and CO_2 at various solvent compositions and pressures is discussed.

3.5. References

1. Finney, M., D. Danehower, and J. Burton, *Gas chromatographic method for the analysis of allelopathic natural products in rye (Secalecereale L.).* Journal of Chromatography A, 2005. **1066**(1-2): p. 249-253.

2. Royer, J., J. Desimone, and S. Khan, *Carbon dioxide-induced swelling of poly (dimethylsiloxane).* Macromolecules, 1999. **32**(26): p. 8965-8973.

3. Chylinski, K. and J. Gregorowicz, *Solubilities of (1-hexanol, or 1, 2-hexanediol, or 2-hydroxypropanoic acid ethyl ester, or 2-hydroxyhexanoic acid ethyl ester) in supercritical CO_2.* The Journal of Chemical Thermodynamics, 1998. **30**(9): p. 1131-1140.

4. Walas, S., *Phase equilibria in chemical engineering.* 1985: Butterworth Boston.

5. Shariati, A. and C. Peters, *Measurements and modeling of the phase behavior of ternary systems of interest for the gas process: I. The system carbon dioxide+ 1-propanol+ salicylic acid.* The Journal of Supercritical Fluids, 2002. **23**(3): p. 195-208.

6. De La Fuente, J.C., S.B. Bottini, and C.J. Peters, *Measurement of the phase behavior of the ternary system carbon dioxide plus acetone plus phenanthrene.* Journal of Chemical and Engineering Data, 2006. **51**(1): p. 2-6.

7. Boukouvalas, C., et al., *Prediction of vapor-liquid equilibria with the LCVM model: Systems containing light gases with medium and high molecular weight compounds.* Ind. Eng. Chem. Res, 1997. **36**(12): p. 5454-5460.

8. Zhong, C. and H. Masuoka, *An EOS/G^E type mixing rule for perturbed hard-sphere equation of state and its application to the calculation of solid solubility in supercritical carbon dioxide.* Fluid Phase Equilibria, 1997. **141**(1-2): p. 13-23.

9. Mendes, M., A. Uller, and F. Pessoa, *Simulation and thermodynamic modeling of the extraction of tocopherol from a synthetic mixture of tocopherol, squalene and CO_2.* Brazilian Journal of Chemical Engineering, 2000. **17**: p. 761-770.

10. Gerszt, R., F. Pessoa, and M. Mendes, *Phase behaviour of sterols and vitamins in supercritical CO_2.* Brazilian Journal of Chemical Engineering, 2000. **17**: p. 261-270.

4. Extraction of Sclareol from Clary Sage Flowers using Mixtures of Ethyl Lactate and CO_2

This chapter was submitted to Journal of Supercritical Fluids for publication.

4.1. Introduction

In this chapter, an extraction method for sclareol utilizing a mixture of dense carbon dioxide and ethyl lactate as the co-solvent is proposed. The ternary phase diagrams of sclareol-ethyl lactate-CO_2 are available in chapter 3 [1], and they were used as a guide for choosing appropriate conditions for the extraction process.

As will be shown, this process offers several advantages over an alternative process using liquid extraction by pure ethyl lactate followed by a CO_2 gas anti-solvent (GAS) process for sclareol recovery. It eliminates the problem of solvent holdup during liquid ethyl lactate extraction and the low sclareol precipitation yield resulting from the GAS process. It is shown that in order for the GAS process to produce high yields of sclareol, the concentration of sclareol in ethyl lactate has to be close to its solubility limit of 11 $\pm$ 1 % (w/w) [1] at room temperature. Baled sage contains only about 3.3 $\pm$ 0.1 % (w/w) sclareol and the ethyl lactate extraction process results in a wet Clary Sage plant material containing between 60 to 70 % (w/w) of ethyl lactate. As a result, it is very challenging to obtain solution with high sclareol concentration for the GAS process that result in high yields and enables convenient recovery of most of the used solvent. For these reasons, the use of ethyl lactate as a co-solvent with CO_2 offers a better processing alternative.

There have been a large number of studies on the extraction of natural compounds using liquid or supercritical CO_2 with co-solvents. Chafer et al. [2] studied the solubility of the antioxidant gallic acid in supercritical CO_2 using ethanol as a co-solvent with ethanol concentrations ranging from 0.7 to 6 mol %. Ethanol was chosen because it is a polar solvent, its use is allowed in the food industry, and it can be easily removed from the extract by evaporation at relatively low temperature. The experiments showed that the solubility of gallic acid decreased with temperature and increased with pressure and ethanol content. Salgin [3] investigated the solubility of jojoba seed oil in supercritical CO_2 as a function of temperature and pressure. The maximum extraction yield obtained was 50.6 % (w/w) at 323.15 K and 60 MPa. Use of *n*-hexane as the co-solvent at a concentration of 5 vol. % improved the yield to 52.2 % (w/w) at lower temperature and pressure (333.15 K and 30 MPa). Machmudah et al. [4] showed that the amount of astaxanthin extracted from *Haematococcus pluvialis* was more than doubled with the use of ethanol as an entrainer and that the extraction could be carried out at a lower pressure.

The extraction experiments of sclareol from Clary Sage flowers using solvent mixtures of ethyl lactate and CO_2 were performed at ambient temperature, various pressures (P = 5.52, 6.89, 10.34 MPa), and various ethyl lactate weight fractions (w_{EL}^{*} = 0-0.9). From the generated results of % sclareol yield versus w_{EL}^{*} and % sclareol purity versus w_{EL}^{*}, it was possible to select the optimum conditions for the extraction process. The experimental extraction yields were compared with the expected yields calculated based on the ternary phase diagrams. In addition, some of the impurities co-extracted with the product were

characterized in consideration of further processing steps required to obtain nearly pure sclareol.

4.2. Experimental Procedure

4.2.1. Materials and Analysis

Field dried Clary Sage was supplied by AVOCA Inc. (Merry Hill, NC). Ethyl lactate (CAS number 687-47-8; 98 % purity) and *n*-hexane (CAS number 110-54-3; 95 % purity) were obtained from Sigma-Aldrich. Carbon dioxide (CAS number 124-38-9; > 99.99 % purity) was purchased from National Welders. These chemicals were used without further purification. The concentration of sclareol in ethyl lactate was determined by gas chromatography (GC) using heptadecanol (CAS number 1454-85-9; 98 % purity) from Sigma-Aldrich as an internal standard. Gas chromatographic analyses [5] were performed using an HP 6890N with conditions of analysis as follows: Column: 30 meter DB-5 (methyl-phenyl bonded phase, J & W Scientific) with a 0.53 mm I.D. and a 0.25 μm phase thickness; Carrier gas: UHP helium (National Welders) at a linear gas velocity of approximately 28 cm/sec; Injector temperature: 275 ^{o}C; FID Detector temperature: 310 ^{o}C; Temperature program: 160 to 310 ^{o}C at 4 degrees/minute. Data was collected using the Perkin-Elmer Total Chrom 6.2 chromatographic analysis system. The spectra of plant extracts were generated using a Jasco V-550 UV/Vis spectrophotometer.

4.2.2. Sclareol Extraction from Baled Sage using Ethyl lactate

The amount of sclareol in the baled sage was determined using *n*-hexane as the extraction solvent. Hexane is the commonly used solvent for industrial extraction of sclareol

from Clary Sage. Since sclareol is found on the surface of sage flowers and leaves, it is not necessary for the baled sage to be ground or chopped into small pieces before being contacted with *n*-hexane. Varying amounts of *n*-hexane (15 and 40 mL) was contacted with 4.082 $\pm$ 0.005 g of baled sage at 298.15 K for 24 hours. For each solvent volume, the experiments were repeated three times. The sclareol concentration in the extract was determined by GC analysis. The total mass of sclareol, neglecting the problem of solvent holdup in the baled sage or extract volume loss during filtration, was calculated from the sclareol concentration multiplied by the *n*-hexane volume used in the extraction process. The amount of sclareol in the baled sage, assuming that all sclareol were completely extracted with *n*-hexane, was determined to be as 3.3 $\pm$ 0.1 % (w/w).

The extraction of sclareol from baled sage using ethyl lactate was performed at 298.15 K and 308.15 K. A given amount of baled sage after the stems were removed (0.504 $\pm$ 0.002 g) was placed in a 20 mL vial containing 1.8 mL ethyl lactate. The mixture was kept in an oven (VWR Scientific, model 1330 FM) and maintained at a fixed temperature for a fixed amount of time. The resulting extract was collected into a 20 mL vial by passing the mixture through a syringeless filter (Whatman Autovial, Teflon® membrane with 0.45 μm pore diameter). The concentration of sclareol in the extract was determined by gas chromatography. To obtain more concentrated solutions of sclareol, the extract was placed in a vacuum oven (VWR Scientific, model 1430 M) for several hours to evaporate the solvent.

4.2.3. Gas Anti-Solvent Process to Precipitate Sclareol from Ethyl Lactate Extract

The sclareol contained in the ethyl lactate extract was recovered via a gas anti-solvent (GAS) process. A schematic diagram of the apparatus is shown in Figure 4-1. The equipment

consists of a 24.1 ± 0.1 mL high-pressure view cell, fabricated from stainless steel (316 SS) and equipped with two sapphire windows (pressure range: 0-69 MPa), a stirring plate (Fisher Scientific) underneath the view cell, a temperature controller (Barnant Company, R/S) with heating tapes (Omega Inc.) to regulate the system temperature with a precision of ± 0.5 K, a syringe pump (ISCO, model 500D) to control the system pressure set point to within ± 0.1 MPa, a heating bath/circulator (Neslab, model ex-111) to maintain the syringe pump at constant temperature, a pressure transducer (Omega Engineering Inc., model PX302, pressure range: 0-69 MPa), a line filter (HIP, pressure range: 0-103 MPa, 0.5 μm filter disc) to trap the precipitates when sampling the supernatant (liquid), and a portable lamp as a light source located at the back of the view cell (Underwriters Laboratories, Inc.). The apparatus is connected with 1/16" OD stainless steel tubing (HIP), with a two-way valve (V1, HIP), a three-way valve (V2, HIP) and a metering valve (V3, Hoke).

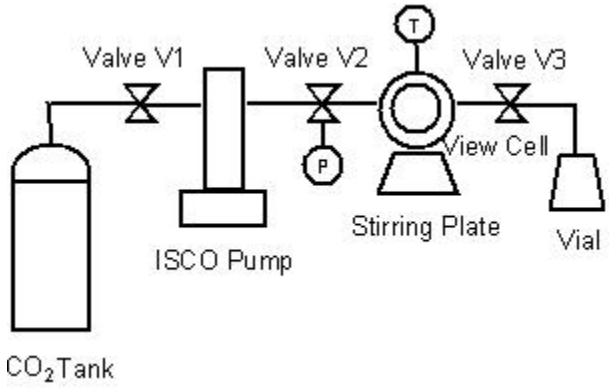

Figure 4-1. Schematic of gas anti-solvent process.

A known volume of ethyl lactate extract with known sclareol concentration was withdrawn using a syringe (Hamilton, model 1005TLL) and placed into the view cell. The

vial containing the extract was weighed before and after the transfer using an analytical balance (Ohaus Explorer Pro, model EP214DC). The difference in weight was determined as the mass of the extract placed into the view cell. The solution in the cell was heated to the desired temperature using the temperature controller. Once the temperature stabilized, CO_2 was delivered into the cell using a syringe pump through the 3-way valve V2 until the desired pressure was achieved. The mixture was then stirred for 45-60 minutes using a 0.2 mL magnetic stir bar (Fisher Scientific). The temperature, pressure, and the amount of CO_2 delivered into the cell were recorded. The liquid extract (supernatant) was collected in a vial at constant system pressure, i.e. by continuously delivering CO_2 from the ISCO pump to the cell. The amount of sclareol in the collected extract was quantified by GC analysis, and was determined as the amount of non-precipitated sclareol.

4.2.4. Sclareol Extraction from Baled Sage using Mixtures of CO_2 and Ethyl Lactate

A schematic diagram of the apparatus for the extraction experiment is shown in Figure 4-2. The equipment consists of an 86 $\pm$ 0.2 mL high-pressure cell, fabricated from stainless steel (316 SS), a temperature controller (Barnant Company, R/S) equipped with heating tape (Omega Inc.) to regulate the system temperature with a precision of $\pm$ 0.5 K, a syringe pump (ISCO, model 500D) to control the system pressure set point to within $\pm$ 0.1 MPa, a heating bath/circulator (Neslab, model ex-111) to maintain the syringe pump at constant temperature, a pressure transducer (Omega Engineering Inc., model PX302, pressure range: 0-69 MPa), and a circulating pump (Micropump Inc., model 1805R/56C, max pressure: 34.47 MPa) to circulate the solvent mixture. The apparatus is connected with 1/16” OD stainless steel tubing

(HIP) and with three-way valves (HIP). The metering valve (V9, Hoke) was used to regulate the sampling volume flow rate.

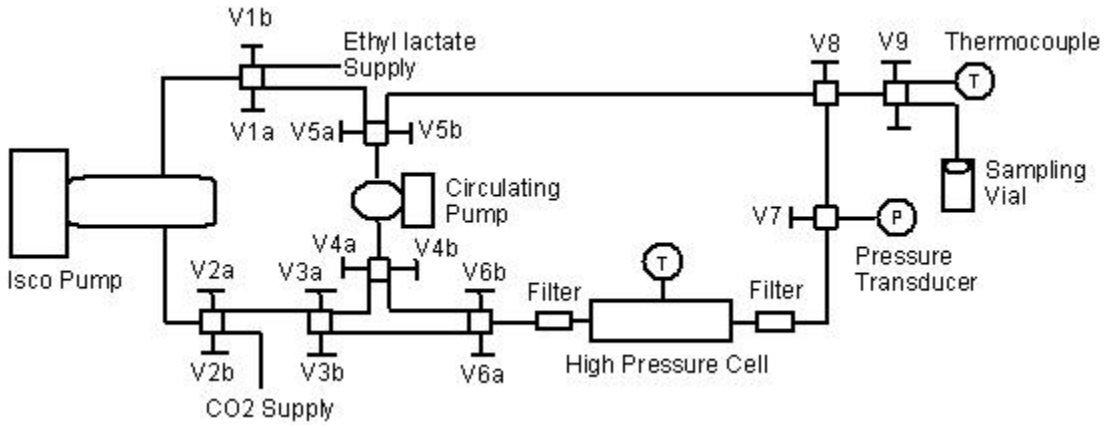

Figure 4-2. Setup for the extraction experiment of sclareol from baled sage using mixtures of CO_2 and ethyl lactate.

A given amount of baled sage after the stems were removed (33.6 $\pm$ 0.3 g) was weighed using an analytical balance (Mettler Toledo, model B3001-S), and loaded into the high-pressure cell. The ISCO pump was refilled with ethyl lactate via valve V1b and refilled with CO_2 via valve V2b. With all valves closed, the pump was pressurized to 20.68 MPa (higher than the desired pressure in order to accelerate the formation of one-phase mixture of CO_2 and ethyl lactate). Valves V1a, V2a, V3a, V4a, and V5a were opened and the circulating pump was switched on for 2 hours. Given the volume of the solvent mixture in the system and the flow rate of the circulating pump (45.9 $\pm$ 0.4 mL/min), this would result in cycling of the solvent mixture 37-40 times during the course of an experiment. After that, the ISCO pump was depressurized to the desired pressure (5.52, 6.89, 10.34 MPa) and the solvent

mixture was delivered to the high-pressure cell at constant pressure and room temperature (valves V3a, V4a, V5a were closed and valves V3b, V4b, V5b, V6a, V6b, V7, and V8 were opened). Subsequently, the solvent mixture containing the dissolved substances was circulated within the system at constant pressure for 1 hour with valve V6a closed. This would result in 30-34 circulations given the mixture volume and the flow rate of the circulating pump. The extract was collected in a vial at constant system pressure, i.e. by continuously delivering the solvent mixture from the ISCO pump to the cell (semi-batch process). In the first sampling, the volume of mixture (ethyl lactate, CO_2, and extracted compounds) collected was approximately the same as the volume of mixture (ethyl lactate and CO_2) delivered to pressurize the system. The addition of fresh solvent mixture into the system during sampling decreased the extracted sclareol concentration in the system with time, and thus would result in the extraction yield lower than expected. In order to improve the extraction yield, sampling was performed for a longer time at the same sampling flow rate, or additional solvent mixture must be fed into the system to replace the amount of extract sampled. One way of doing this is to repeat the sampling procedure, which is referred to here as the 2^{nd} sampling.

Subsequently after sampling, the volume of the collected extract was measured, and the amount of sclareol in the collected extract was quantified by GC analysis. The purity of sclareol in the collected extract in terms of weight fraction was also determined. Finally, the system was depressurized and the remaining extract in the system was collected in a vial during depressurization. The temperature, pressure, and volume of the ISCO pump as well as the temperature and pressure of the cell were recorded after each step.

4.3. Results and Discussions

4.3.1. Sclareol Extraction from Baled Sage using Ethyl Lactate

The extraction with ethyl lactate was performed at 298.15, 308.15 K and various contact times, as summarized in Table 4-1 and Table 4-2. The ethyl lactate volume used in each experiment is 1.8 mL. The results show that ethyl lactate is an excellent solvent for sclareol. The extraction with ethyl lactate achieved ostensibly 100 % extraction yield in a matter of seconds. Some experimental data show extracted sclareol masses higher than expected. This is possibly due to the variation in the sclareol content in the sage flowers and leaves, or possibly that ethyl lactate is a better solvent than hexane in extracting all of the sclareol. Moreover, since virtually complete sclareol extraction can be achieved at ambient temperature, there is no advantage to be gained from the extraction at a higher temperature. The sclareol percentage in the extracted materials was determined by evaporating the solvent from a known volume of extract, evaluating gravimetrically the mass of the extract after complete solvent removal, and then determining the sclareol mass in the extract by GC analysis. From this experiment, the % sclareol purity in the extracted material was calculated to be in the range of 40-50 % (w/w). The problem of the solvent holdup during liquid extraction is discussed in the next section.

Table 4-1. Sclareol extraction from baled sage using ethyl lactate at 298.15 K and various contact times.

T = 298.15 K

Contact times (hr)	Baled sage mass (g)	Sclareol concentration in the extract (g/L)	Total mass of sclareol in the extract (mg)	Expected sclareol mass (mg)
15-30 sec	0.503	8.9	16.0	16.6
0.5	0.506	8.6	15.5	16.7
1	0.502	9.4	16.8	16.6
1.5	0.503	11.4	20.5	16.6
2	0.504	11.1	20.0	16.6
4	0.503	11.0	19.9	16.6
24	0.506	9.5	17.0	16.7

Table 4-2. Sclareol extraction from baled sage using ethyl lactate at 308.15 K and various contact times.

Contact times (hr)	Baled sage mass (g)	Sclareol concentration in the extract (g/L)	Total mass of sclareol in the extract (mg)	Expected sclareol mass (mg)
0.5	0.507	8.8	15.8	16.7
1	0.502	9.9	17.9	16.6
1.5	0.505	9.4	16.8	16.7
2	0.505	10.6	19.2	16.7
4	0.505	12.4	22.4	16.7
24	0.505	8.7	15.6	16.7

4.3.2. Gas Anti-Solvent Process to Precipitate Sclareol from Ethyl Lactate Extract

The initial plan of the extraction experiment was to extract sclareol from baled sage using ethyl lactate and to recover the sclareol from the ethyl lactate via a GAS process using CO_2. The ternary phase diagram of sclareol-ethyl lactate-CO_2 system at 298.15 K and 6.89 MPa (Figure 4-3) was used as a basis for choosing the starting concentration of sclareol in ethyl lactate for the GAS process. To achieve high % yields of sclareol precipitation, the starting concentration of sclareol must be close to the saturation concentration of sclareol in ethyl lactate, which is 11 $\pm$ 1 % (w/w) or 129 $\pm$ 1.5 g/L at 298.15 K. Since baled sage contains only 3.3 $\pm$ 0.1 % (w/w) of sclareol and the wet sage mat contains approximately 60-

70 % (w/w) ethyl lactate, a large amount of solvent is required to extract a given amount of sclareol, and this must be followed by evaporation of the solvent to achieve a mixture with sufficiently high sclareol concentration to result in a high yield for the GAS process. To illustrate this point, two mixtures of different sclareol concentrations were prepared for GAS experiments, as summarized in Table 4-3. To achieve a final sclareol concentration of 46.2 g/L for Mixture 1 and 100.3 g/L for Mixture 2, 71 and 143 mL of solvent respectively had to be evaporated.

Table 4-3. Sclareol extraction from baled sage using ethyl lactate at 298.15 K for gas anti-solvent precipitation experiments.

	Mixture 1	Mixture 2
Mass of sage (g)	17.5	35
Volume of ethyl lactate used (mL)	120	240
Volume of collected extract (mL)	78	149
Sclareol concentration before solvent evaporation (g/L)	4.3	4.2
Sclareol concentration after solvent evaporation (g/L)	46.2	100.3

The GAS experiment was performed at 298.15 K and 6.89 MPa. At these conditions, ethyl lactate and carbon dioxide are completely miscible with each other, forming a single phase. The experimental conditions for the GAS process and the resulting sclareol yields are summarized in Table 4-4.

Table 4-4. Results summary of GAS process at 298.15 K and 6.89 MPa.

	Experiment 1	Experiment 2	Experiment 3
Volume of extract (mL)	5	1	1
Sclareol concentration before GAS (g/L)	100.3	100.3	46.2
Mass of CO_2 introduced (g)	17.49	18.19	18.16
Sclareol concentration after GAS (g/L)	98.5	80.6	45.7
Precipitates observed	yes	yes	yes
% sclareol precipitated	1.79	19.64	1.08
% expected sclareol precipitation	46.3	70.4	36.1

For all the cases, once CO_2 was introduced into the extract, the solution became cloudy and precipitation was observed. In order to calculate the amount of sclareol precipitated, the supernatant of the mixture was collected and its sclareol concentration was determined by GC. The results showed significant precipitation of sclareol for experiment 2. Together with sclareol, some impurities including plant pigments were also precipitated.

By neglecting the presence of impurities, the compositions of sclareol in ethyl lactate (before CO_2 addition) and in the mixture of ethyl lactate and CO_2 were calculated and plotted in the ternary phase diagram of pure sclareol in terms of weight fraction, as shown in Figure 4-3 and Figure 4-4. The method to estimate the ternary phase equilibrium of the sclareol-ethyl lactate-CO_2 system was described in a previous chapter [1]. In Figure 4-3, Point A is the starting composition for experiment 1 while point B is for experiment 2. Points A^1 and B^1 are the compositions after addition of CO_2 and just before precipitation occurred. The same relationships apply for point C and C^1 (experiment 3) in Figure 4-4. The addition of CO_2 diluted the mixture and brought the solutions closer to the ethyl lactate-CO_2 edge. The location of these points can be more clearly observed in the plot of the solubility of sclareol as a function of CO_2 content ($w_{Sclareol}$ versus w_{CO_2}) in Figure 4-5.

With the given starting volume, sclareol concentration, pressure, and temperature, the theoretically expected % sclareol precipitation results based on pure sclareol behavior for all the three cases were calculated. The results were as follows: 46.3 % for experiment 1, 70.4 % for experiment 2, and 36.1 % for experiment 3. These results are listed in Table 4-4 as % expected sclareol precipitation. The expected % sclareol precipitation yields based on experiments done with pure sclareol in ethyl lactate solution were significantly higher than

those obtained from precipitations done with the plant extract material. The results from the plant extract are also shown in Table 4-4, indicating precipitation yields of 1.79 % for experiment 1, 19.64 % for experiment 2, and 1.08 % for experiment 3 respectively. Clearly the precipitation yield results with pure sclareol are much greater than those obtained with the natural plant material. It is speculated that a significant number of the impurities in the extract act as co-solvents for sclareol and thus inhibit the precipitation of sclareol compared to pure sclareol in ethyl lactate solution.

These GAS experiments with the extract from the natural plant were repeated at a higher pressure of 10.34 MPa. The results showed that the increase in pressure from 6.89 to 10.34 MPa and the resulting increase in CO_2 concentration did not significantly change the sclareol precipitation yield and selectivity. Point B in Figure 4-3 was the starting point for the experiment at 10.34 MPa. At this pressure, the experimental sclareol precipitation yield was 20 %, which was approximately the same as the result obtained at 6.89 MPa. The expected sclareol precipitation yield based on pure sclareol solubility was 82.6 %. This experiment also is consistent with the supposition that the inhibition of sclareol precipitation in the natural extract is due to impurities acting as co-solvents for sclareol. This effect was seen at both the low and high pressure GAS process.

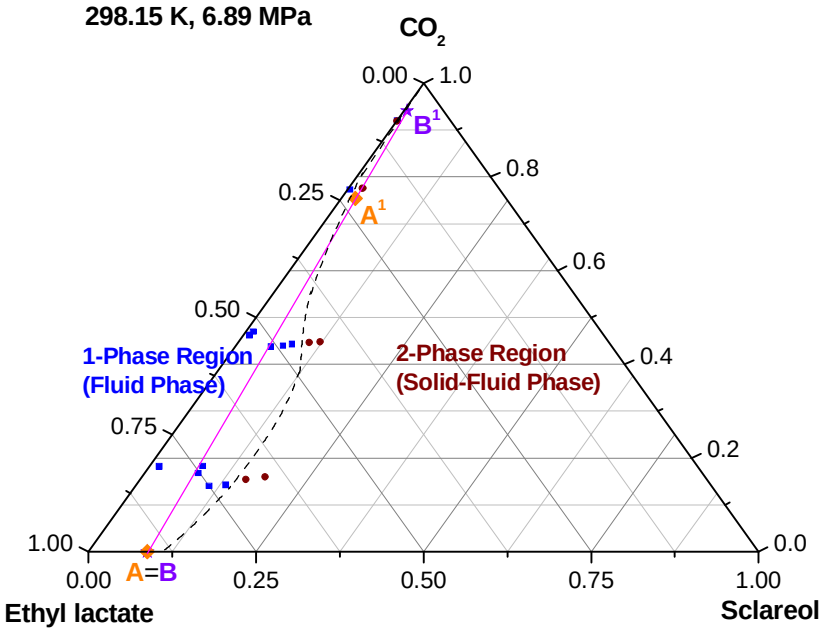

Figure 4-3. Experimental ternary phase diagram at 298.15 K and 6.89 MPa obtained from static synthetic observations. Squares represent the one-phase region (fluid phase) and circles represent the two-phase region (solid-fluid phase). Point A=B represents the starting compositions of sclareol in ethyl lactate in Experiments 1 and 2 whereas both point A^1 and point B^1 represent the final composition after introduction of CO_2 (GAS process) with different amount of CO_2.

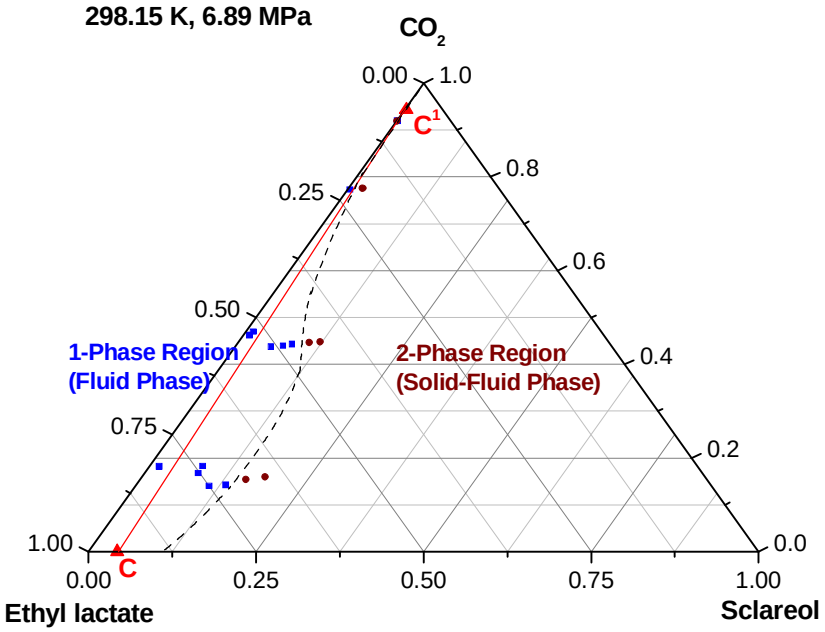

Figure 4-4. Experimental ternary phase diagram at 298.15 K and 6.89 MPa obtained from static synthetic observations. Squares represent the one-phase region (fluid phase) and circles represent the two-phase region (solid-fluid phase). Point C represents the starting composition of sclareol in ethyl lactate in Experiment 3 whereas point C^1 represents the final composition after introduction of CO_2 (GAS process).

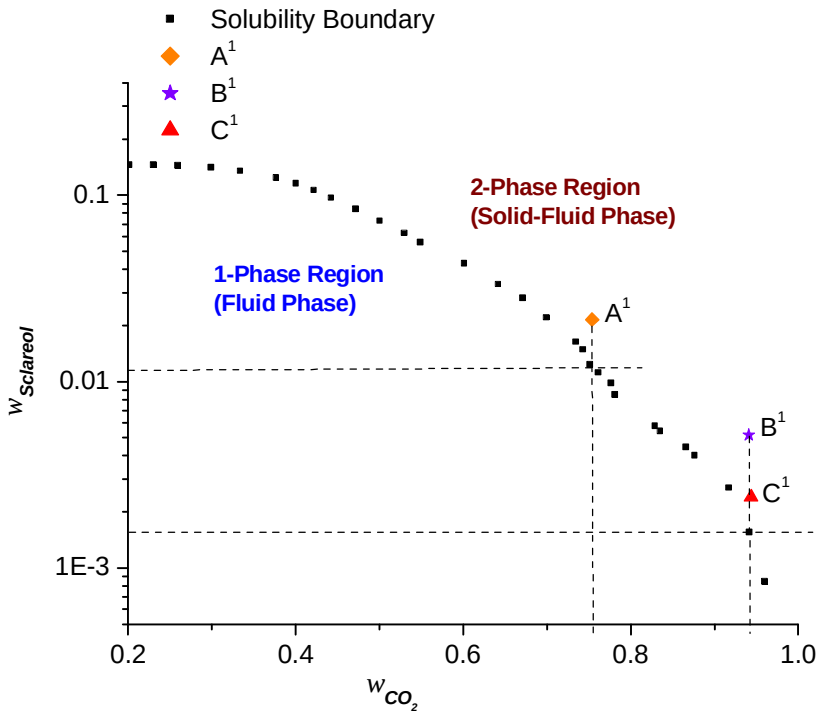

Figure 4-5. Plot of the sclareol solubility in an ethyl lactate-CO_2 mixture at 298.15 K and 6.89 MPa. Points A^1, B^1, and C^1 represent the composition of sclareol in ethyl lactate-CO_2 mixture for experiments 1, 2, and 3 in Table 4, respectively. The calculation neglects the presence of impurities in the mixture.

In summary, the extraction of sclareol from baled sage using ethyl lactate followed by gas anti-solvent precipitation resulted in some significant challenges. The solvent holdup during liquid extraction required the use of large volumes of ethyl lactate to extract a given amount of sclareol, resulting in extracts with very dilute sclareol concentration. For effective operation of the GAS process, on the other hand, the extract should contain high sclareol concentration, and therefore it was necessary to concentrate the extract by evaporating a significant amount of ethyl lactate. Moreover, the GAS results from the extract showed a much lower precipitation yield than the expected yield according to the solubility behavior of

pure sclareol, probably as a result of impurities acting as co-solvents for sclareol in the ethyl lactate. Finally, the GAS process was not very selective for sclareol. The precipitates contained other substances besides sclareol. Based on this modest result with GAS, it was decided to pursue an alternative route that would reduce the amount of ethyl lactate used and would significantly increase the yield of sclareol obtained.

4.3.3. Sclareol Extraction from Baled Sage using Mixtures of CO_2 and Ethyl Lactate

Since ethyl lactate is such an excellent solvent for sclareol and also completely miscible with CO_2 under certain conditions, the use of ethyl lactate as a co-solvent for extraction of sclareol is attractive and compelling. The presence of CO_2 increases the solvent diffusivity and significantly reduces its viscosity relative to pure ethyl lactate, thus eliminating the problem of solvent holdup. It was also hoped that CO_2 might also increase the extract purity since polar compounds and high molecular weight compounds, such as plant pigments, are sparingly soluble in carbon dioxide at relatively low pressures and temperatures. The solubility of some natural hydrophobic substances, such as xanthophylls, carotenes, and chlorophyll in liquid CO_2 (253.15 to 293.15 K) and supercritical CO_2 at less than 30 MPa are fairly low, in spite of their low polarity [6].

The section that follows describes the extraction of sclareol from baled sage using mixtures of ethyl lactate and CO_2 at various ethyl lactate compositions. All the experiments were performed at 298.15 K, pressures of 5.52, 6.89, and 10.34 MPa, and a range of solvent compositions at which the ethyl lactate and CO_2 are completely miscible. At 298.15 K and

5.52 MPa, carbon dioxide is immiscible with ethyl lactate at w_{CO_2} > 0.73 (or w_{EL} < 0.27) as shown in Figure 4-6.

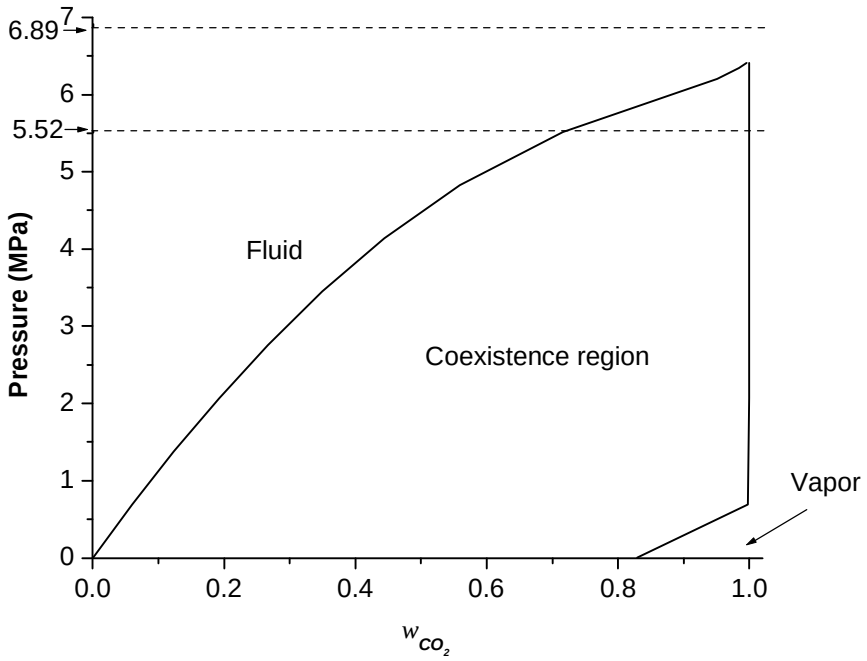

Figure 4-6. Computed vapor liquid equilibrium data of ethyl lactate-CO_2 system at 298.15 K and various pressures using Peng-Robinson EOS with linear combination of Vidal and Michelsen mixing rules (PR-LCVM) model.

Estimation of theoretical % sclareol yield

Given a set of experimental conditions, namely extraction vessel size, temperature, and pressure, the ternary phase equilibrium data can be used to generate a plot of the estimated % sclareol yield as a function of co-solvent (ethyl lactate) composition. Figure 4-3 and Figure 4-7 show the solubility boundary of sclareol in the ethyl lactate-CO_2 mixtures as a function of ethyl lactate weight fraction at 298.15 K, and two different pressures (6.89 and 10.34 MPa, respectively).

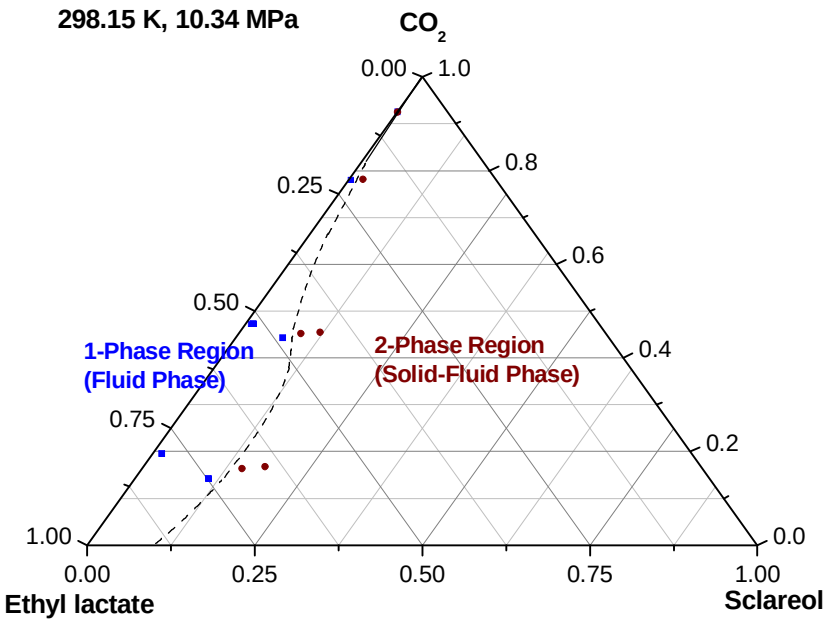

Figure 4-7. Experimental ternary phase diagram at 298.15 K and 10.34 MPa obtained from static synthetic observations. Squares represent the one-phase region (fluid phase) and circles represent the two-phase region (solid-fluid phase).

The phase envelopes in the ternary phase diagrams in Figure 4-3 and Figure 4-7 show the transition from a single phase to a two-phase (solid-fluid) system, and they fix the solubility of sclareol at given concentrations of CO_2 and ethyl lactate ($w_{Sclareol}, w_{EL}, w_{CO_2}$). The precipitated solid is assumed to be pure sclareol. The equivalent weight fraction of ethyl lactate in the remaining binary mixture made up of CO_2 and ethyl lactate, w_{EL}^{*}, is calculated as follows,

$$w_{EL}^{*} = \frac{w_{EL}}{w_{EL} + w_{CO_2}} \tag{2}$$

The mass of solvent mixture used to pressurize the system, and to extract sclareol from a given amount of baled sage (33.6 $\pm$ 0.3 g) can then be determined from the formula,

$$m_{CO_2+EL} = r_{CO_2+EL} * V_{CO_2+EL} \quad (3)$$

In this expression the density of the carbon dioxide and ethyl lactate mixture, r_{CO_2+EL}, varies with w_{EL}^{*} and pressure, and can be estimated from the Peng-Robinson Equation of State [7] with the Linear Combination of Vidal and Michelsen mixing rules (PR-LCVM) model [8]. The calculation of solvent mixture density using the PR-LCVM model is described in the Appendix A.2. The volume of the carbon dioxide and ethyl lactate mixture (V_{CO_2+EL}) used in the extraction step is determined from the difference in the ISCO pump volumes before and after pressurizing the system with the solvent mixture. Finally, the theoretical % sclareol yield is obtained from the expressions,

$$m_{Sclareol} = \frac{w_{Sclareol}}{w_{EL}} * w_{EL}^{*} * m_{CO_2+EL} \quad (4)$$

$$\%\cdot Sclareol\cdot yield = \frac{m_{Sclareol}}{m_{\exp ected}} * 100\% \quad (5)$$

Here $m_{\exp ected}$ is the total mass of sclareol in the known amount of baled sage, considering that baled sage contains 3.3 $\pm$ 0.1 % (w/w) of sclareol. Figure 4-8 shows the plot of theoretical % sclareol yield versus w_{EL}^{*} at 298.15 K and pressures of 6.89, 10.34 MPa.

These curves indicate that, in theory, sclareol should be completely extracted from baled sage at a weight fraction of ethyl lactate w_{EL}^{*} greater than 0.25 at 6.89 MPa and greater than 0.22 for 10.34 MPa at 298.15 K.

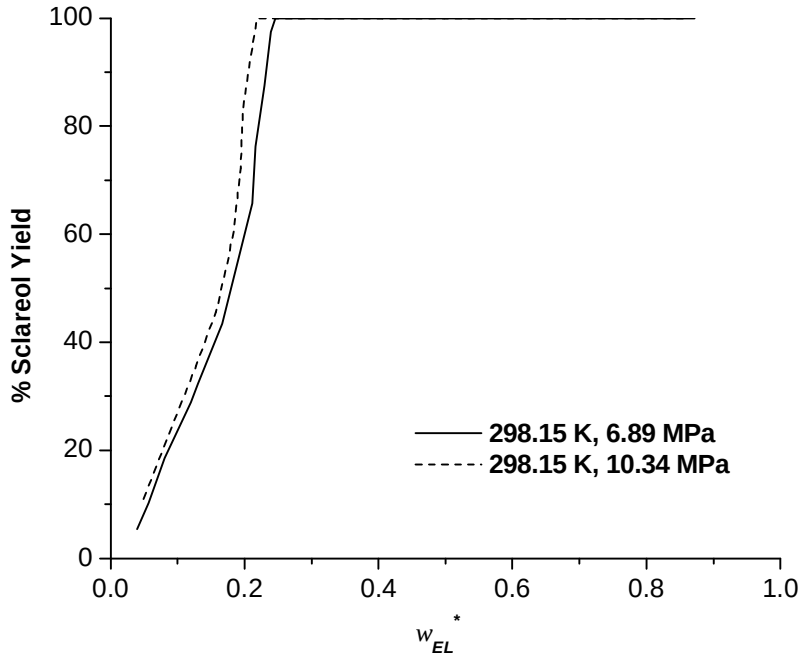

Figure 4-8. Estimated % sclareol yield as a function of ethyl lactate compositions in the ethyl lactate-CO_2 mixtures given the experimental extraction conditions.

Experimental % sclareol yield and % sclareol purity

Sclareol extraction experiments from baled sage were performed at various ethyl lactate compositions using the setup depicted in Figure 4-2. The high-pressure cell was packed with 33.6 $\pm$ 0.3 g of baled sage. The solvent mixture was prepared by metering ethyl lactate and CO_2 into the solvent loop using valves 1 and 2 and was then delivered into the cell until the desired pressure was achieved. The circulation pump was used to circulate the solvent mixture to promote sclareol extraction. Subsequently, the extract was sampled at constant

pressure by continuously delivering the solvent mixture from the ISCO pump into the system while collecting the extract in the sampling vial. Two samples were taken for each experiment. Figure 4-9 shows the % sclareol extraction yield based on the total collected mass of sclareol during the 1st sampling and 2nd sampling. It is clear that experimental sclareol extraction yields are well approximated by the theoretically predicted in the w_{EL}^{*} range of 0.2 to 0.9. Also shown in Figure 4-9, the experimental extraction yields for w_{EL}^{*} > 0.3 are independent of the ethyl lactate concentration and pressure, in the range of 80 to 95 %.

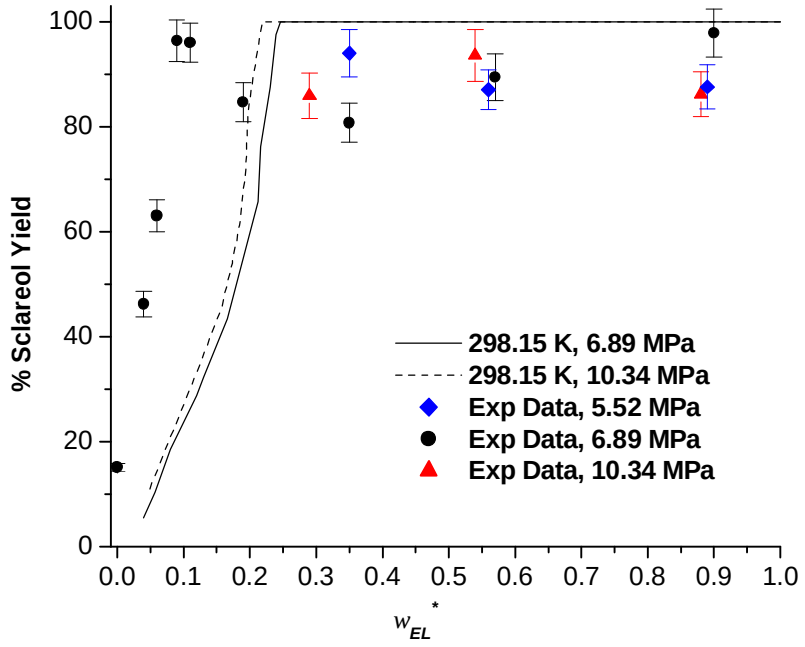

Figure 4-9. Estimated and experimental % sclareol yield as a function of ethyl lactate compositions in the ethyl lactate-CO_2 mixtures at 298.15 K and various pressures. The experimental data is calculated based on the total collected mass of sclareol, combining the first and second sampling.

The sclareol purity of each extract (% sclareol) was determined by evaporating the solvents (CO_2 and ethyl lactate) from a known volume of extract, measuring the mass of the extract gravimetrically after complete solvent removal, and then determining the sclareol mass in the extract by GC analysis. The impurities of the extract vary with the ethyl lactate concentration in the extraction medium w_{EL}^{*}, as shown in Figure 4-10. The results also show that at 6.89 MPa, the experiments performed with w_{EL}^{*} of approximately 0.09-0.1 produce extracts with the highest sclareol purity, in the range of 65-70 % (w/w). At high CO_2 concentrations or $w_{EL}^{*} < 0.09$, higher purity extracts were expected since the solubility of many plant pigments in CO_2 are relatively low [6]. Experimentally, it was found that these extracts obtained at low ethyl lactate weight fractions have relatively high purity as well as some of the highest yields. Apparently, the other components in the extract that helped to enhance the solubility of sclareol in the extracts with low ethyl lactate concentration to result in high yield, are not very good solvents for a significant number of other impurity types that would lower the sclareol purity.

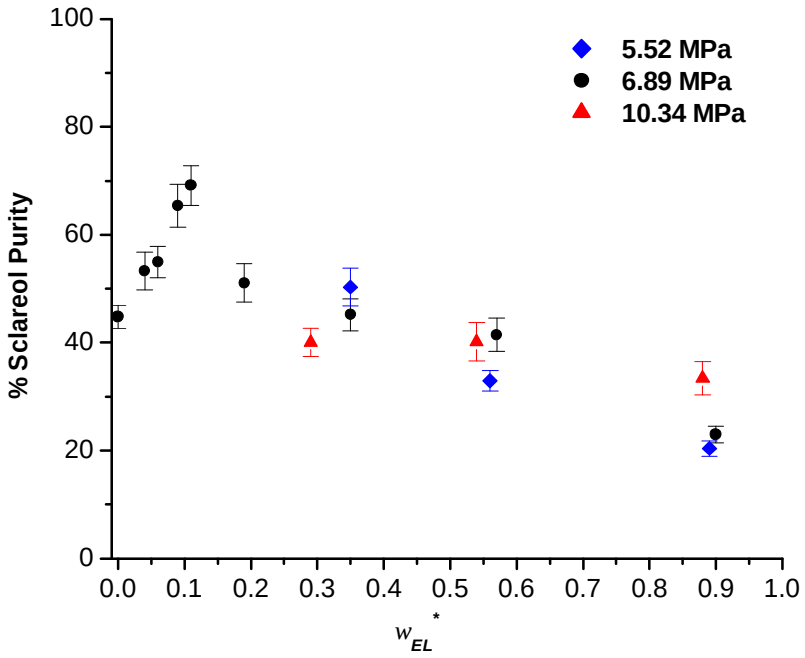

Figure 4-10. Experimental % sclareol purity as a function of ethyl lactate compositions in the ethyl lactate-CO_2 mixtures at 298.15 K and various pressures.

4.3.4. Characterization of Plant Extracts

The color of the extracts obtained varied from yellow green to dark green depending on the ethyl lactate composition in the extraction solvent. Representative pictures of the extracts are shown in Figure 4-11. The green color of the extracts is most likely due to the presence of chlorophylls. All green plants contain chlorophyll *a* and chlorophyll *b* in their chloroplasts [9]. In higher plants, chlorophyll *a* is the major pigment and chlorophyll *b* is an accessory pigment. Chlorophylls are green in color because they absorb strongly in the red and blue regions of the visible spectrum. The small differences in the structures of the two chlorophylls produce differences in the absorption spectra.

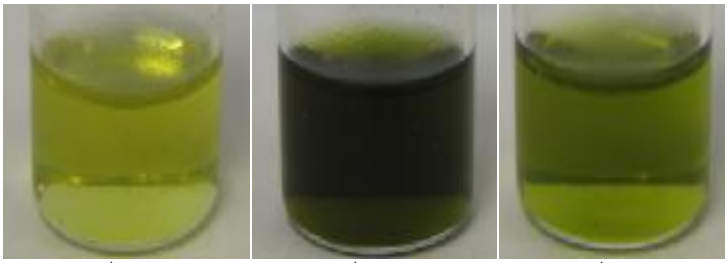

$w_{EL}^{*} = 0.1$ $w_{EL}^{*} = 0.35$ $w_{EL}^{*} = 0.9$

Figure 4-11. Pictures of extracts obtained at 6.89 MPa. The sclareol concentration and % sclareol purity in each extract are different. For w_{EL}^{*} = 0.1, 0.35, and 0.9, sclareol concentration is 69.1± 3.5, 14.4 ± 0.7, 5.9 ± 0.3 g/L while % sclareol purity is 69.2 ± 3.7, 45.2 ± 2.9, 23 ± 1.5 % (w/w), respectively.

Gross et al. [9] reported that in diethyl ether, chlorophyll *a* has approximate absorbance maxima of 430 nm and 662 nm while chlorophyll *b* has absorbance maxima of 453 nm and 642 nm. The absorption spectra of chlorophyll *a* and *b* in diethyl ether are described in Figure 4-12. The exact positions and intensity of the maximum vary slightly with the nature of the solvents used [9, 10]. The representative absorption spectra of the extracts obtained at 6.89 MPa and various w_{EL}^{*} are illustrated in Figure 4-13.

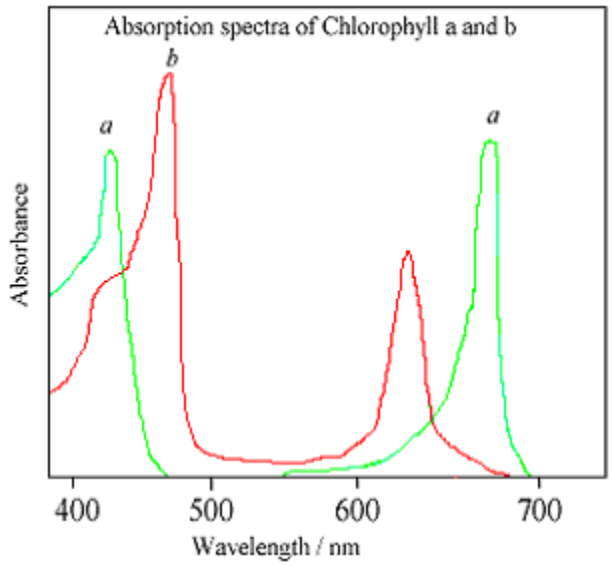

Figure 4-12. Absorption spectra of chlorophylls *a* and *b* in diethyl ether [9].

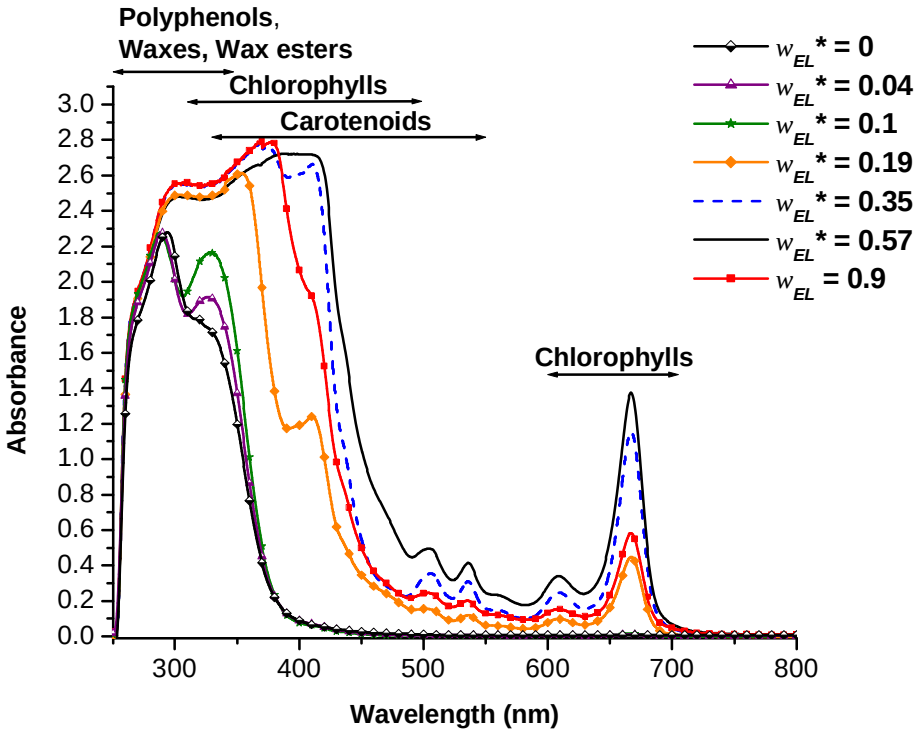

Figure 4-13. Absorption spectra of ethyl lactate and CO_2 extracts obtained at 6.89 MPa and various ethyl lactate compositions. Each extract is diluted to contain the same sclareol concentration.

The spectra of the extracts also demonstrate an absorbance maximum of 663 nm for chlorophyll *a*. There is also an absorbance maximum at around 615 nm, which may indicate the presence of chlorophyll *b*. Due to the presence of impurities which absorb in the range of 280-500 nm, such as polyphenols, carotenoids, monoterpenes and sesquiterpenes, linalool, and linalyl acetate, it was not possible to distinguish the absorbance maxima of chlorophyll *a* and *b* in the blue region (lower wavelength). However, based on the presence of the band in the red region, it can be surmised that chlorophylls contributed to the impurities of the plant

extracts. The intensity of the peaks obviously varied with the amount of ethyl lactate in the extracts.

The amount of chlorophyll *a* in each extract was determined according to the Beer-Lambert law [11]. By measuring the absorption spectra of relatively pure chlorophyll *a* (Sigma Aldrich; CAS number 479-61-8; ~ 95 % purity) in ethyl lactate at various concentrations, the molar extinction coefficient could be determined as 66.91 g/(L.cm) at a maximum peak of 665 nm. The percentage of chlorophyll *a* was then calculated and plotted as a function of w_{EL}^{*} in Figure 4-14. The results showed that chlorophyll *a* constitutes a relatively small percentage of all impurities, < 0.5 % (w/w). The extracts with w_{EL}^{*} = 0.5-0.6 contained the highest percentage of chlorophyll *a* while the extracts with w_{EL}^{*} < 0.1 contained negligible amount of chlorophyll *a*.

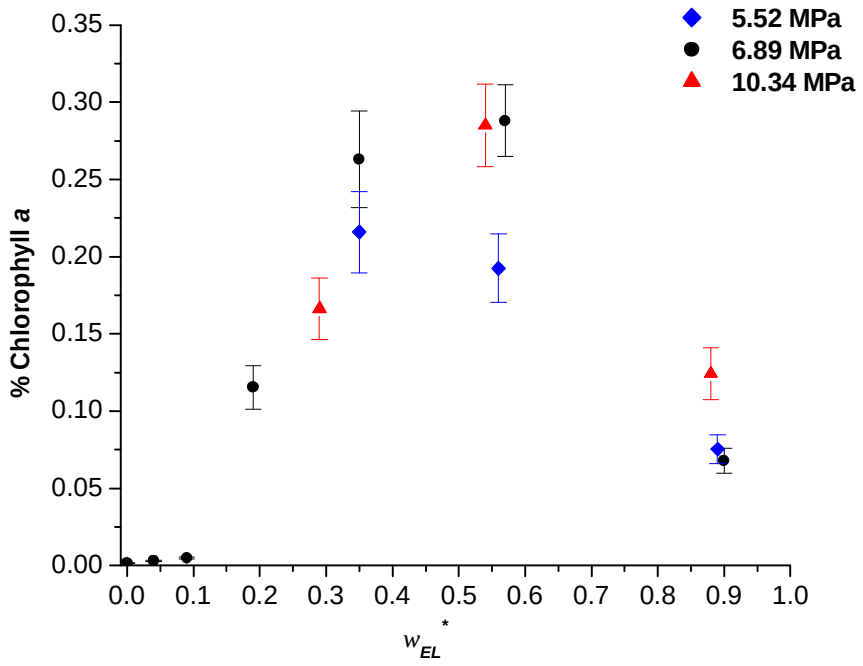

Figure 4-14. Plot of % chlorophyll *a* in CO_2+EL extracts obtained at various w_{EL}^* and pressures.

Along with chlorophylls, the chloroplast also contains a family of pigments called carotenoids [9, 12]. Each carotenoid absorbs light in the UV and visible region of the spectrum. A typical absorbance spectrum of carotenoids contains three bands, and the positions of the absorption maxima are affected by the length of the chromophore and the position of the terminal double bond in the chain or ring [9]. The solvents used also influence the position of the absorption maxima [9, 13]. Carotenoids absorb mainly in the blue (430-470 nm), but they also absorb in the blue-green (470-500 nm) and green (500-530 nm) regions of the spectrum. Absorption maxima of some common carotenoids of plants are shown in Table 4-5. The spectra of the extracts (Figure 4-13) show absorbance in the range of 250-550 nm, and therefore it is likely that carotenoids are present in the extracts and

responsible for the yellow color of the extracts. Comparison of UV-visible spectra alone, however, is not sufficient to confirm the presence of carotenoids since many other compounds may absorb in the same range as carotenoids.

Other possible impurities contained in the extracts are mono- and sesquiterpenes, fatty acids, oils, polyphenols, waxes, wax esters, pigments and their degradation products [14]. A combination of several analytical techniques would be necessary for characterizing all constituents that contribute to the impurities of extracts.

Table 4-5. Absorption maxima of some common carotenoids of plants in petroleum ether [9].

Carotenoid	Absorption maximum (nm)
Phytofluene	331, 348, 367
z-Carotene	380, 400, 424
Lycopene	447, 472, 504
b-Zeacarotene	405, 428, 455
a-Carotene	423, 444, 473
b-Carotene	425, 451, 478
Zeaxanthin	425, 451, 478
Antheraxanthin	420, 444, 472
Mutatoxanthin	404, 427, 453
Violaxanthin	418, 440, 470
Violeoxanthin	415, 436, 464
Capsanthin	476

4.4. Conclusions

The extraction of sclareol from Clary Sage using ethyl lactate, followed by gas anti-solvent (GAS) precipitation process presented challenges for obtaining pure sclareol in high yield. The process required the use of a large amount of ethyl lactate to extract a given amount of sclareol from Clary sage, and subsequent evaporation of a large amount of ethyl lactate to concentrate the solution in order to achieve a high yield of sclareol upon

precipitation with the GAS process. Furthermore, it was found that the experimental yield of sclareol by precipitation was much lower than the expected yield based on the solubility behavior of pure sclareol. This is likely due to impurities acting as co-solvents for sclareol in the ethyl lactate. Finally, the GAS process was not very selective for sclareol. The sclareol obtained by precipitation was impure.

The extraction of sclareol with a mixture of ethyl lactate and CO_2 offers some advantages. The presence of CO_2 increases the solvent diffusivity and significantly reduces its viscosity relative to pure ethyl lactate, thus minimizing the problem of solvent holdup. The extraction experiments were performed at 298.15 K, pressures of 5.52, 6.89, 10.34 MPa, and various ethyl lactate concentrations (w_{EL}^{*}). The results showed that the extract yield and purity varied with the ethyl lactate concentration. The experimental extraction yields were close to the theoretically predicted values in the w_{EL}^{*} range of 0.2 to 0.9. At certain ethyl lactate compositions (w_{EL}^{*} = 0.09-0.1), ambient temperature, and pressure of 6.89 MPa, the extraction process achieved 95-100 % sclareol extraction yield with highest sclareol purity, i.e. 65-70 % (w/w).

The UV visible spectra analysis of the plant extracts confirmed the presence of chlorophyll a responsible for the green color of the extract. The calculation of % chlorophyll showed that chlorophyll *a* contributed to a small percentage of impurities (< 0.5 % (w/w)), and the extracts with $w_{EL}^{*} < 0.1$ contained negligible amount of chlorophyll *a*. A detailed discussion on the process to purify and recover sclareol from the ethyl lactate and CO_2 extracts is presented in chapter 5.

4.5. References

1. Tombokan, X.C., et al., *Three-component phase behavior of the sclareol-ethyl lactate-carbon dioxide system for GAS applications.* The Journal of Supercritical Fluids. Selected contributions from 1st Iberoamerican Conference on Supercritical Fluids, Prosciba Iguassu Falls, April 10-13, 2007, 2008. **45**(2): p. 146-155.

2. Chafer, A., et al., *Solubility of the natural antioxidant gallic acid in supercritical CO_2 + ethanol as a cosolvent,* in *Journal of chemical and engineering data*. 2007. p. 116-121.

3. Salgin, U., *Extraction of jojoba seed oil using supercritical CO_2+ ethanol mixture in green and high-tech separation process.* The Journal of Supercritical Fluids, 2007. **39**(3): p. 330-337.

4. Machmudah, S., et al., *Extraction of astaxanthin from Haematococcus pluvialis using supercritical CO_2 and ethanol as entrainer.* Ind. Eng. Chem. Res., 2006. **45**(10): p. 3652-3657.

5. Finney, M., D. Danehower, and J. Burton, *Gas chromatographic method for the analysis of allelopathic natural products in rye (Secalecereale L.).* Journal of Chromatography A, 2005. **1066**(1-2): p. 249-253.

6. Mukhopadhyay, M., *Natural extracts using supercritical carbon dioxide*. 2000: CRC Press.

7. Peng, D. and D. Robinson, *A new two-constant equation of state.* Industrial & Engineering Chemistry Fundamentals, 1976. **15**(1): p. 59-64.

8. Boukouvalas, C., et al., *Prediction of vapor-liquid equilibrium with the LCVM model: A linear combination of the vidal and michelsen mixing rules coupled with the original UNIFAC.* Fluid Phase Equilibria, 1994. **92**: p. 75-106.

9. Gross, J., *Pigments in vegetables: Chlorophylls and carotenoids.* 1991: Van Nostrand Reinhold, New York.

10. Schoefs, B., *Chlorophyll and carotenoid analysis in food products. Properties of the pigments and methods of analysis.* Trends in Food Science & Technology, 2002. **13**(11): p. 361-371.

11. Clark, B., T. Frost, and M. Russell, *UV spectroscopy: Techniques, instrumentation, data handling*. 1993: Springer.

12. Mihalik, E., et al., *Photosynthetic and morphological characters of leaves of the annual and biennial salvia sclarea biotypes.* Acta Biologica Szegediensis, 2005. **49**(1-2): p. 161-163.

13. Zang, L., O. Sommerburg, and F. Van Kuijk, *Absorbance changes of carotenoids in different solvents.* Free Radical Biology and Medicine, 1997. **23**(7): p. 1086-1089.

14. Diaz-Reinoso, B., et al., *Supercritical CO_2 extraction and purification of compounds with antioxidant activity.* J. Agric. Food Chem., 2006. **54**(7): p. 2441-2469.

5. Purification and Recovery of Sclareol from a Dense CO_2-Ethyl Lactate Extract

5.1. Introduction

The extraction of sclareol from Clary sage was performed using a binary mixture of ethyl lactate and CO_2 at 298.15 K, pressures of 5.52, 6.89, 10.34 MPa, and variable ethyl lactate concentrations (w_{EL}^{*}). At a solvent composition of w_{EL}^{*} = 0.09-0.1 at ambient temperature and 6.89 MPa of pressure, this extraction process achieved 95-100 % sclareol extraction yield and 65-70 % (w/w) of sclareol purity. The likely impurities contained in this extract are mono- and sesquiterpenes, fatty acids, oils, polyphenols, waxes, wax esters, plant pigments (chlorophylls and carotenoids), and their degradation products. The detailed extraction procedure and results are presented in chapter 4 [1]. In this chapter, we examine methods for further purification and recovery of sclareol from the initial plant extract. Our approach involved the addition of activated carbon to further purify the crude liquid extract and subsequent application of a liquid anti-solvent process, using water as the antisolvent, to precipitate high purity sclareol.

Activated carbon is a common adsorbent used in a wide variety of purification processes. It is a microcrystalline, non-graphitic form of carbon that has been processed to develop high internal porosity. This porosity creates a surface area that has the capability to selectively adsorb certain gases and vapors from composite gases and dissolved or dispersed substances from liquids. Liquid phase applications account for about 85 % of activated carbon usage and have proven to be an economical and convenient tool in the processing of

food and pharmaceutical products. The application of activated carbon as a food processing aid was given independent verification of the safety and health aspects by a group of scientists from the Select Committee on GRAS substances in 1981 [2]. Some examples of activated carbon applications in the liquid phase are water purification treatment in the food and beverage industry, decaffeination by selective adsorption of caffeine from aqueous solutions, removal of amino acid content for long-term stored apple juices, decolorization of malt beer, adsorption of undesirable flavors to achieve high ethanol recovery in Saccharomyces cerevisiae fermentation of glucose to ethanol, etc [2]. In this work, the introduction of activated carbon into the crude liquid extract selectively adsorbed contaminants resulting in an increase in sclareol purity. Subsequently, sclareol in the purified extract was recovered by a liquid antisolvent process.

Antisolvent processes have been used to selectively separate many types of solid and liquid compounds from their solutions. One advantage of this process is that it eliminates the use of thermal energy that might degrade the biological activity of molecules, such as in pharmaceutical applications. In liquid antisolvent processes, water has generally been used as an antisolvent for hydrophobic compounds, while alcohols or other organic solvents have been used for hydrophilic compounds [3-5]. The introduction of the antisolvent results in preferential interactions between the solvent and antisolvent, with a concomitant disruption in the solvent-solute interaction, resulting in near instantaneous supersaturation and subsequent solute precipitation or liquid compound separation. A key factor in the antisolvent process is the degree of solubility between the solvent and the antisolvent. In the case of sclareol precipitation, the essential key is the degree of miscibility between ethyl

lactate and water. As is the case with ethanol, ethyl lactate is completely miscible with water. As a result, the addition of a given amount of water to the purified ethyl lactate extract resulted in a nearly complete precipitation of pure sclareol.

5.2. Experimental Procedure

5.2.1. Materials and Analysis

Field dried Clary Sage was supplied by Avoca Inc. (Merry Hill, NC). Ethyl lactate (CAS number 687-47-8; 98 % purity), ethyl acetate (CAS number 141-78-6; 99.9 % purity), and sclareol (CAS number 515-03-7; > 95 % purity) were supplied by Sigma-Aldrich. Carbon dioxide (CAS number 124-38-9; > 99.99 % purity) was supplied by National Welders. These chemicals were used without further purification. Activated carbon (CAS number 7440-44-0, 50-200 mesh or 74-297 μm particle size) was supplied by Fisher Scientific. The concentration of sclareol in ethyl lactate was determined by gas chromatography-Flame Ionization Detection (GC-FID). GC analyses [11] were performed using an HP 6890N GC with conditions of analysis as follows: Column: 30 meter DB-5 (methyl-phenyl bonded phase, J & W Scientific) with a 0.32 mm I.D. and a 0.25 μm phase thickness; Carrier gas: UHP Helium (National Welders) at a linear gas velocity of approximately 28 cm/sec; Injector temperature: 275 ^{o}C; FID Detector temperature: 310 ^{o}C; Temperature program: 60 to 310 ^{o}C at 4 degrees/minute. Data was collected using the Perkin-Elmer Total Chrom 6.2 chromatographic analysis system. GC-MS analyses were performed using an Agilent 19091S-433 with conditions of analysis as follows: Column: 30 meter HP-5MS (5 % phenyl methyl siloxane) with a 0.25 mm I.D. and a 0.25 μm phase thickness; Carrier gas: Helium at

an average velocity of 38 cm/sec; Injector temperature: 275 ^{o}C; Temperature program: 160-350 ^{o}C at 4 degrees/minute. The absorption spectra of the plant extracts were generated using a Jasco V-550 UV/Vis spectrophotometer.

5.2.2. Purification of the Ethyl Lactate and CO_2 Extract with Activated Carbon

The purification of the plant extract (w_{EL}^{*} = 0.09, 6.89 MPa) using activated carbon was performed at 323.15 $\pm$ 1 K. The effects of contact times (30-210 min) and activated carbon concentrations (14-242 g/L) on the extract purity were investigated. A given activated carbon concentration was added to a vial containing 2 mL extract, which was kept in an oven (VWR Scientific, model 1330 FM) maintained at a fixed temperature. The solution was then stirred for a specified time. Subsequently, the solution was quickly transferred into another vial through a syringeless filter (Whatman Autovial, Teflon® membrane with 0.45 μm pore diameter) to trap the spent carbon. The volume of the collected extract was measured, and the amount of sclareol in the collected extract was quantified by GC analysis. The purity of sclareol in the collected extract in terms of weight fraction was determined. In addition, the UV visible spectra, GC, and GC-MS chromatograms of the extracts before and after treatment with the activated carbon were generated in order to determine which compounds were removed by adsorption.

5.2.3. Recovery of Sclareol from the Purified Extract via Water Anti-Solvent Process

Solubility of sclareol in the mixture of ethyl lactate and water

The solubility of sclareol in the mixture of ethyl lactate and water was determined at 298.15 $\pm$ 1 K. Mixtures of ethyl lactate and water with various compositions were prepared.

An excess amount of pure sclareol was then added to each mixture. The solution was stirred to allow the system to rapidly reach equilibrium. After 4 hours, the solution was quickly transferred into a vial through a syringeless filter to trap any un-dissolved sclareol. A known volume of the filtered solution was withdrawn and placed into a pre-weighed vial. The solvent was evaporated in the oven for 2-3 days at 318.15 $\pm$ 1 K and the weight of the vial plus residue was regularly monitored. After complete solvent removal, the weight of sclareol was recorded and compared with the results from GC analysis. For GC, a known volume of ethyl lactate was added to the vial to re-dissolve sclareol. The solution was then injected into the GC in order to determine the sclareol concentration. Subsequently, the solubility value for sclareol under the conditions of the experiment was evaluated and the ternary phase diagram was generated.

Water antisolvent process

The performance of water as an antisolvent for sclareol in extracts with variable sclareol purity was examined. A known volume of the purified extract with known sclareol concentration was prepared. Water was added to the extract until the desired concentration was achieved. This was determined from the solubility data of sclareol in mixtures of ethyl lactate and water. Once water was added, the solution became cloudy. The mixture was then cooled (278.15 $\pm$ 1 K) overnight to enhance sclareol precipitation. At a given level of solution purity, resulting from contacting with various ratios of activated carbon to sclareol extract, the formation of three phases was observed: an oily phase lighter than water-ethyl lactate phase; a water-ethyl lactate phase; and a solid precipitate phase consisting primarily

of sclareol. The solid precipitate phase was separated from the solution via vacuum filtration (Millipore, PVDF membrane with 0.45 μm pore diameter). The oil phase, consisting of a thin film floating on the top of the solution, could be easily separated with a spatula.

After drying each of the phases in an oven for 2-3 days (318.15 K) in order to remove residual solvent, the concentration of sclareol in each phase was determined by GC-FID and expressed as a weight fraction. A known weight of the solid precipitate or oil phase was dissolved in a known volume of ethyl lactate, and the amount of sclareol in the solution was quantified by GC analysis. Afterward, the percentage weight ratio of the sclareol to the extract was determined as the extract purity. The amount of the non-precipitated sclareol was determined from the GC analysis of the sclareol concentration in the water-ethyl lactate phase. The total mass of the oil and the solid precipitate phases as well as the distribution of the phase-separated sclareol in each phase was determined from the mass balance calculation.

5.3. Results and Discussions

5.3.1. Purification of the Ethyl Lactate and CO_2 Extract with Activated Carbon

The process of purification by activated carbon involves the adsorption of impurities from the crude liquid extract by strong physicochemical bonding within the porous structure of the carbon. One important factor in the carbon adsorption process is the contact time between the solution and the carbon, which should be chosen to be sufficiently long to achieve adsorption equilibrium [7, 8]. The experiment to study the effect of contact time on the adsorption capability was performed at approximately 0.1 volume ratio of activated

carbon to extract and at 323.15 $\pm$ 1 K. The activated carbon (~120 mg) was mixed with the solution (2 mL) using a 0.2 mL magnetic stir bar (Fisher Scientific) for a fixed period of time, ranging from 30 to 210 minutes. The solution was then filtered and sclareol concentration in the solution was quantified by GC analysis. Under these experimental conditions, the sclareol concentration after treatment with the activated carbon is relatively the same as its concentration in the original solution, thus demonstrates negligible adsorption of sclareol onto the activated carbon. The extract purity after treatment with the activated carbon was also determined. By knowing the extract purity and the sclareol concentration in the solution before and after treatment with activated carbon, the percentage of sclareol and impurities adsorbed could be calculated, as illustrated in Figure 5-1. The adsorption of impurities increased as the contact time increased from 30 to 90 minutes, while a contact time longer than 90 minutes did not markedly enhance the adsorption of impurities. Therefore, for the remaining purification experiments, 90 minutes was selected as the contact time for adsorption on activated carbon. A shorter contact time can possibly be achieved if the mixing method between the solution and the activated carbon is improved.

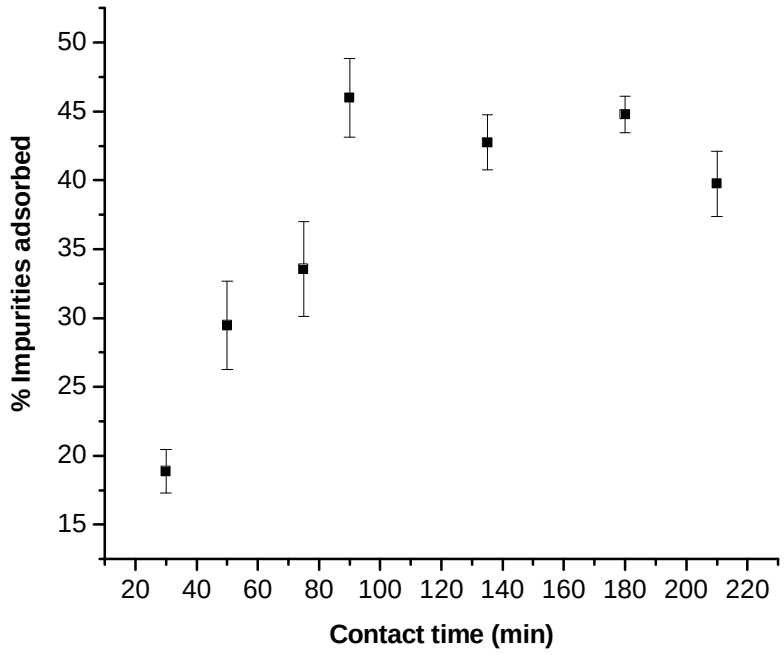

Figure 5-1. Plot of % total impurities adsorbed as a function of contact time.

The effect of the proportion of activated carbon to crude sclareol extract on the extract purity and sclareol yield was investigated. Different amounts of activated carbon were added to vials containing 2.0 mL extract. The amounts of activated carbon used in the experiments are summarized in Table 5-1. After stirring the mixture for 90 minutes, the solution was filtered, and the volume of collected extract, the sclareol concentration in the collected extract, and the extract purity were analyzed.

Figure 5-2 shows the % sclareol yield as a function of activated carbon concentration. Percent sclareol purity increased with increasing activated carbon concentration. Sclareol purity was increased from 64.8 to 79 % (w/w) of sclareol when 60 g/L of activated carbon was introduced. Further addition of activated carbon up to 242 g/L did not significantly

increase the extract purity. Figure 5-2 also shows the % sclareol yield based on the difference in the sclareol concentration before and after treated with the activated carbon. The decrease in % sclareol yield as the activated carbon concentration increases beyond 60 g/L of extract indicates that up to approximately 8 % of sclareol is adsorbed onto the carbon.

The % sclareol yield in Figure 5-3 was calculated from the difference in the total mass of sclareol in the extract before and after treatment with the activated carbon. This calculation took into account the loss of the extract volume during treatment with the activated carbon due to the holdup of liquid in the activated carbon particles. For the range of conditions studied, the % liquid holdup varied from 12 to 35 vol. %. In a real-world process, filtration and recovery would likely be improved by applying vacuum or pressure [7].

Table 5-1. Various amounts of activated carbon used for purification experiments.

Sample	Activated Carbon Conc. (g/L)	Activated Carbon/Extract Volume Ratio
1	14	0.02
2	32	0.05
3	60	0.1
4	121	0.2
5	242	0.4

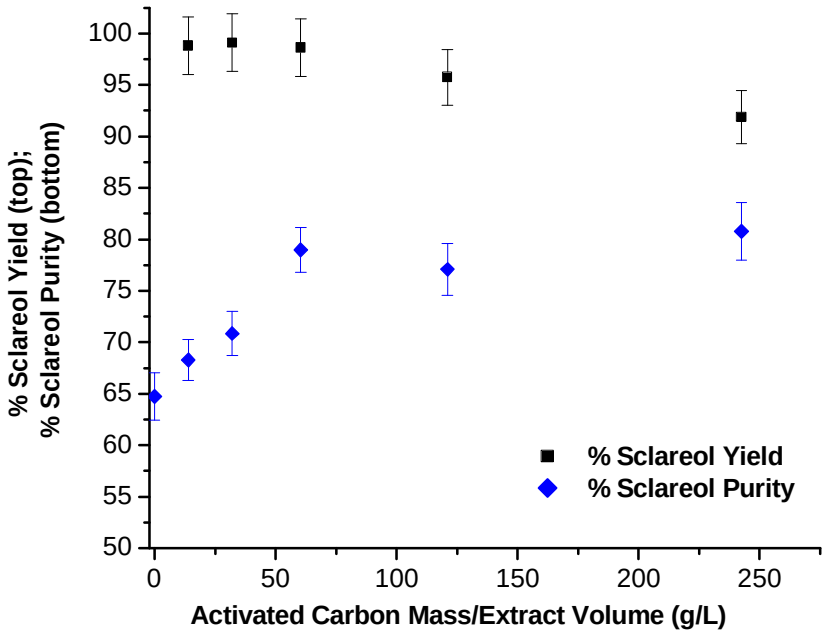

Figure 5-2. Plot of % sclareol yield and % sclareol purity as a function of activated carbon concentration. The calculation of yield assumes negligible loss of the extract volume during activated carbon treatment.

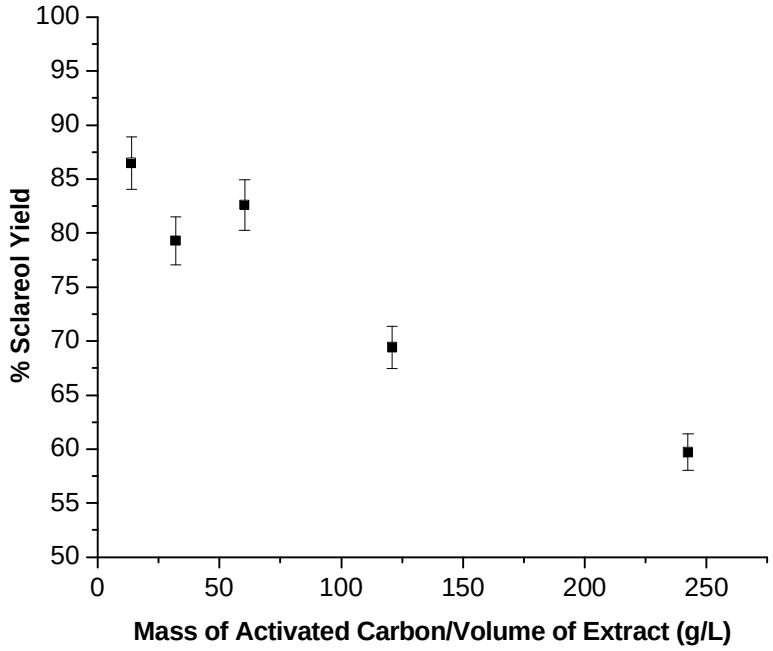

Figure 5-3. Plot of % sclareol yield versus activated carbon concentration. The calculation of yield takes into account the loss of the extract volume during activated carbon treatment.

Likely impurities contained in the plant extract include mono- and sesquiterpenes, fatty acids, polyphenols, waxes, wax esters, plant pigments such as chlorophylls and carotenoids and their degradation products [9]. Figure 5-4 compares the absorption spectra of the extracts before and after treatment with various amounts of activated carbon. The extract absorption in the wavelength range of 250-400 nm is partially due to the presence of polyphenols, waxes, and wax esters which mainly absorb at 250-350 nm and some kinds of carotenoids (or similar compounds) which generally absorb at 320-550 nm. A significant decrease in absorption intensity in the wavelength range of 250-400 nm is clearly observed in Figure 5-4 as the amount of activated carbon is increased. These absorption spectra permit qualitative observation of the removal of some impurities with the activated carbon.

Chlorophylls are minor impurities in the extract. As is seen in Figure 5-4, there is a relatively small peak observed in the absorption range of chlorophylls (600-700 nm). Gross et al. [10] reported that in diethyl ether, chlorophyll *a* (major pigment in green plants) has approximate absorbance maxima of 430 nm and 662 nm while chlorophyll *b* has absorbance maxima of 453 nm and 642 nm. The amount of chlorophyll *a* in the extract before and after treatment with activated carbon was determined according to the Beer-Lambert law [11]. By measuring the absorption spectra of relatively pure chlorophyll *a* (Sigma Aldrich; CAS number 479-61-8; ~ 95 % purity) in ethyl lactate at various concentrations, the molar extinction coefficient could be determined as 66.91 g/(L.cm) at a maximum peak of 665 nm. The percentage of chlorophyll *a* in each extract was then calculated and plotted as a function of w_{EL}^{*} in Figure 5-5, assuming that the absorbance in the range of 600-700 nm is solely due to chlorophyll *a*. It is observed from this plot that there is a decrease in the amount of chlorophyll *a* at increasing activated carbon concentrations.

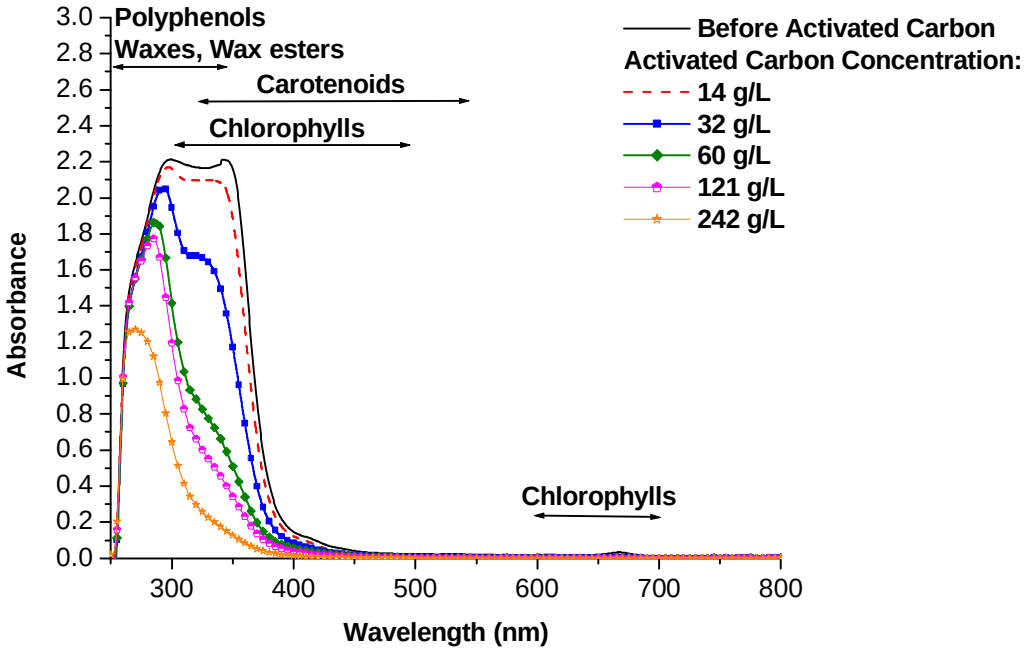

Figure 5-4. UV-Visible spectra of the extracts before and after treatment with various activated carbon concentrations.

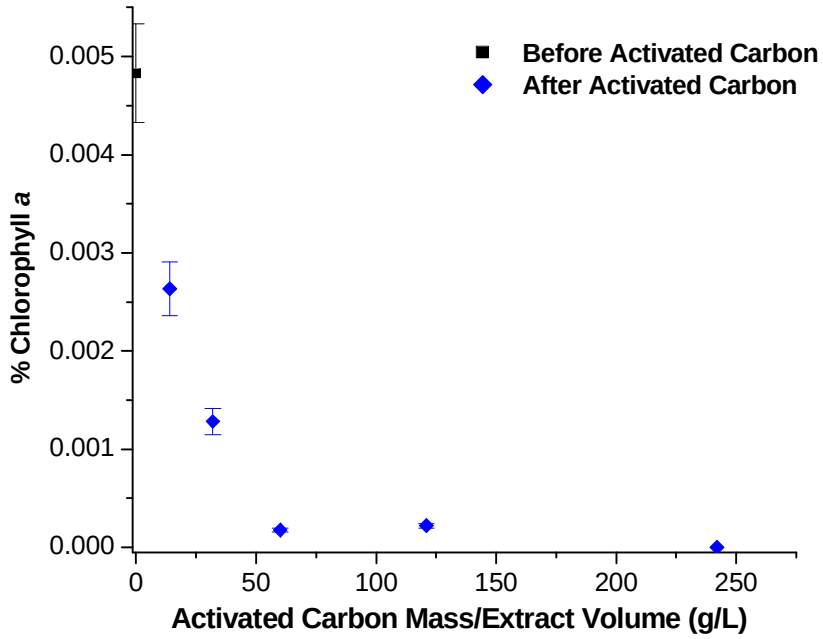

Figure 5-5. Plot of % chlorophyll *a* as a function of activated carbon concentration.

Figure 5-6 displays the chromatograms of the plant extracts before and after treatment with two different activated carbon concentrations, 32 and 242 g/L respectively. For this analysis, the extract solvent (ethyl lactate) was completely evaporated and the extract was re-dissolved in ethyl acetate. This step is necessary to minimize the interference of the solvent impurities in the analysis. Due to solvent evaporation, however, we would most likely lose some of the impurities that have boiling points close to ethyl lactate or lower, such as linalyl acetate, linalool, monoterpenes, and sesquiterpenes. In addition, some of the relatively high molecular weight components possibly present in the extract, such as plant pigments, waxes, and wax esters, are not observed in the chromatogram due to the instrument limitation.

Figure 5-6 qualitatively shows a decrease in the intensity of the peaks at increasing amounts of activated carbon, more appreciably for the peaks eluting after the sclareol peak. This is confirmed by the GC-MS analysis of the extracts shown in Figure 5-7 and Figure 5-8. In Figure 5-7, the amount of hydrocarbons and plant sterols noticeably decreased as the activated carbon concentration increased. In Figure 5-8, a qualitative reduction of some monocyclic and bicyclic diterpenes and diterpenoids, such as cembrene, manool, manoyl oxide, was examined.

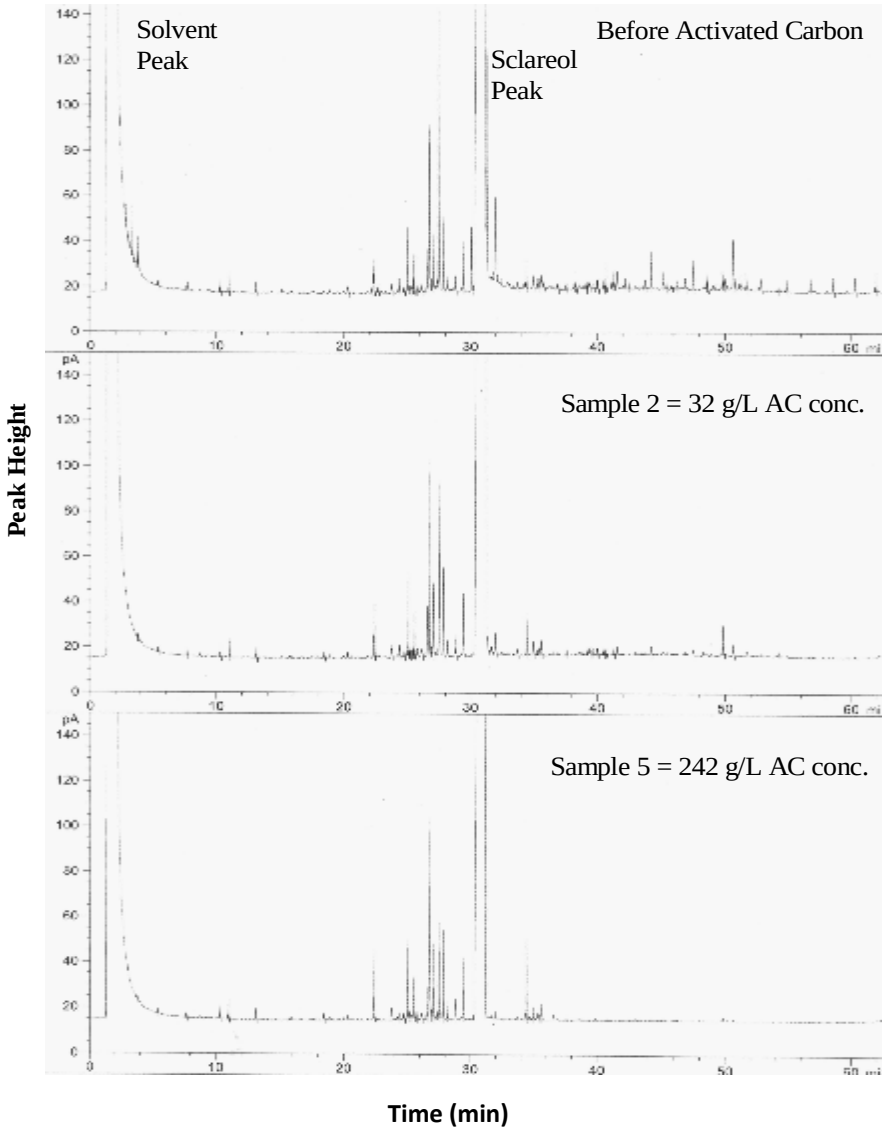

Figure 5-6. Chromatograms of the extracts before and after treatment with two different activated carbon concentrations.

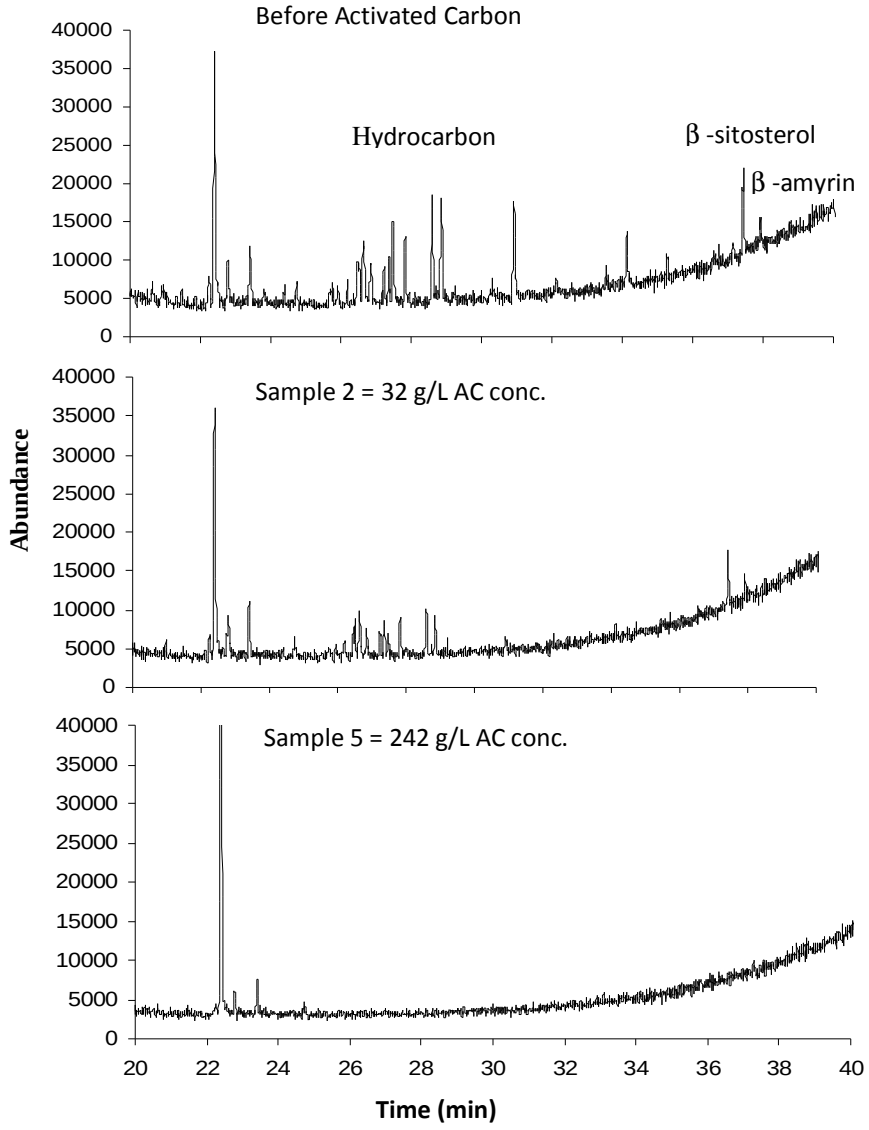

Figure 5-7. GC-MS chromatograms showing the peaks of impurities that elute after sclareol.

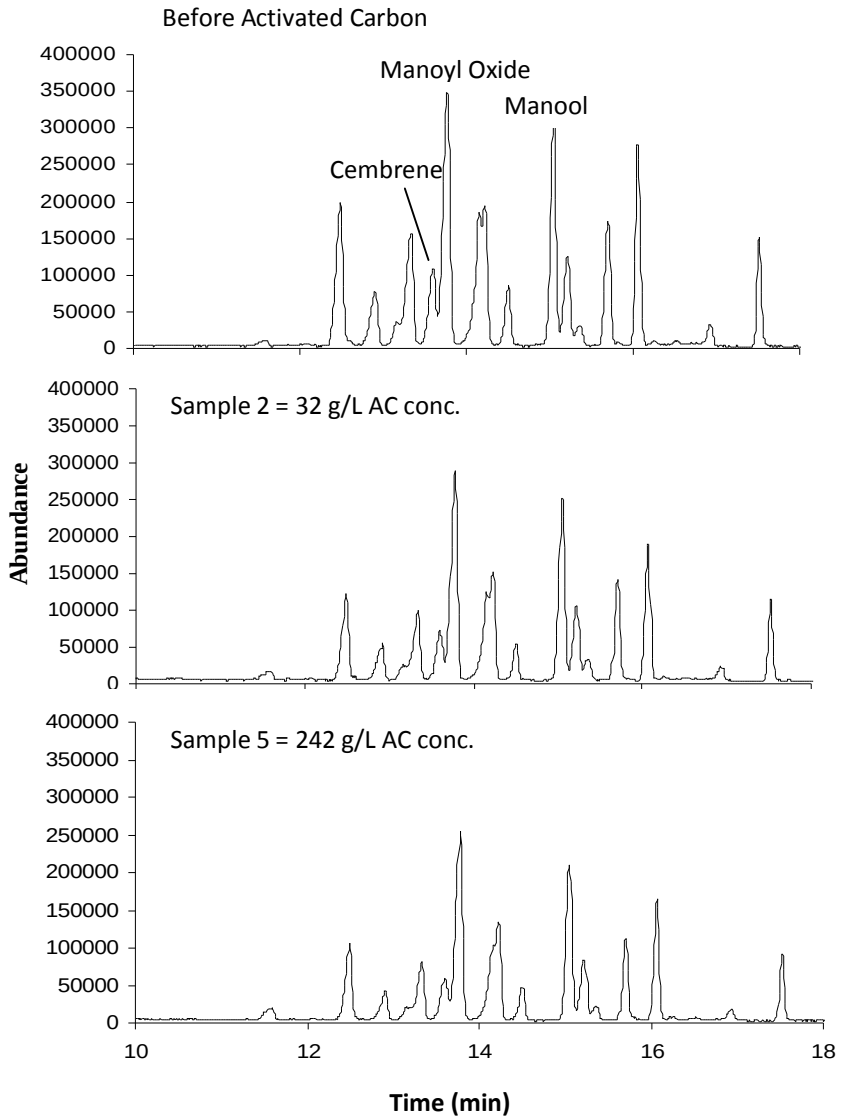

Figure 5-8. GC-MS chromatograms showing the peaks of impurities that elute before sclareol.

In summary, activated carbon can be used to remove some impurities in the plant extract, and the adsorption of the sclareol on the carbon is relatively small under the conditions investigated.

While not a part of this investigation, it is important to note that in terms of an industrial process, the spent activated carbon used for partial purification of sclareol can be regenerated by one of several methods, including thermal, chemical, and steam treatments [7]. In thermal regeneration, the contaminants adsorbed are removed by heating the exhausted carbon in the kilns at high temperatures typically ranging from 773.15-1073.15 K. This method is effective at regeneration, however, it requires large amount of energy and expensive equipment. There is also a characteristic loss of 5-10 % of the carbon from excessive burn off [12]. Some advantages of the steam and chemical regeneration over thermal method are higher recovery of regenerated carbon, possible recovery of valuable adsorbates, and potential reuse of the solvents after proper subsequent treatments [13]. Since the stream regeneration is only effectively used to remove volatile compounds, the chemical regeneration is therefore the most promising method for our system and further research must be conducted for selecting the proper chemical (organic solvents) that can facilitate affinity or solubility [12, 14].

5.3.2. Recovery of Sclareol from the Purified Extract via Water Anti-Solvent Process

Sclareol is highly insoluble in water whereas ethyl lactate and water are completely miscible. When water is added into the liquid extract, it preferentially interacts with the ethyl lactate solvent, effectively preventing it from solvating the sclareol and remaining impurities in the solution. This results in solute precipitation. The solubility of pure sclareol in various compositions of ethyl lactate and water was investigated at 298.15 $\pm$ 1 K. The results are plotted in Figure 5-9. It is observed that complete precipitation of sclareol is achieved when the percentage of water in the solvent mixture approaches 75 % (w/w). This concentration of water was therefore selected as the starting point for the water antisolvent experiments.

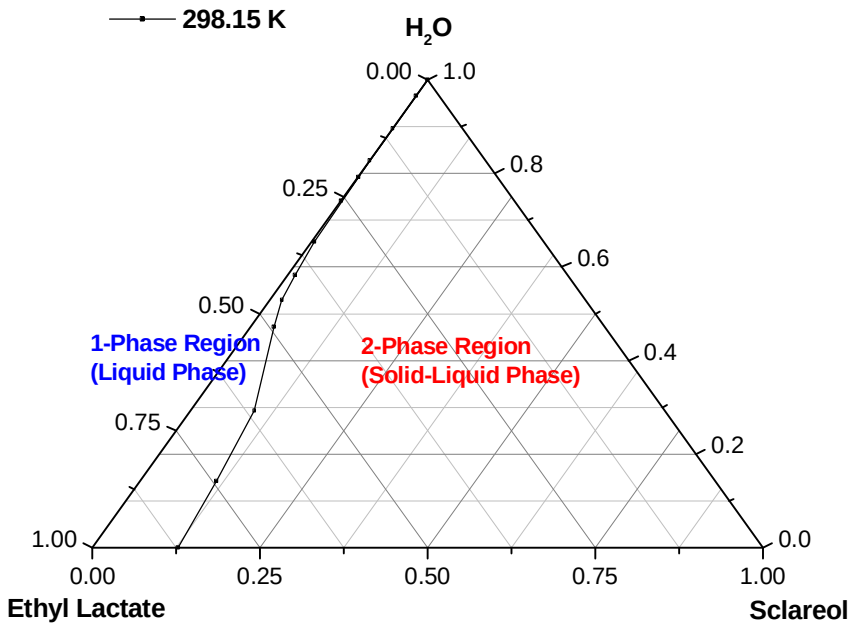

Figure 5-9. Experimental ternary phase diagram of sclareol-ethyl lactate-water at 298.15 K and ambient pressure.

Five samples with varying sclareol content and extract purity were obtained from the activated carbon purification experiments. These extracts were used in the water antisolvent precipitation experiments. The experiments were performed at a constant ratio of water to ethyl lactate, which was set at ~ 78 % (w/w) of water to ethyl lactate solution. Once water was added, the solution became cloudy, as shown in Figure 5-10, and the previously homogeneous solution immediately separated into three phases, consisting of a yellowish upper oil phase, an ethyl lactate-water phase, and a solid precipitate phase, for all samples except for sample 5. Sample 5 was treated with the highest amount of activated carbon, and

resulted in near-complete removal of the components responsible for the formation of the oil phase.

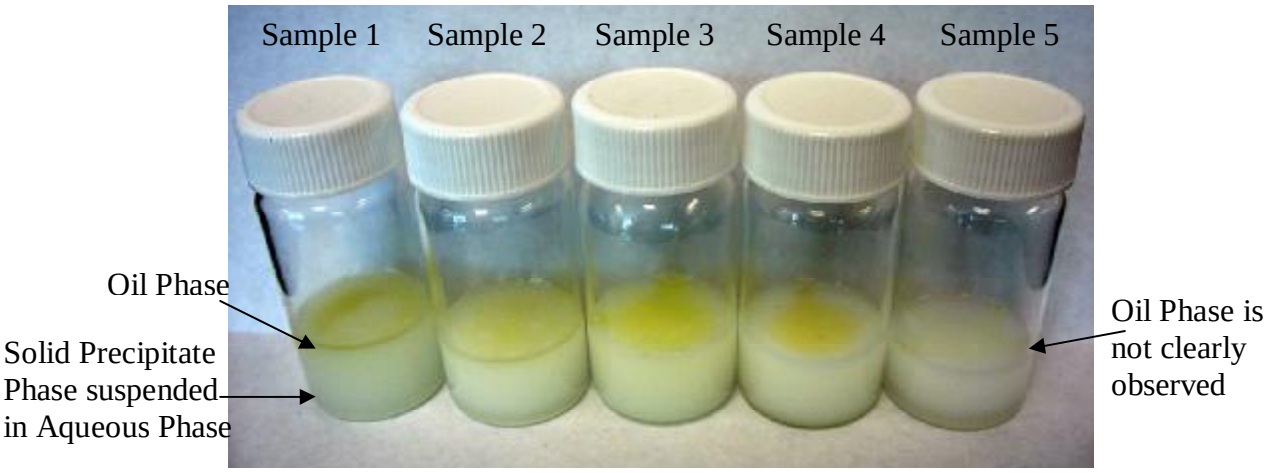

Figure 5-10. Picture of the various extracts after water is added. The purity of the extract before water is added in % (w/w): sample 1 = 68.3, sample 2 = 70.9, sample 3 = 77.6, sample 4 = 79, sample 5 = 80.8. The activated carbon concentration used to purify the extract in g/L: sample 1 = 14, sample 2 = 32, sample 3 = 60, sample 4 = 121, sample 5 = 242.

The calculation of % sclareol purity in the oil and precipitate phase showed that the solid precipitate phase purity ranged from 92-97 % (w/w) while the sclareol content of the oil phase ranged from 63-77 % (w/w), as illustrated in Figure 5-11. The GC analysis of the sclareol concentration in the water-ethyl lactate (aqueous) phase implied the nearly complete phase separation of sclareol (97-99 %). From the mass balance calculation, the distribution of the phase-separated sclareol in each phase was determined and plotted as a function of the extract purity before it was mixed with water in Figure 5-12 and Figure 5-13. The slight increase in the extract purity by addition of the largest ratio of activated carbon has a considerable effect on the formation of the phases. The formation of the oil phase becomes indistinct with a relatively slight increase in the extract purity.

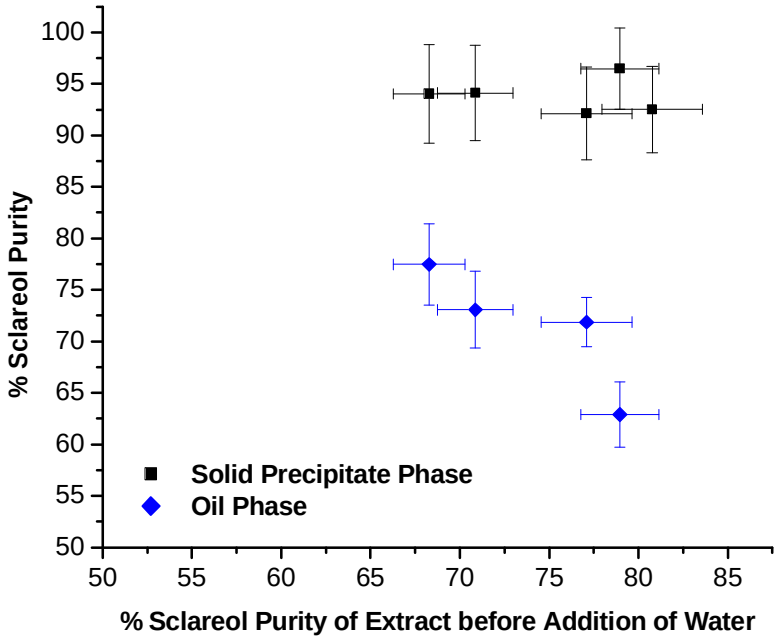

Figure 5-11. The percentage of sclareol in the oil and solid precipitate phases as a function of the sclareol purity of the ethyl lactate extract before mixing with water.

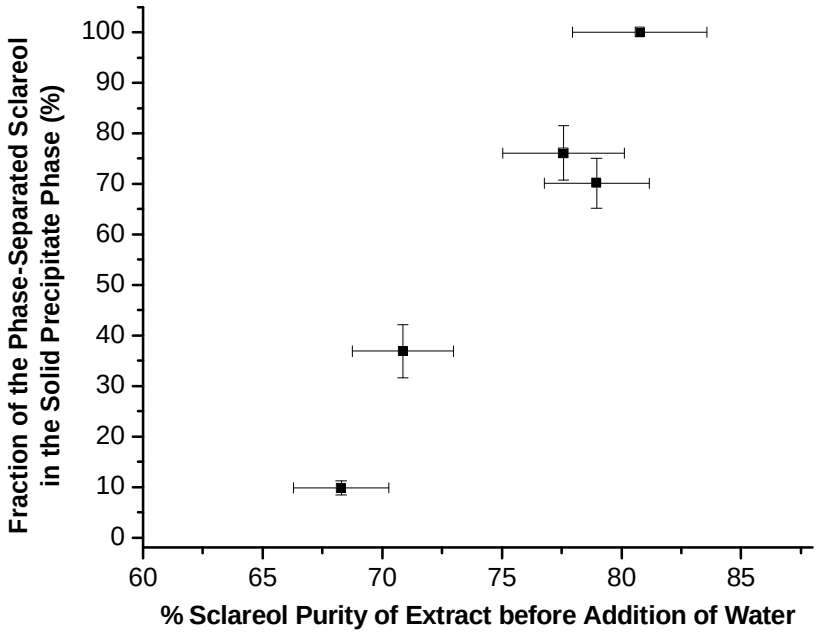

Figure 5-12. The percentage of sclareol from the total mass of phase-separated sclareol found in the solid precipitate phase, as a function of % sclareol purity in the ethyl lactate extract before water is added.

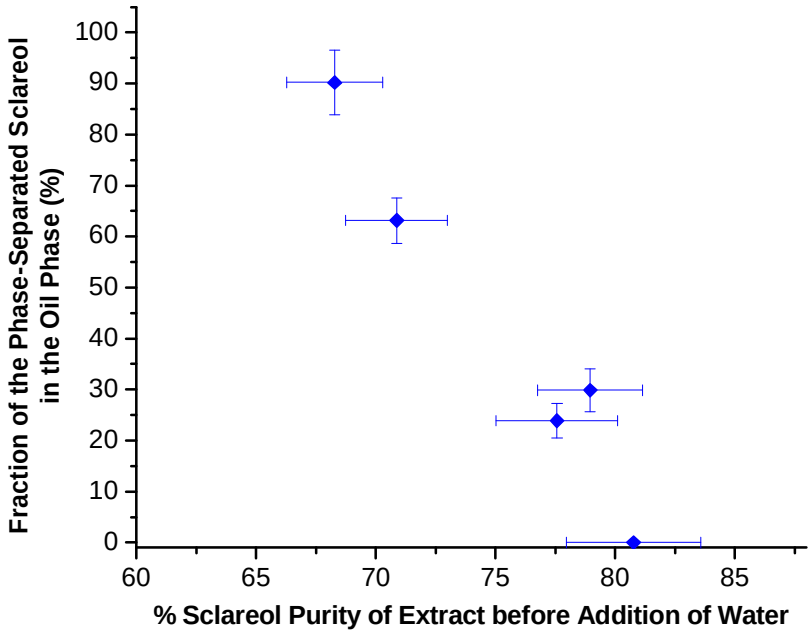

Figure 5-13. The percentage of sclareol from the total mass of phase-separated sclareol in the oil phase, as a function of % sclareol purity in the ethyl lactate extract before water is added.

The analysis of the aqueous ethyl lactate phase revealed that almost all sclareol was phase separated upon mixing the ethyl lactate extract with water. Notably, some of the impurities that are relatively more hydrophilic than sclareol remained dissolved in the solution. Figure 5-14 describes the % sclareol in the total mass of substances that phase-separated, as a function of the % sclareol purity before the ethyl lactate extract was mixed with water. The data in this plot all falls above the 45^{o} line, and this clearly shows the increase in the extract purity with the addition of water as some impurities remained dissolved in the solution.

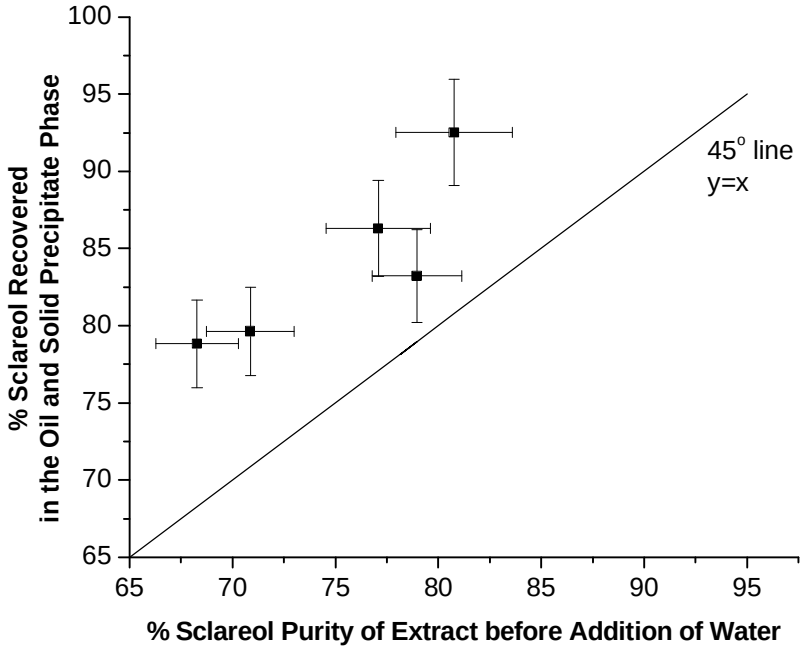

Figure 5-14. The total percentage of sclareol recovered in both the oil and solid precipitate phases, as a function of % sclareol purity of extract before water is added.

5.4. Conclusions

Activated carbon can be used to remove some of the impurities found in the initial CO_2-ethyl lactate extraction of Clary Sage. These impurities include such components as polyphenols, waxes, wax esters, etc., in the CO_2 + EL extract (w_{EL}^{*} = 0.09, 6.89 MPa). The purity of the extract increases while the sclareol yield decreases with the use of higher amount of activated carbon. The mixing of water (> 75 % (w/w)) in the residual ethyl lactate extract remaining after venting of the CO_2 from the mixture results in the formation of a three phase mixture consisting of an oil phase, an aqueous ethyl lactate phase, and a solid precipitate phase. Extract purity governs the formation of these phases to a significant extent.

The extract treated with the highest activated carbon concentration did not demonstrate the formation of an appreciable quantity of oil phase upon addition of water. In summary, the purification of the CO_2 + EL extract using activated carbon followed by sclareol precipitation with water is promising. Applying 60 g/L activated carbon increased the extract purity from 65 to 79 % (w/w) of sclareol, and addition of water to this extract caused ~ 70 % of the phase-separated sclareol to go in the solid precipitate phase in approximately 97 % (w/w) purity. The application of 242 g/L of activated carbon did not significantly enhance the extract purity and resulted in lower sclareol yield due to some adsorption of sclareol by the activated carbon and the holdup of the liquid extract in the activated carbon. At this high activated carbon level, the formation of oil phase did not occur upon addition of water, and sclareol with a purity of 93 % (w/w) was obtained as the precipitate.

5.5. Separation of Ethyl Lactate and Water using Vacuum Distillation

The remaining solution after purification of the plant extract with activated carbon and recovery of sclareol using water as the antisolvent is a mixture of ethyl lactate and water. In an industrial process, the ethyl lactate-water phase would need to be separated and the individual liquid components recovered using vacuum distillation. The ethyl lactate could then be recycled for re-use in the extraction step of the process while the recovered water could be re-used for the liquid antisolvent step of the process. In this section, we discuss a simple vacuum distillation process simulation for ethyl lactate and water using Aspen Plus 2004.1.

Distillation is a unit operation used for the separation of constituents of mixtures by partial evaporation. It is based on the fact that vapor is relatively richer in the component

with the highest vapor pressure, which is the more volatile component. Industrial-scale distillation at moderate vacuum can be characterized by the use of conventional distillation equipment. Its lowest pressure limit is on the order of 1 torr or 0.00013 MPa [15]. Vacuum distillation increases the relative volatility of the key components in many applications, which means that the components are more separable. As a result, it requires fewer number of equilibrium stages in the distillation column to achieve the same separation between overhead and bottom products. Consequently, it reduces the capital cost of the equipment. In addition, the reduced temperature requirement at lower pressure decreases the possibility of product degradation. The drawback of vacuum distillation is the relatively higher operating costs.

In distillation calculation using Aspen, one important issue is the selection of an appropriate physical property method that will accurately describe the phase equilibrium of the chemical component system [16]. The program Aspen Plus has a large number of alternative methods. For liquid systems, NRTL and UNIQUAC are commonly employed. The available isothermal vapor liquid equilibrium data for the water and ethyl lactate system, as described in Figure 5-15 were used to regress the model parameters in Aspen. The calculated data from NRTL and UNIQUAC are compared with experimental data in Figure 5-16, Figure 5-17, Figure 5-18, and Figure 5-19. As shown in these figures, the system has an azeotrope, occurring at 5-7 mol % ethyl lactate [17].

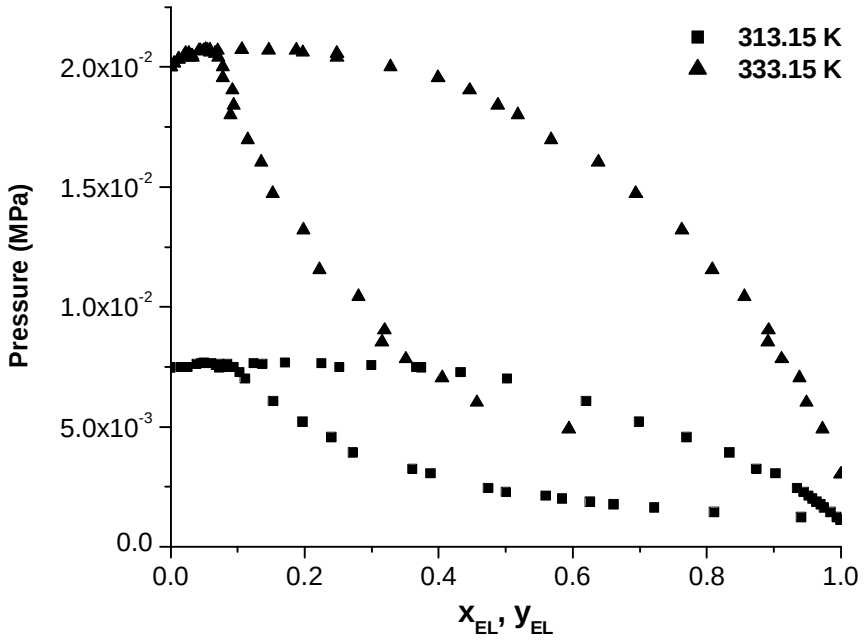

Figure 5-15. Isothermal vapor liquid equilibrium data of ethyl lactate and water system at 313.15 and 333.15 K [17].

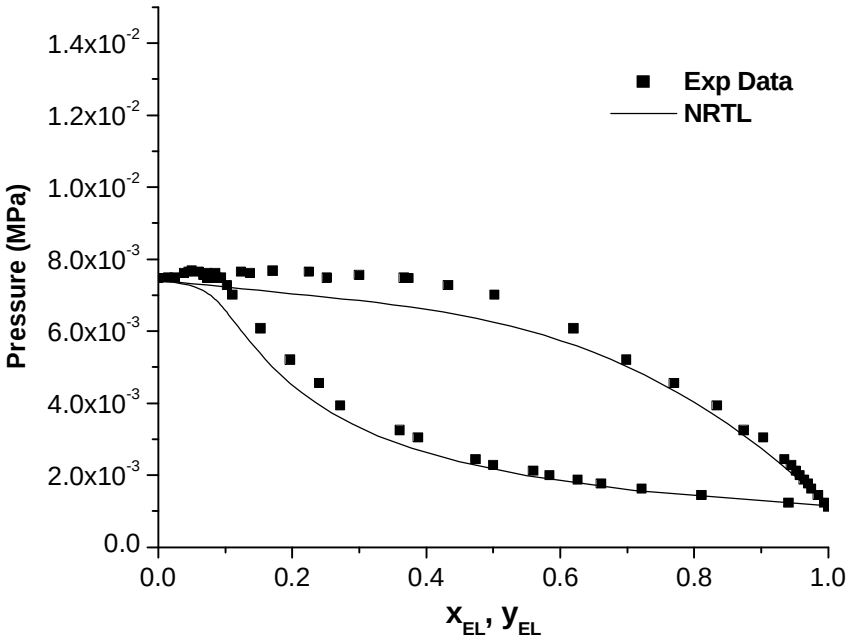

Figure 5-16. Comparison of experimental and calculated vapor liquid equilibrium data of ethyl lactate and water system using NRTL at 313.15 K.

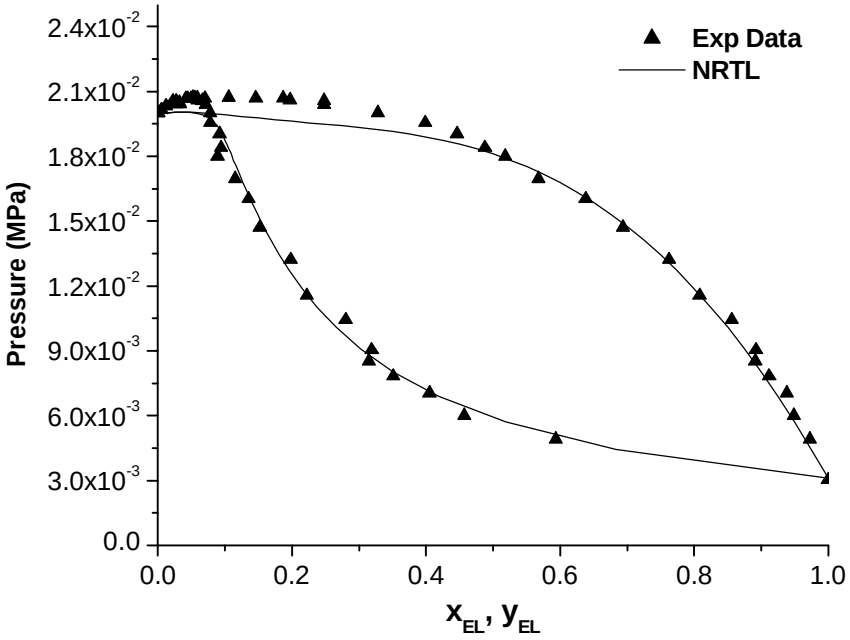

Figure 5-17. Comparison of experimental and calculated vapor liquid equilibrium data of ethyl lactate and water system using NRTL at 333.15 K.

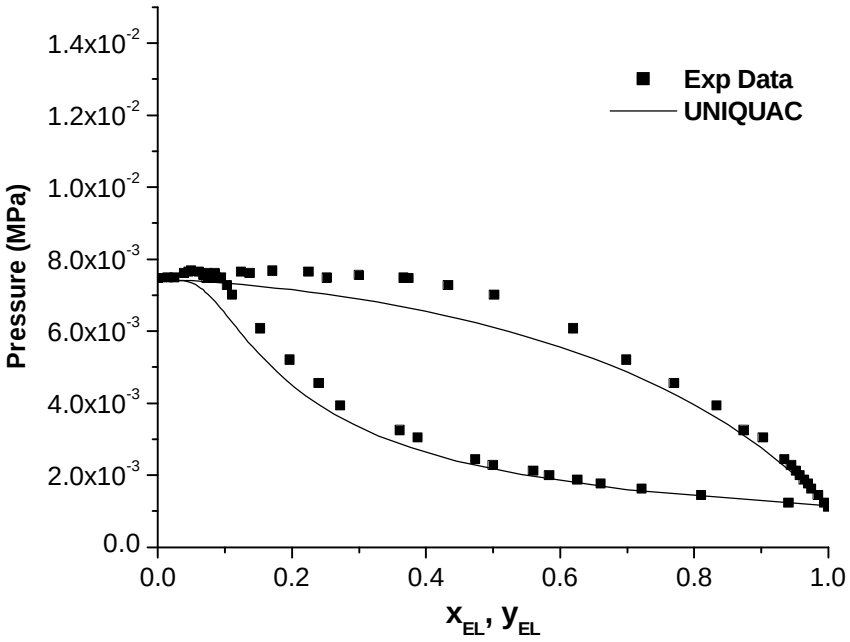

Figure 5-18. Comparison of experimental and calculated vapor liquid equilibrium data of ethyl lactate and water system using UNIQUAC at 313.15 K.

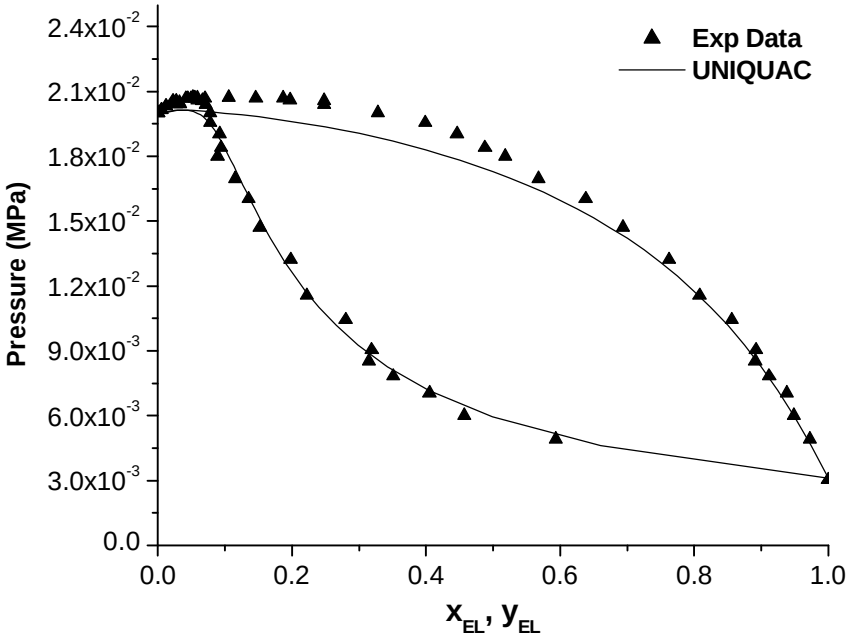

Figure 5-19. Comparison of experimental and calculated vapor liquid equilibrium data of ethyl lactate and water system using UNIQUAC at 333.15 K.

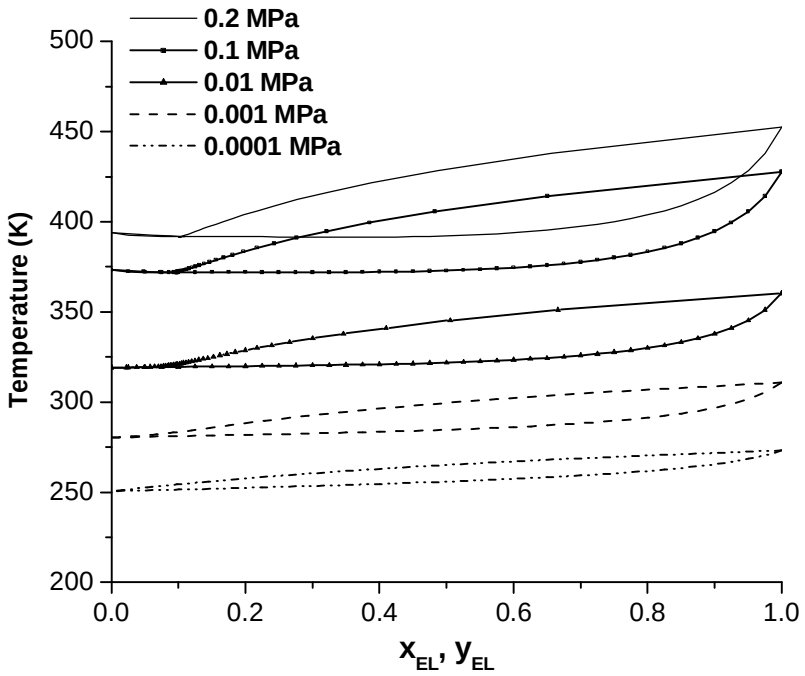

Figure 5-20. Calculated vapor liquid equilibrium data of ethyl lactate and water system using NRTL at various pressures.

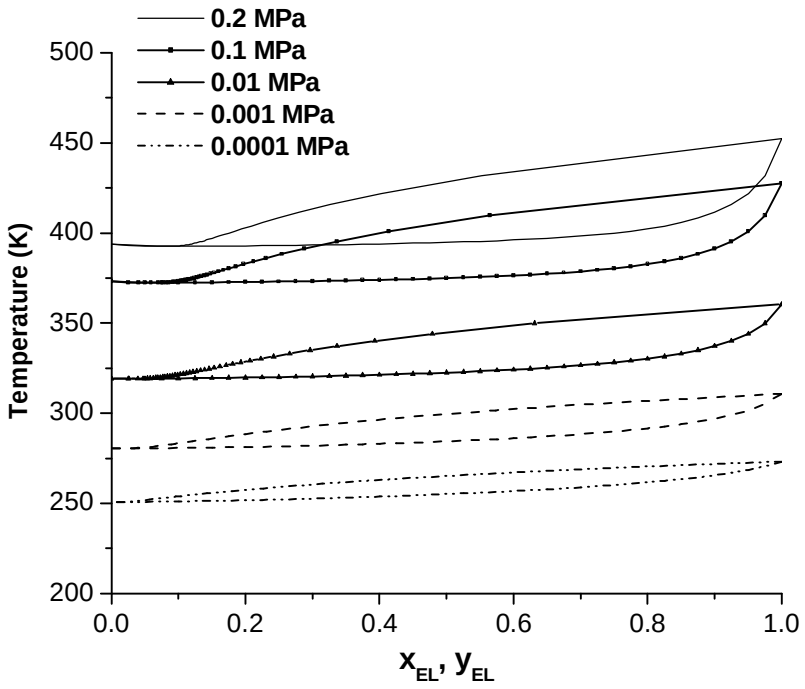

Figure 5-21. Calculated vapor liquid equilibrium data of ethyl lactate and water system using UNIQUAC at various pressures.

From Figure 5-20 and Figure 5-21, it is observed that as pressure is reduced the system azeotrope occurs at a lower molar composition of ethyl lactate, and breaks at a pressure lower than 0.001 MPa. These VLE data indicate that vacuum distillation should be applied to our system in order to obtain products with 99.9 mol % water in the distillate and 99.9 mol % ethyl lactate in the bottom. In the next paragraphs, we discuss the required parameters and the effect of varying some parameters in the process simulation. The schematic of the distillation process is shown in Figure 5-22.

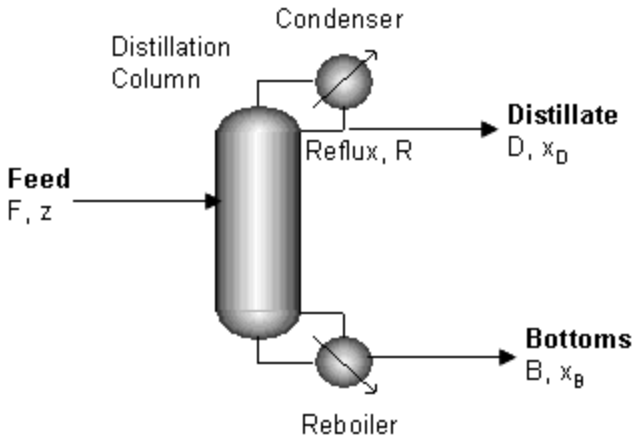

Figure 5-22. Schematic of distillation process.

The design of distillation column involves many parameters: product compositions, product flowrates, operating pressure P, total number of trays N_T, feed tray location N_F, distillate D, reflux ratio RR (a ratio of liquid reflux R to distillate D), reboiler heat input, condenser heat removal, column diameter, and column height. In typical distillation design, the feed conditions (temperature T_F, pressure P_F, flow rate F, and composition z) and the desired product compositions (the heavy-key impurity in the distillate $x_{D,HK}$ and the light-key impurity in the bottoms $x_{B,LK}$) are given.

In simulating the distillation process to separate ethyl lactate and water, the feed composition was specified as 96 mol % water. This value was calculated from the sclareol precipitation process using water as the antisolvent. The feed temperature and pressure were set at ambient conditions. For achieving the 99.9 mol % of ethyl lactate in the bottom and 99.9 mol % water in the distillate, the distillate rate D was calculated as 0.96 mol/s according to equation (1) by assuming the feed molar flow rate of 1 mol/s [16].

$$D = F\left(\frac{z - x_B}{x_D - x_B}\right) \quad (1)$$

where F is the feed flow rate and z, x_B, x_D are the light component molar compositions in the feed, bottom, and distillate, respectively.

The simulation was run at various pressures with constant feed conditions and distillate rate, and NRTL was chosen for the physical property model. Using the "Design Spec/Vary" function, the reflux ratio was manipulated to achieve the desired product compositions [16]. With the specified number of stages, the feed stage was varied to find the minimum reboiler heat consumption [18]. With the fixed ratio of the total number of stages to the feed stage, the number of stages was decreased until the required reflux ratio became large.

Table 5-2 shows the effect of operating pressure on the required condenser temperature. A decrease in pressure causes a decrease in temperature, which finally results in higher heat removal expense since refrigeration must be used in the condenser. Cooling water is the typical heat sink used in the condenser. It is commonly available at 305 K and is less expensive than refrigeration. Hence, condenser temperature is one important criterion in selecting the proper operating pressure. Table 5-3 shows the effect of pressure on the required number of stages as well as the reboiler heat duty. It can be seen that the required number of stages decreases with the operating pressure, which results in the reduced capital cost. At a certain pressure and number of stages, the feed stage was chosen to provide the minimum reboiler heat duty. The ratio of the number of stages to feed stage is close to a fixed value for each pressure, which is approximately 1.2 for 0.007 and 0.005 MPa, 2.6 for

0.001 MPa, and 1.7 for 0.0001 MPa. Additionally, it is shown in Table 5-3 that increasing the number of stages lowers the reflux ratio and the heat duty in the reboiler, consequently decreasing the operating cost and increasing the capital cost.

Table 5-2. Effect of pressure on condenser temperature.

Pressure (MPa)	Condenser temperature (K)
0.007	312.39
0.005	306.26
0.001	280.33
0.0001	250.54

Table 5-3. Effect of pressure on number of stages and reboiler heat duty.

P = 0.007 MPa

Number of stages (N_T)	Feed stage (N_F)	Reflux ratio (RR)	Heat duty (Watt)
90	83	10.67	4.88E+05
70	64	13.5	6.05E+05
50	37	38.03	1.63E+06

P = 0.005 MPa

Number of stages (N_T)	Feed stage (N_F)	Reflux ratio (RR)	Heat duty (Watt)
30	26	10.28	4.74E+05
27	23	15.85	7.06E+05
24	21	54.44	2.32E+06

P = 0.001 MPa

Number of stages (N_T)	Feed stage (N_F)	Reflux ratio (RR)	Heat duty (Watt)
15	6	5.09	2.60E+05
13	5	10	4.70E+05
11	4	48.47	2.11E+06

P = 0.0001 MPa

Number of stages (N_T)	Feed stage (N_F)	Reflux ratio (RR)	Heat duty (Watt)
10	6	0.89	7.99E+04
9	5	1.64	1.13E+05
8	5	18.76	8.61E+05

The height of a distillation column can be calculated using equation (2) if the number of stages (N_T) is known [16]. The diameter of the column is determined by the maximum vapor velocity. Since the vapor flow rates change from stage to stage in a nonequimolal overflow system, the stage with the highest vapor velocity will set the minimum column diameter. In the Aspen calculation, the cross-sectional area of the column is determined by dividing the volumetric vapor flow rate with the maximum vapor velocity. Table 5-4 summarizes the height and diameter of the column, corresponding to the number of stages and operating pressures.

$$L(meter) = 1.2(0.61)(N_T - 2) \quad (2)$$

Table 5-4. Height and diameter of the column at varied operating pressures and number of stages.

P = 0.007 MPa

Number of stages (N_T)	Feed stage (N_F)	Reflux ratio (RR)	Length (m)	Column diameter (m)
90	83	10.67	64.42	1.06
70	64	13.5	49.78	1.19
50	37	38.03	35.14	1.93

P = 0.005 MPa

Number of stages (N_T)	Feed stage (N_F)	Reflux ratio (RR)	Length (m)	Column diameter (m)
30	26	10.28	20.50	1.17
27	23	15.85	18.30	1.42
24	21	54.44	16.10	2.59

P = 0.001 MPa

Number of stages (N_T)	Feed stage (N_F)	Reflux ratio (RR)	Length (m)	Column diameter (m)
15	6	5.09	9.52	1.41
13	5	10	8.05	1.89
11	4	48.47	6.59	4.02

P = 0.0001 MPa

Number of stages (N_T)	Feed stage (N_F)	Reflux ratio (RR)	Length (m)	Column diameter (m)
10	6	0.89	5.86	1.59
9	5	1.64	5.12	1.89
8	5	18.76	4.39	5.23

It is clear that the lower operating pressures allow for the design of shorter columns with reasonable heights albeit with larger column diameters. In conclusion, the separation of ethyl lactate from water can be performed using a vacuum distillation process. Several parameters, such as operating pressure, number of stages, feed stage, etc. must be carefully considered in designing an efficient process. Aspen calculations show that the required number of stages decreases with pressure, which results in a decrease in capital cost and an increase in operating cost due to the need for refrigeration in the condenser. Moreover, the length of the distillation column is significantly dependent on the number of stages whereas its diameter is

dependent on the volumetric vapor flow rate and maximum vapor velocity, which are reliant on the operating conditions.

5.6. References

1. Tombokan, X., et al., *Extraction of sclareol from clary sage flower using mixtures of carbon dioxide and ethyl lactate.* Submitted to Journal of Supercritical Fluids.

2. Roy, G., *Activated carbon applications in the food and pharmaceutical industries*. 1995: CRC Press.

3. Zhao, H., et al., *Controlled liquid antisolvent precipitation of hydrophobic pharmaceutical nanoparticles in a microchannel reactor.* Industrial & Engineering Chemistry Research, 2007. **46**(24): p. 8229-8235.

4. Park, S., S. Jeon, and S. Yeo, *Recrystallization of a pharmaceutical compound using liquid and supercritical antisolvents.* Ind. Eng. Chem. Res, 2006. **45**(7): p. 2287-2293.

5. Settings, M., *Crystallization of sulfamethizole using the supercritical and liquid antisolvent processes.* The Journal of Supercritical Fluids, 2004. **30**(3): p. 315-323.

6. Finney, M., D. Danehower, and J. Burton, *Gas chromatographic method for the analysis of allelopathic natural products in rye (Secalecereale L.).* Journal of Chromatography A, 2005. **1066**(1-2): p. 249-253.

7. Cheremisinoff, P. and F. Ellerbusch, *Carbon adsorption handbook.* Ann Arbor Science Publishers Inc. Ann Arbor, Mich.,(04: 07 CHE), 1978: p. 1063.

8. How, J. and C. Morr, *Removal of phenolic compounds from soy protein extracts using activated carbon.* Journal of Food Science, 1982. **47**(3): p. 933-940.

9. Diaz-Reinoso, B., et al., *Supercritical CO_2 extraction and purification of compounds with antioxidant activity.* J. Agric. Food Chem., 2006. **54**(7): p. 2441-2469.

10. Gross, J., *Pigments in vegetables: Chlorophylls and carotenoids.* 1991: Van Nostrand Reinhold, New York.

11. Clark, B., T. Frost, and M. Russell, *UV spectroscopy: Techniques, instrumentation, data handling*. 1993: Springer.

12. Leng, C., *An investigation of the mechanisms of chemical regeneration of activated carbon*, in Industrial & engineering chemistry research. 1996. p. 2024-2031.

13. Cooney, D., A. Nagerl, and A. Hines, *Solvent regeneration of activated carbon.* Water Research, 1983. **17**(4): p. 403-410.

14. Chiang, P., E. Chang, and J. Wu, *Comparison of chemical and thermal regeneration of aromatic compounds on exhausted activated carbon.* Water Science & Technology., 1997. **35**(7).

15. Shi, J., *Molecular distillation of palm oil distillates: Evaporation rates, relative volatility, and distribution coefficients of tocotrienols and other minor components.* Separation Science and Technology, 2007. **42**(14): p. 3029-3048.

16. Luyben, W.L., American Institute of Chemical Engineers., and Arnold Addison & Mildred Barner Jackson Library Endowment., *Distillation design and control using Aspen simulation*. 2006, Hoboken, N.J.: Wiley-Interscience. xiii, 345 p.

17. Vu, D., *Vapor-liquid equilibria in the systems ethyl lactate plus ethanol and ethyl lactate plus water*, in *Journal of chemical and engineering data*. 2006. p. 1220-1225.

18. Gil, I., et al., *Separation of ethanol and water by extractive distillation with salt and solvent as entrainer: Process simulation.* Braz. J. Chem. Eng, 2008. **25**(1).

6. General Conclusions and Future Recommendations

The ternary phase behavior of pure sclareol-ethyl lactate-CO_2 system at 298.15, 308.15 K and various pressures provides essential information for the design of an extraction process of sclareol from the Clary Sage plants. The phase diagrams, which were constructed using the static synthetic method, exhibited a cybotactic region in CO_2-ethyl lactate mixture, with the solubility increasing with increasing pressure at a fixed temperature. CO_2 acted as a co-solvent to ethyl lactate at lower pressure and/or lower CO_2 concentrations and as an anti-solvent at higher pressure and/or higher CO_2 concentrations. The PR-LCVM model was able to qualitatively but not quantitatively predict the ternary phase behavior of sclareol-ethyl lactate-CO_2 system. This model, however, could provide a good prediction for ethyl lactate-CO_2 system, and thus was useful for analyzing the region of miscibility of the two components at various pressures and temperatures.

The sclareol extraction from Clary Sage plants using ethyl lactate, followed by GAS precipitation process did not produce the desired quantity or purity of sclareol. The process required the use of a large amount of ethyl lactate to extract a given amount of sclareol from Clary Sage, and subsequent evaporation of a large amount of ethyl lactate to concentrate the solution for achieving a high yield of sclareol upon precipitation with the GAS process. Some impurities, extracted together with sclareol by ethyl lactate, acted as a co-solvent for sclareol and inhibited the precipitation of sclareol. Furthermore, the GAS process was not very selective for sclareol. The sclareol obtained by precipitation was impure.

An alternative extraction process using a mixture of ethyl lactate and CO_2 at subcritical conditions (6.89 MPa, 298.15 K) is promising. The process could achieve high sclareol extraction yield (95-100 %) and highest purity (65-70 % (w/w) of sclareol) at ethyl lactate concentrations in the range of w_{EL}^{*} = 0.09-0.1. Increasing the pressure to 10.34 MPa at a fixed temperature did not improve the product purity while decreasing the pressure to 5.52 MPa and lower created the region of immiscibility between ethyl lactate and CO_2.

The purification of the liquid extract (w_{EL}^{*} = 0.09, 6.89 MPa) with the activated carbon resulted in a 5-15 % increase in the extract purity, depending on the activated carbon concentration. Increasing the activated carbon concentration decreased the sclareol yield due to some adsorption of sclareol and the increase of liquid extract holdup in the activated carbon. The recovery of sclareol from the purified liquid extract can be achieved by applying ~ 78 % (w/w) of water. Generally, three phases were formed upon addition of water: an oil phase containing 63-77 % (w/w) of sclareol, a solid precipitate phase containing 92-97 % (w/w) of sclareol, and a water-ethyl lactate phase with negligible amount of sclareol. The extract treated with the highest activated carbon concentration did not demonstrate the formation of an appreciable quantity of oil phase upon addition of water, thus most of the sclareol was obtained in the solid precipitate phase.

In an industrial process, the ethyl lactate-water phase can be separated and the individual liquid components recovered using a vacuum distillation. The ethyl lactate can then be recycled for re-use in the extraction step of the process while the recovered water can be re-used for the liquid antisolvent step of the process. Water and ethyl lactate are not only miscible, but also form an azeotrope. We used Aspen Plus 2004.1 simulation to model the

separation process. The calculation employed a simple distillation setup and neglected the presence of impurities in the ethyl lactate-water mixture. It is estimated that, for a given water composition of 78 % (w/w), the complete separation of water and ethyl lactate can be reasonably achieved using a vacuum pressure of < 0.007 MPa.

Figure 6-1 and Figure 6-2 summarize the overall process of extraction, purification, and recovery of sclareol from the plant materials, respectively, for two purification conditions. In Figure 6-1, applying 60 g/L activated carbon increased the extract purity from 65 to 79 % (w/w) of sclareol, and addition of water to this extract caused ~ 70 % of the phase-separated sclareol in the solid precipitate phase with 97 % (w/w) of sclareol. Consequently, as shown in Figure 6-2, applying 242 g/L of activated carbon did not significantly enhance the extract purity and a lower sclareol yield was obtained due to some adsorption of sclareol and the holdup of the liquid extract in the activated carbon. The formation of oil phase did not noticeably occur upon addition of water, and sclareol with a purity of 93 % (w/w) was obtained as the precipitate. To conclude, it is preferable to apply 60 g/L activated carbon in the purification step of our process. With this reasonable amount of activated carbon, we can achieve high enough extract purity. The drawback is the dissolution of some sclareol in the oil phase upon addition of water. It is necessary to perform further investigation on the process to purify the oil phase and subsequently recover sclareol from that phase.

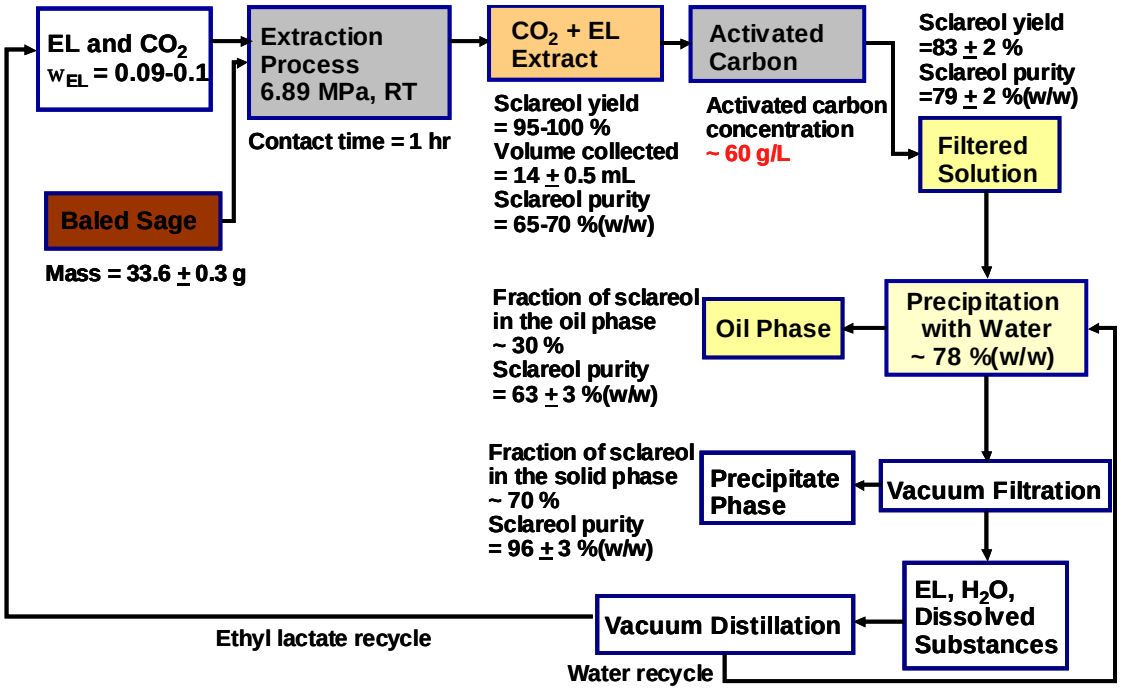

Figure 6-1. Process flow diagram for the extraction, purification, and recovery process of sclareol from Clary Sage plants. The purification was performed with 60 g/L activated carbon.

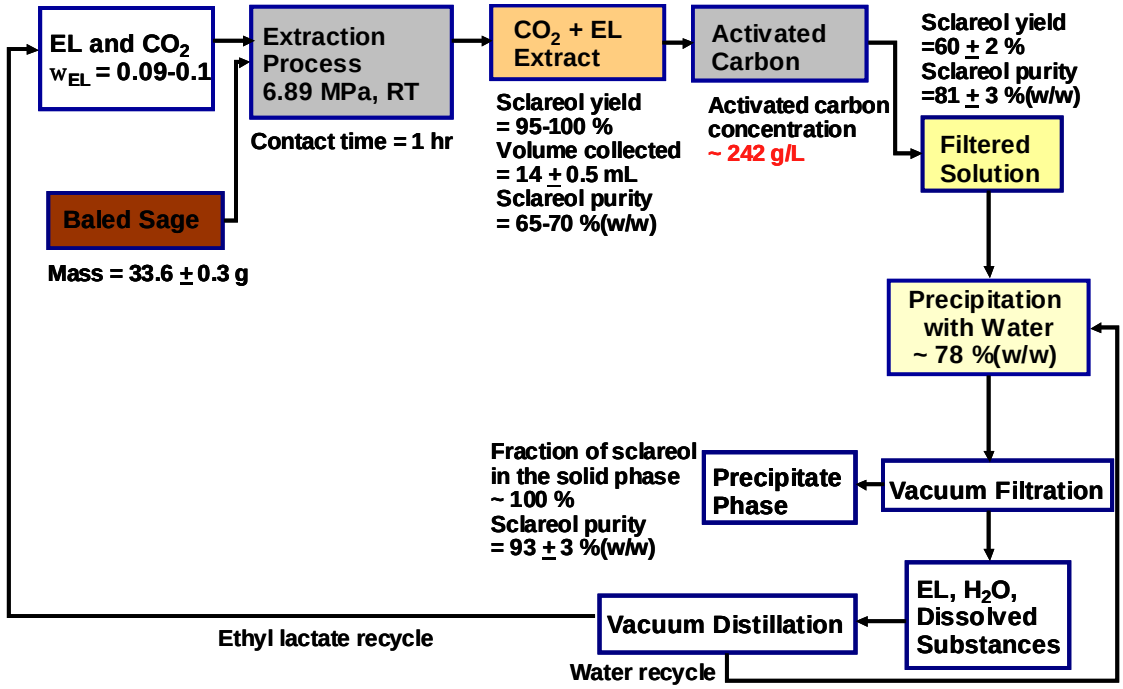

Figure 6-2. Process flow diagram for the extraction, purification, and recovery process of sclareol from Clary Sage plants. The purification was performed with 242 g/L activated carbon.

Future work pertaining to the improvement of the extraction methods to increase the extract purity or sclareol selectivity includes investigating other GRAS solvent-CO_2 pairs and reducing the contact time between the plant materials with the solvent mixtures since sclareol was found on the surface of sage flowers and could be extracted in a matter of minutes. Using a more volatile GRAS extraction solvent can be advantageous because these solvents can be easily evaporated and the extract after complete solvent removal, presumably with the reasonably high purity, can be directly subjected for the re-crystallization process to achieve the almost pure product.

In the purification part, investigation on other types of activated carbons for removal of the dominant impurities in the extract must be pursued. An alternative to activated carbon, such as using another GRAS solvent to selectively extract sclareol from the ethyl lactate extract can also be examined. Finally, water as the antisolvent for sclareol can be replaced by other hydrophobic GRAS solvents, which can be easily separated from ethyl lactate using a conventional distillation process.

Appendix

A. Thermodynamic Modeling of the Ternary System of Sclareol-Ethyl Lactate-CO_2

A.1. LCVM Mixing Rules Coupled with the Original UNIFAC and PR-EOS

Vidal Mixing Rule [1]:

$$a_V = \frac{1}{A_V} \cdot \frac{G^E}{RT} + \sum x_i a_i \tag{A.1}$$

For the PR EOS, Vidal suggested a value of -0.623.

Michelsen Mixing Rule [2]:

$$a_M = \frac{1}{A_M}\left[\frac{G^E}{RT} + \sum x_i \ln\left(\frac{b}{b_i}\right)\right] + \sum x_i a_i \tag{A.2}$$

where A_M is an EOS-dependent parameter that depends additionally on the linear approximation used in describing the $q(a)$ vs. a, as derived in the following equations. Introduction of $a = \frac{a}{bRT}$ and $u = \frac{V}{b}$ into PR EOS pressure explicit as shown in Equation (A.3) yields Equation (A.4).

$$P = \frac{RT}{v-b} - \frac{a(T)}{v(v+b)+b(v-b)} \tag{A.3}$$

$$\frac{Pb}{RT} = \frac{1}{u-1} - \frac{a}{u^2 + 2u - 1} \tag{A.4}$$

where u is related to a through the PR EOS for P = 0:

$$\frac{1}{u-1} = \frac{a}{u^2 + 2u - 1} \Rightarrow u = \frac{1}{2}\left[(a-2) - \sqrt{a^2 - 8a + 8}\right] \tag{A.5}$$

The function $q(a)$ is defined for $a > 4 + 2\sqrt{2} = 6.83$. If we plot $q(a)$ vs. a and replace the curve with the linear approximation: $q(a) = q_0 + q_1 a$, we obtain $q_1 = -0.52$ for the a range of 6.83 to 20. By employing the linear approximation to Equation (A.2), we find that $A_M = q_1 = -0.52$.

LCVM mixing rules:

In this model, a linear combination of Vidal and Michelsen mixing rules [3] is used to calculate the attractive term parameter a in PR EOS, as expressed in the following equation:

$$a = \left(\frac{l}{A_V} + \frac{1-l}{A_M}\right) \cdot \frac{G^E}{RT} + \frac{1-l}{A_M} \cdot \sum x_i \ln\left(\frac{b}{b_i}\right) + \sum x_i a_i \tag{A.6}$$

where $a = \frac{a}{bRT}$ (A.7)

and l is a parameter that determines their relative contributions to a. The value of l was determined by applying the model for calculation of bubble point pressures of known binary systems, including systems with considerable size differences in their components. It was found out that suggested value for l is 0.36 when the original UNIFAC G^E model is incorporated in this mixing rule.

Multiplying each side of Equation (A.6) with the total number of moles, n, and deriving each side with respect to number of moles of each species *i* at constant T and P, n_i, gives the expression of parameter *a* for species *i* in the mixture:

$$\bar{a}_i = \left[\frac{\partial n a}{\partial n_i}\right]_{T,P,n_{j\neq i}} = \left(\frac{l}{A_V} + \frac{1-l}{A_M}\right)\cdot \ln g_i + \frac{1-l}{A_M}\cdot\left(\ln\frac{b}{b_i} + \frac{b_i}{b} - 1\right) + a_i \qquad \text{(A.8)}$$

where g_i represents the activity coefficient of species *i*, which is calculated from UNIFAC model. The fugacity coefficient for species *i* in the mixture, Φ_i, can be derived from PR EOS as shown in Equation (A.9). Applying Equation (A.8) into Equation (A.9) results in the fugacity coefficient of species *i* in the mixture in terms of activity coefficient of species *i*, as shown below:

$$\Phi_i = \exp\left[\frac{b_i}{b}\cdot(Z-1) - \ln(Z-B) - \frac{A}{2\sqrt{2}B}\left(\frac{2\sum_j x_j a_{ji}}{a} - \frac{b_i}{b}\right)\ln\left(\frac{Z+2.414B}{Z-0.414B}\right)\right] \qquad \text{(A.9)}$$

$$\Phi_i = \exp\left[\frac{b_i}{b}\cdot(Z-1) - \ln(Z-b) - \frac{\bar{a}_i}{2\sqrt{2}}\ln\left(\frac{Z+2.414B}{Z+0.414B}\right)\right] \qquad \text{(A.10)}$$

Group Contribution UNIFAC:

The activity coefficient of species *i* in a mixture is described as:

$$g_i = \exp\left[\ln g_i^{Combinatorial} + \ln g_i^{Residual}\right] \tag{A.11}$$

The combinatorial part accounts for differences in the size and shape of the molecules in the mixture whereas the residual part comprises the energy interactions. The following equations describe the combinatorial and residual activity coefficients:

$$\ln g_i^{Combinatorial} = \ln\frac{\Phi_i}{x_i} + \frac{z}{2} q_i \ln\frac{q_i}{\Phi_i} + l_i - \frac{\Phi_i}{x_i}\sum_j x_j l_j \tag{A.12}$$

$$\ln g_i^{Residual} = \sum_k v_k^{(i)}\left[\ln\Gamma_k - \ln\Gamma_k^{(i)}\right] \tag{A.13}$$

$$\text{where } l_i = \frac{z}{2}(r_i - q_i) - (r_i - 1); z = 10 \tag{A.14}$$

$$r_i = \sum_k v_k^{(i)} R_k \tag{A.15}$$

$$q_i = \sum_k v_k^{(i)} Q_k \tag{A.16}$$

$$q_i = \frac{q_i x_i}{\sum_j q_j x_j} \tag{A.17}$$

$$\Phi_i = \frac{r_i x_i}{\sum_j r_j x_j} \tag{A.18}$$

$$\ln\Gamma_k = Q_k\left[1 - \ln\left(\sum_m \Theta_m \Psi_{mk}\right) - \sum_m\left(\frac{\Theta_m \Psi_{km}}{\sum_n \Theta_n \Psi_{nm}}\right)\right] \tag{A.19}$$

$$\Psi_{mn} = \exp\left[\frac{U_{mn} - U_{nn}}{RT}\right] = \exp\left(\frac{a_{mn}}{T}\right) \tag{A.20}$$

In these equations: R_k and Q_k are the group volume and surface area parameters, respectively; $v_k^{(i)}$ is the number of groups of type k in molecule i; q_i and Φ_i are the area and segment fraction, which is similar to the volume fraction, respectively; a_{mn} is the group interaction parameter, which is evaluated from the experimental phase equilibrium data.

A.2. Two-Component System: Ethyl Lactate and CO_2

A.2.1. Flowchart of Binary VLE

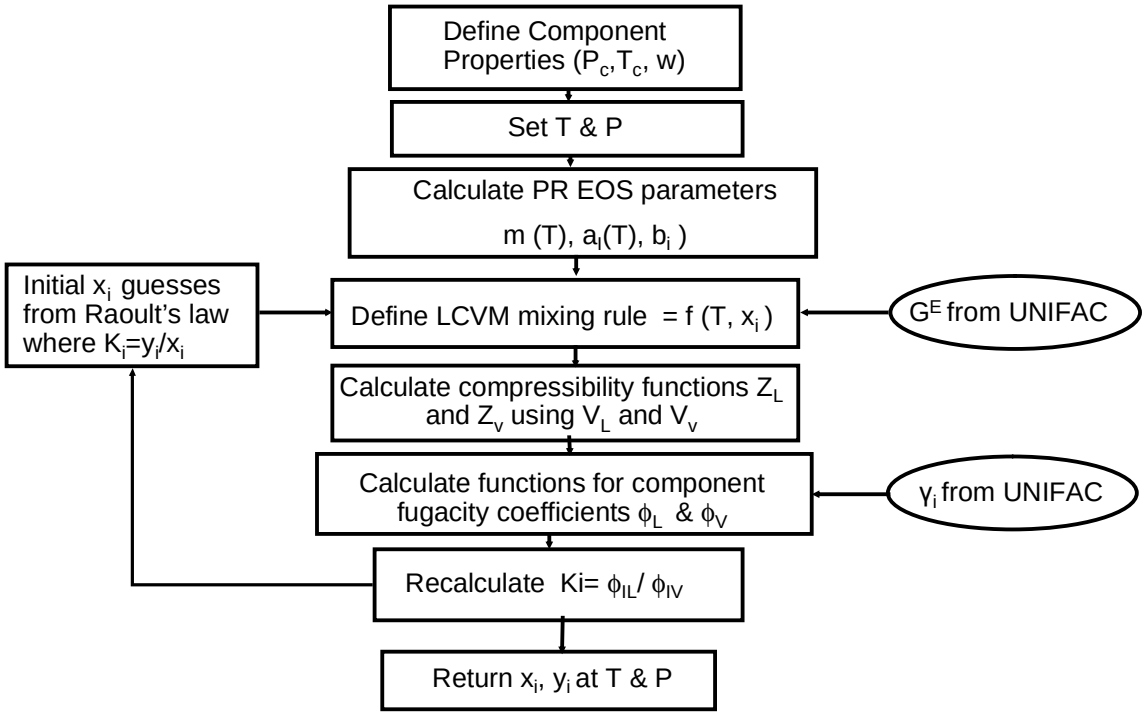

A.2.2. Matlab Code of Binary VLE: Ethyl Lactate-CO_2

```
function [g1new,g2new] = LCVM_CO2_Ethyllactate(PB)
% PB = system pressure; g1new = K_i = f_L / f_V
T = 15+273.15;
R = 8.31451;
z = 10;
%  1 = CO2; 2 = ethyl lactate, Critical temperature (Tc) in terms of K, Critical pressure (Pc) in terms of Pa
Tc(1) = 304.19; w(1) = 0.225; Pc(1) = 7.3815e6;
Tc(2) = 588; w(2) = 0.6; Pc(2) = 3.86e6;
for i = 1:2
K(i) = 0.37464 + 1.5422*w(i) - 0.26992*w(i)^2;
alfa(i) = ( 1 + K(i)*( 1 - sqrt(T/Tc(i)) ) )^2;
ai(i) = 0.45724*R^2*Tc(i)^2/Pc(i)*alfa(i);
bi(i) = 0.07780*R*Tc(i)/Pc(i);
end
g1 = 40;
g2 = 0.02;
g1new = 50;
Ethyllactate_sat=0.5;
g2new = Ethyllactate_sat/PB;

while abs(g1new-g1) + abs(g2new-g2) > 10.^(-10)
   g1 = g1new;
   g2 = g2new;
   x(1) = (g2-1)/(g2-g1)
   x(2) = 1-x(1)
   y(1) = g1*x(1)
   y(2) = 1-y(1)

% LIQUID CALCULATION
   bL = bi*x'
% New mixing rule incorporating UNIFAC
   ulambda=0.36;
   Av=-0.623;
   Am=-0.52;
_____________________________________________________________________________
% PART A
%CO2 = 1; CH3 = 2; CH  = 3; OH = 4; COOCH2 = 5;
r(1) = 1.2960; r(2) = 0.9011; r(3) = 0.4469; r(4) = 1.000; r(5) = 1.6764;
q(1) = 1.261; q(2) = 0.848; q(3) = 0.228; q(4) = 1.200; q(5) = 1.420;
Rv(1) = 1*r(1);
Q(1) = 1*q(1);
Rv(2) = 2*r(2)+1*r(3)+1*r(4)+1*r(5);
Q(2) = 2*q(2)+1*q(3)+1*q(4)+1*q(5);
_____________________________________________________________________________

for i=1:2
  Rsigma = Rv*x'
  Qsigma = Q*x'
```

```
      theta(i) = Rv(i)*x(i)/Rsigma;
                pi(i) = Q(i)*x(i)/Qsigma;
                l(i) = z/2*(Rv(i)-Q(i))-(Rv(i)-1);

  sigma = l*x';
  ln_gamma_combinatorial(i) = log(theta(i)/x(i)) + z/2*Q(i)*log(pi(i)/theta(i)) + l(i) -  theta(i)/x(i)*lsigma;
end

%a is in degree K
a = [0,110.6,110.6,87.1,-126.9
     116.7,0,0,986.5,232.1
     116.7,0,0,986.5,232.1
     471.83,156.4,156.4,0,101.1
     102.75,114.8,114.8,245.4,0];
 for i=1:5
  for  j=1:5
   wU(i,j) = exp(-a(i,j)/T);
 end
end
```

```
% PART B
   %For pure CO2
   %p indicates pure
   %CO2 = 1;
   X_p1(1) = 1; X_p1(2) = 0; X_p1(3) = 0; X_p1(4) = 0; X_p1(5) = 0;

   for i=1:5
    Area_thetaSigma_p1 = q*X_p1';
          Area_theta_p1(i) = q(i)*X_p1(i)/Area_thetaSigma_p1;
   end
b1(1) = log( Area_theta_p1(1)*wU(1,1) );
c1(1) = 1;
     ln_t_p1(1) = q(1) * (1 - b1(1) - c1(1));
```

```
% PART C
   %For pure Ethyl Lactate
   %p indicates pure
   X_p2(1) = 0; X_p2(2) = 2/5; X_p2(3) = 1/5; X_p2(4) = 1/5; X_p2(5) = 1/5;

   for i=1:5
          Area_thetaSigma_p2 = q*X_p2'
         Area_theta_p2(i) = q(i)*X_p2(i)/Area_thetaSigma_p2;
   end

        for i=2:5
         b2(i) = log(Area_theta_p2(2)*wU(2,i) + Area_theta_p2(3)*wU(3,i) +  Area_theta_p2(4)*wU(4,i)
         + Area_theta_p2(5)*wU(5,i) );
         c2(i)=
         Area_theta_p2(2)*wU(i,2)/(Area_theta_p2(2)*wU(2,2)+Area_theta_p2(3)*wU(3,2)+Area_theta_
         p2(4)*wU(4,2)+Area_theta_p2(5)*wU(5,2))+...
         Area_theta_p2(3)*wU(i,3)/(Area_theta_p2(2)*wU(2,3)+Area_theta_p2(3)*wU(3,3)+Area_theta_
         p2(4)*wU(4,3)+Area_theta_p2(5)*wU(5,3))+...
```

```
            Area_theta_p2(4)*wU(i,4)/(Area_theta_p2(2)*wU(2,4)+Area_theta_p2(3)*wU(3,4)+Area_theta_
            p2(4)*wU(4,4)+Area_theta_p2(5)*wU(5,4))+...
            Area_theta_p2(5)*wU(i,5)/(Area_theta_p2(2)*wU(2,5)+Area_theta_p2(3)*wU(3,5)+Area_theta_
            p2(4)*wU(4,5)+Area_theta_p2(5)*wU(5,5))
        ln_t_p2(i) = q(i) * (1 - b2(i) - c2(i))

end
```

```
% PART D
  %For Binary
  Xsigma = x(1)*1 + x(2)*5;
  X(1) = (x(1)*1 + x(2)*0)/Xsigma;
  X(2) = (x(1)*0 + x(2)*2)/Xsigma;
  X(3) = (x(1)*0 + x(2)*1)/Xsigma;
  X(4) = (x(1)*0 + x(2)*1)/Xsigma;
  X(5) = (x(1)*0 + x(2)*1)/Xsigma;

  for i=1:5
Area_thetaSigma = q*X';
   Area_theta(i) = q(i)*X(i)/Area_thetaSigma;
  end

  for i=1:5
      b(i)=log(Area_theta(1)*wU(1,i)+Area_theta(2)*wU(2,i)+Area_theta(3)*wU(3,i)+Area_theta(4)*w
      U(4,i)+Area_theta(5)*wU(5,i) );
      c(i)=
      Area_theta(1)*wU(i,1)/(Area_theta(1)*wU(1,1)+Area_theta(2)*wU(2,1)+Area_theta(3)*wU(3,1)+
      Area_theta(4)*wU(4,1)+Area_theta(5)*wU(5,1))+...
      Area_theta(2)*wU(i,2)/(Area_theta(1)*wU(1,2)+Area_theta(2)*wU(2,2)+Area_theta(3)*wU(3,2)+
      Area_theta(4)*wU(4,2)+Area_theta(5)*wU(5,2))+...
      Area_theta(3)*wU(i,3)/(Area_theta(1)*wU(1,3)+Area_theta(2)*wU(2,3)+Area_theta(3)*wU(3,3)+
      Area_theta(4)*wU(4,3)+Area_theta(5)*wU(5,3))+...
      Area_theta(4)*wU(i,4)/(Area_theta(1)*wU(1,4)+Area_theta(2)*wU(2,4)+Area_theta(3)*wU(3,4)+
      Area_theta(4)*wU(4,4)+Area_theta(5)*wU(5,4))+...
      Area_theta(5)*wU(i,5)/(Area_theta(1)*wU(1,5)+Area_theta(2)*wU(2,5)+Area_theta(3)*wU(3,5)+
      Area_theta(4)*wU(4,5)+Area_theta(5)*wU(5,5));
    ln_t(i) = q(i) * (1 - b(i) - c(i))
  end

  ln_gamma_residual(1) = 1*( ln_t(1) - ln_t_p1(1) );
  ln_gamma_residual(2) = 2*( ln_t(2) - ln_t_p2(2) ) + 1*( ln_t(3) - ln_t_p2(3) ) + 1*( ln_t(4) -
  ln_t_p2(4) ) + 1*( ln_t(5) - ln_t_p2(5) ) ;
  ln_gamma_total(1) = ln_gamma_combinatorial(1) + ln_gamma_residual(1);
  ln_gamma_total(2) = ln_gamma_combinatorial(2) + ln_gamma_residual(2);
```

```
% Introduction of GE function

GE=(x(1)*ln_gamma_total(1)+x(2)*ln_gamma_total(2))*R*T;

%Inserting the new mixing rule incorporating UNIFAC
```

```
   for i=1:2
      bratio(i) = log(bL/bi(i));
      alphai(i) = ai(i)/bi(i);
   end

   aL1=(ulambda/Av + (1-ulambda)/Am)*GE/R/T;
   aL2=((1-ulambda)/Am)*(x*bratio');
   aL3= x*alphai';
   jL= aL3*bL;
   wL= (aL1+aL2)*R*T*bL;
   aL= jL+wL;
   AL = aL*PB/(R^2*T^2);
   BL = bL*PB/(R*T);
   %   L(1)*X^N + ... + L(N)*X + L(N+1)
   %   Peng Robinson coefficients of the cubic eq.
   L(1) = 1;
   L(2) = BL - 1;
   L(3) = AL - 3*BL^2 - 2*BL;
   L(4) = BL^3 + BL^2 - AL*BL;
   %   Solve for the roots
   ZtempL = roots(L)
   %   I will consider only the smallest value. For vapor phase, consider the largest value.
   j = 1;
   for i = 1:3
      if imag(ZtempL(i))==0
         zL(j) = ZtempL(i);
         j = j + 1;
      end
   end
   ZL = min(zL)

for i = 1:2
    alpha_prime(i)=(ulambda/Av+(1-ulambda)/Am)*ln_gamma_total(i)+(1-ulambda)/Am*(log(bL/bi(i))+
    bi(i)/bL-1) + ai(i)/bi(i)/R/T
    phiL(i)=exp(bi(i)/bL*(ZL-1)-log(ZL-BL)-alpha_prime(i)/2.828*log((ZL+2.414*BL)/(ZL-0.414*BL)))
end
```

% VAPOR CALCULATION

% the same calculation procedure as the liquid phase can be applied to obtain the fugacity coefficient in the vapor phase

```
         g1new = phiL(1)/phiV(1)
         g2new = phiL(2)/phiV(2)
end
```

A.3. Three-Component System: Sclareol-Ethyl Lactate-CO_2

A.3.1. Flowchart of Ternary SVLE

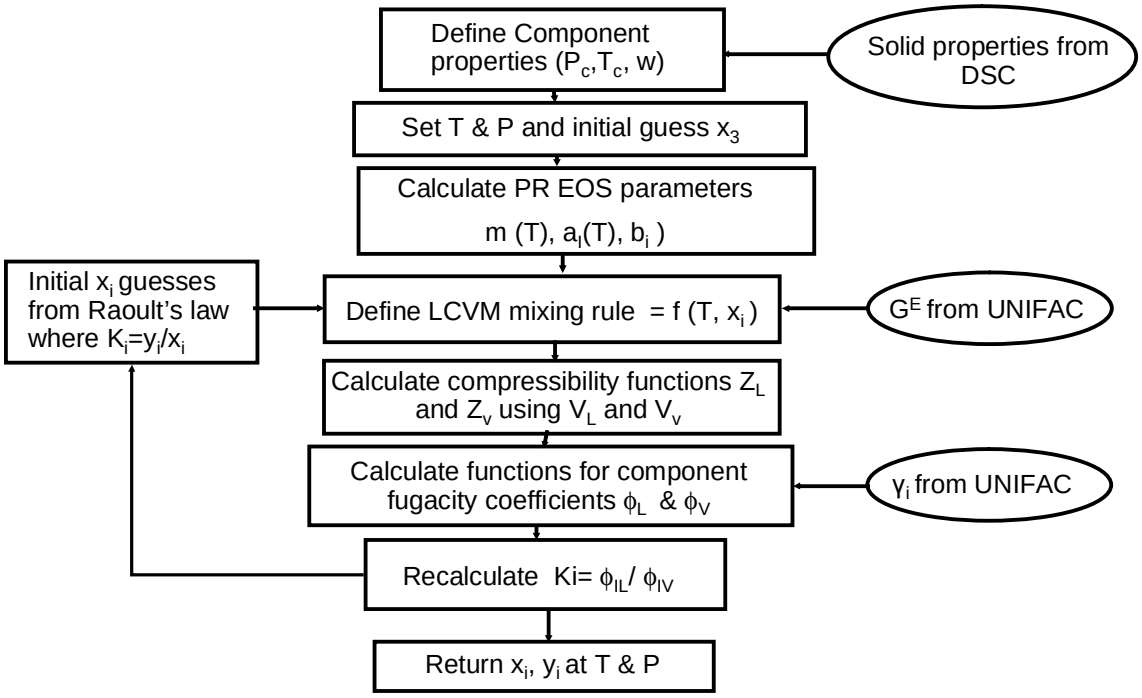

A.3.2. Matlab Code of Ternary VLE

```
function [x2] = LCVM_vaporliquid_ternary_corrected(x3)

T = 273.15+25;
R = 8.31451;
%  1 = CO2; 2 = Ethyl lactate; 3 = Sclareol

Tc(1) = 304.2; w(1) = 0.225; Pc(1) = 7.3815e6;
Tc(2) = 588; w(2) = 0.6; Pc(2) = 3.86e6;
Tc(3) = 845.5; w(3) = 1.023; Pc(3) = 1.58e6;

PB = 600*6894.757; z = 10;

% Sclareol physical properties
Ptp = 1e4; v3s = .300e-3; DeltaH_fus = 26225; Ttp = 376.46; DeltaCp = 0.0;
```

```
for i = 1:3
   K(i) = 0.37464 + 1.5422*w(i) - 0.26992*w(i)^2;
   alfa(i) = ( 1 + K(i)*( 1 - sqrt(T/Tc(i)) ) )^2;
   ai(i) = 0.45724*R^2*Tc(i)^2/Pc(i)*alfa(i);
   bi(i) = 0.07780*R*Tc(i)/Pc(i);
end

x(2) = 0.0000001; x2 = 0.01;

g1new = 50;
Ethyllactate_sat=40;
g2new = Ethyllactate_sat/PB;
Sclareol_sat = 4;
g3new = Sclareol_sat/PB;

while abs(x(2)-x2) > 10^(-6)
   x(3) = x3;
   x(2) = (1+(g1new-g3new)*x(3)-g1new)/(g2new-g1new);
   x(1) = 1-x(3)-x(2);

   y1 = g1new*x(1); y2 = g2new*x(2); y3 = g3new*x(3);
   m = y1 + y2 + y3;
   y(1) = y1/m; y(2) = y2/m; y(3) = y3/m;

% VAPOR CALCULATION
     bV = bi*y';
 % New mixing rule incorporating UNIFAC
   ulambda=0.36;
   Av=-0.623;
   Am=-0.52;
 %Inserting UNIFAC Excess Gibbs Energy function
%C02 (1) : C02=1;
%Ethyl-s-Lactate(2) : nCH2COO = 1; nCH3 = 2; nOH = 1; nCH = 1;
%Sclareol(3) : nCH3 = 5; nCH2 = 7; nCH = 2; nC = 4; nCH2=CH2 = 1; nOH = 2;
%r = Volume parameters
%q = Area parameters
%z = coordination number
```

```
% PART E
%CH3 = 1; CH2 = 2; CH = 3; C = 4; C=C = 5; OH = 6; CH2COO = 7; CO2 =8;
r(1) = 0.9011; r(2) = 0.6744; r(3) = 0.4469; r(4) = 0.2195; r(5) = 1.3454; r(6) = 1.000; r(7) = 1.6764; r(8) =
1.2960;
q(1) = 0.848; q(2) = 0.540; q(3) = 0.228; q(4) = 0.000; q(5) = 1.176; q(6) = 1.200; q(7) = 1.420; q(8) =
1.261;

Rv(1) = 1*r(8);
Rv(2) = 2*r(1)+1*r(3)+1*r(6)+1*r(7);
Rv(3) = 5*r(1)+7*r(2)+2*r(3)+4*r(4)+1*r(5)+2*r(6);
Q(1) = 1*q(8);
Q(2) = 2*q(1)+1*q(3)+1*q(6)+1*q(7);
Q(3) = 5*q(1)+7*q(2)+2*q(3)+4*q(4)+1*q(5)+2*q(6);
```

```
for i=1:3
Rsigma_V = Rv*y;
Qsigma_V = Q*y' ;
    theta_V(i) = Rv(i)*y(i)/Rsigma_V;
    pi_V(i) = Q(i)*y(i)/Qsigma_V;
    l(i) = z/2*(Rv(i)-Q(i))-(Rv(i)-1);
end
lsigma_V = y*l' ;
for i=1:3
ln_gamma_combinatorial_V(i)=log(theta_V(i)/y(i))+z/2*Q(i)*log(pi_V(i)/theta_V(i))+l(i)-
theta_V(i)/y(i)*lsigma_V;
end

 %a is in degree K
 a = [0, 0, 0, 0,-200.0, 986.5, 232.1, 116.7
      0, 0, 0, 0, -200.0, 986.5, 232.1, 116.7
      0, 0, 0, 0, -200.0, 986.5, 232.1, 116.7
      0, 0, 0, 0, -200.0, 986.5, 232.1, 116.7
      2520, 2520, 2520, 2520, 0, 693.9, 71.23, 48.57
      156.4, 156.4, 156.4, 156.4, 8694, 0, 101.1,471.83
      114.8, 114.8, 114.8, 114.8, 269.3, 245.4, 0, 102.75
      110.6,110.6,110.6,110.6,55.74,87.1,-126.9,0];

for i=1:8
  for  j=1:8
    w(i,j) = exp(-a(i,j)/T);
  end
end
```

```
% PART F
   %For pure CO2
   %p indicates pure
   %CO2 = 1
   Y_p1(1)=0; Y_p1(2)=0; Y_p1(3)=0; Y_p1(4)=0; Y_p1(5)=0; Y_p1(6)=0; Y_p1(7)=0;Y_p1(8) = 1;
    Area_thetaSigma_p1_V=q*Y_p1';

   for i=1:8
      Area_theta_p1_V(i) = q(i)*Y_p1(i)/Area_thetaSigma_p1_V;
   end
      b1_V(8) = log( Area_theta_p1_V(8)*w(8,8) );
      c1_V(8) = 1;
      ln_t_p1_V(8) = q(8) * (1 - b1_V(8) - c1_V(8));
```

```
% PART G
   %For pure Ethyl lactate
   %p indicates pure
   Y_p2(1)=2/5; Y_p2(2)=0; Y_p2(3)=1/5; Y_p2(4)=0; Y_p2(5)=0; Y_p2(6)=1/5; Y_p2(7)=1/5;
   Y_p2(8) = 0;
    Area_thetaSigma_p2_V=q*Y_p2';
   for i=1:8
      Area_theta_p2_V(i) = q(i)*Y_p2(i)/Area_thetaSigma_p2_V;
```

```
b2_V(i)=log(Area_theta_p2_V(1)*w(1,i)+Area_theta_p2_V(3)*w(3,i)+ Area_theta_p2_V(6)*w(6,i) +
Area_theta_p2_V(7)*w(7,i) );
c2_V(1)=
Area_theta_p2_V(1)*w(i,1)/(Area_theta_p2_V(1)*w(1,1)+Area_theta_p2_V(3)*w(3,1)+
Area_theta_p2_V(6)*w(6,1) + Area_theta_p2_V(7)*w(7,1)) +...
Area_theta_p2_V(3)*w(i,3)/(Area_theta_p2_V(1)*w(1,3)+Area_theta_p2_V(3)*w(3,3)+
Area_theta_p2_V(6)*w(6,3) + Area_theta_p2_V(7)*w(7,3)) +...
Area_theta_p2_V(6)*w(i,6)/(Area_theta_p2_V(1)*w(1,6)+Area_theta_p2_V(3)*w(3,6)+
Area_theta_p2_V(6)*w(6,6) + Area_theta_p2_V(7)*w(7,6)) +...
Area_theta_p2_V(7)*w(i,7)/(Area_theta_p2_V(1)*w(1,7)+Area_theta_p2_V(3)*w(3,7)+
Area_theta_p2_V(6)*w(6,7) + Area_theta_p2_V(7)*w(7,7));
ln_t_p2_V(i) = q(i) * (1 - b2_V(i) - c2_V(i));
end
```

```
% PART H
%For pure Sclareol
    %p indicates pure
    Y_p3(1)=5/21; Y_p3(2)=7/21; Y_p3(3)=2/21; Y_p3(4)=4/21; Y_p3(5)=1/21;
    Y_p3(6)=2/21; Y_p3(7) 0; Y_p3(8)=0;
    Area_thetaSigma_p3_V = q*Y_p3';

  for i=1:8
     Area_theta_p3_V(i) = q(i)*Y_p3(i)/Area_thetaSigma_p3_V;
    b3_V(i)=log(Area_theta_p3_V(1)*w(1,i)+Area_theta_p3_V(2)*w(2,i)+Area_theta_p3_V(3)*w(3,i)+
    Area_theta_p3_V(4)*w(4,i) + Area_theta_p3_V(5)*w(5,i) + Area_theta_p3_V(6)*w(6,i) );
    c3_V(i)=
    Area_theta_p3_V(1)*w(i,1)/(Area_theta_p3_V(1)*w(1,1)+Area_theta_p3_V(2)*w(2,1)+
    Area_theta_p3_V(3)*w(3,1)+Area_theta_p3_V(4)*w(4,1)+Area_theta_p3_V(5)*w(5,1)+
    Area_theta_p3_V(6)*w(6,1))+...
    Area_theta_p3_V(2)*w(i,2)/(Area_theta_p3_V(1)*w(1,2)+Area_theta_p3_V(2)*w(2,2)+
    Area_theta_p3_V(3)*w(3,2)+Area_theta_p3_V(4)*w(4,2)+Area_theta_p3_V(5)*w(5,2)+
    Area_theta_p3_V(6)*w(6,2))+...
    Area_theta_p3_V(3)*w(i,3)/(Area_theta_p3_V(1)*w(1,3)+Area_theta_p3_V(2)*w(2,3)+
    Area_theta_p3_V(3)*w(3,3)+Area_theta_p3_V(4)*w(4,3)+Area_theta_p3_V(5)*w(5,3)+
    Area_theta_p3_V(6)*w(6,3))+...
    Area_theta_p3_V(4)*w(i,4)/(Area_theta_p3_V(1)*w(1,4)+Area_theta_p3_V(2)*w(2,4)+
    Area_theta_p3_V(3)*w(3,4)+Area_theta_p3_V(4)*w(4,4)+Area_theta_p3_V(5)*w(5,4)+
    Area_theta_p3_V(6)*w(6,4))+...
    Area_theta_p3_V(5)*w(i,5)/(Area_theta_p3_V(1)*w(1,5)+Area_theta_p3_V(2)*w(2,5)+
    Area_theta_p3_V(3)*w(3,5)+Area_theta_p3_V(4)*w(4,5)+Area_theta_p3_V(5)*w(5,5)+
    Area_theta_p3_V(6)*w(6,5))+...
    Area_theta_p3_V(6)*w(i,6)/(Area_theta_p3_V(1)*w(1,6)+Area_theta_p3_V(2)*w(2,6)+
    Area_theta_p3_V(3)*w(3,6)+Area_theta_p3_V(4)*w(4,6)+Area_theta_p3_V(5)*w(5,6)+
    Area_theta_p3_V(6)*w(6,6));
    ln_t_p3_V(i) = q(i) * (1 - b3_V(i) - c3_V(i));
  end
```

```
% PART I
  %For Ternary
  Ysigma = y(1)*1+y(2)*5+y(3)*21;
  Y(1) = (y(1)*0 + y(2)*2 + y(3)*5)/Ysigma;
```

```
Y(2) = (y(1)*0 + y(2)*0 + y(3)*7)/Ysigma;
Y(3) = (y(1)*0 + y(2)*1 + y(3)*2)/Ysigma;
Y(4) = (y(1)*0 + y(2)*0 + y(3)*4)/Ysigma;
Y(5) = (y(1)*0 + y(2)*0 + y(3)*1)/Ysigma;
Y(6) = (y(1)*0 + y(2)*1 + y(3)*2)/Ysigma;
Y(7) = (y(1)*0 + y(2)*1 + y(3)*0)/Ysigma;
Y(8) = (y(1)*1 + y(2)*0 + y(3)*0)/Ysigma;

Area_thetaSigma_V=q*Y';

for i=1:8
    Area_theta_V(i) = q(i)*Y(i)/Area_thetaSigma_V;
  b_V(i)=log(Area_theta_V(1)*w(1,i)+Area_theta_V(2)*w(2,i)+Area_theta_V(3)*w(3,i)+Area_theta_V
  (4)*w(4,i)+Area_theta_V(5)*w(5,i)+Area_theta_V(6)*w(6,i)+Area_theta_V(7)*w(7,i)+
  Area_theta_V(8)*w(8,i));
  c_V(i)=
  Area_theta_V(1)*w(i,1)/(Area_theta_V(1)*w(1,1)+Area_theta_V(2)*w(2,1)+Area_theta_V(3)*w(3,1)
  +Area_theta_V(4)*w(4,1)+Area_theta_V(5)*w(5,1)+Area_theta_V(6)*w(6,1)+Area_theta_V(7)*w(7,
  1)+Area_theta_V(8)*w(8,1))+...
  Area_theta_V(2)*w(i,2)/(Area_theta_V(1)*w(1,2)+Area_theta_V(2)*w(2,2)+Area_theta_V(3)*w(3,2)
  +Area_theta_V(4)*w(4,2)+Area_theta_V(5)*w(5,2)+Area_theta_V(6)*w(6,2)+Area_theta_V(7)*w(7,
  2)+Area_theta_V(8)*w(8,2))+...
  Area_theta_V(3)*w(i,3)/(Area_theta_V(1)*w(1,3)+Area_theta_V(2)*w(2,3)+Area_theta_V(3)*w(3,3)
  +Area_theta_V(4)*w(4,3)+Area_theta_V(5)*w(5,3)+Area_theta_V(6)*w(6,3)+Area_theta_V(7)*w(7,
  3)+Area_theta_V(8)*w(8,3))+...
  Area_theta_V(4)*w(i,4)/(Area_theta_V(1)*w(1,4)+Area_theta_V(2)*w(2,4)+Area_theta_V(3)*w(3,4)
  +Area_theta_V(4)*w(4,4)+Area_theta_V(5)*w(5,4)+Area_theta_V(6)*w(6,4)+Area_theta_V(7)*w(7,
  4)+Area_theta_V(8)*w(8,4))+...
  Area_theta_V(5)*w(i,5)/(Area_theta_V(1)*w(1,5)+Area_theta_V(2)*w(2,5)+Area_theta_V(3)*w(3,5)
  +Area_theta_V(4)*w(4,5)+Area_theta_V(5)*w(5,5)+Area_theta_V(6)*w(6,5)+Area_theta_V(7)*w(7,
  5)+Area_theta_V(8)*w(8,5))+...
  Area_theta_V(6)*w(i,6)/(Area_theta_V(1)*w(1,6)+Area_theta_V(2)*w(2,6)+Area_theta_V(3)*w(3,6)
  +Area_theta_V(4)*w(4,6)+Area_theta_V(5)*w(5,6)+Area_theta_V(6)*w(6,6)+Area_theta_V(7)*w(7,
  6)+Area_theta_V(8)*w(8,6))+...
  Area_theta_V(7)*w(i,7)/(Area_theta_V(1)*w(1,7)+Area_theta_V(2)*w(2,7)+Area_theta_V(3)*w(3,7)
  +Area_theta_V(4)*w(4,7)+Area_theta_V(5)*w(5,7)+Area_theta_V(6)*w(6,7)+Area_theta_V(7)*w(7,
  7)+Area_theta_V(8)*w(8,7))+...
  Area_theta_V(8)*w(i,8)/(Area_theta_V(1)*w(1,8)+Area_theta_V(2)*w(2,8)+Area_theta_V(3)*w(3,8)
  +Area_theta_V(4)*w(4,8)+Area_theta_V(5)*w(5,8)+Area_theta_V(6)*w(6,8)+Area_theta_V(7)*w(7,
  8)+Area_theta_V(8)*w(8,8));
   ln_t_V(i) = q(i) * (1 - b_V(i) - c_V(i));
 end

ln_gamma_residual_V(1)=1*( ln_t_V(8) - ln_t_p1_V(8) );
ln_gamma_residual_V(2)=2*( ln_t_V(1) - ln_t_p2_V(1) )+1*( ln_t_V(3) - ln_t_p2_V(3) )+1*(   ln_t_V(6)
- ln_t_p2_V(6) ) + 1*( ln_t_V(7) - ln_t_p2_V(7) );
ln_gamma_residual_V(3)=5*( ln_t_V(1) - ln_t_p3_V(1) )+7*( ln_t_V(2) - ln_t_p3_V(2) )+2*( ln_t_V(3)
- ln_t_p3_V(3) ) + 4*( ln_t_V(4) - ln_t_p3_V(4) ) + 1*( ln_t_V(5) - ln_t_p3_V(5) ) + 2*( ln_t_V(6) -
ln_t_p3_V(6) );

  ln_gamma_total_V(1) = ln_gamma_combinatorial_V(1) + ln_gamma_residual_V(1);
  ln_gamma_total_V(2) = ln_gamma_combinatorial_V(2) + ln_gamma_residual_V(2);
  ln_gamma_total_V(3) = ln_gamma_combinatorial_V(3) + ln_gamma_residual_V(3);
```

```
% Introduction of GE function

   GE_V=(y(1)*ln_gamma_total_V(1)+y(2)*ln_gamma_total_V(2)+y(3)*ln_gamma_total_V(3))*R*T;

   %Inserting the new mixing rule incorporating UNIFAC

   for i=1:3
      bratioV(i) = log(bV/bi(i));
      alphai(i) = ai(i)/bi(i);
   end

   aV1=(ulambda/Av + (1-ulambda)/Am)*GE_V/R/T;
   aV2=((1-ulambda)/Am)*(y*bratioV');
   aV3=y*alphai';
   jV= aV3*bV;
   wV= (aV1+aV2)*R*T*bV;
   aV= jV+wV;

   AV = aV*PB/(R^2*T^2);
   BV = bV*PB/R/T;

   %   V(1)*X^N + ... + V(N)*X + V(N+1)
   %   Peng Robinson coefficients of the cubic eq.
   V(1) = 1;
   V(2) = BV - 1;
   V(3) = AV - 3*BV^2 - 2*BV;
   V(4) = BV^3 + BV^2 - AV*BV;
   %   Solve for the roots.
   ZtempV = roots(V);
   %   I will consider only the largest value. The smallest value for liquid phase.
   j = 1;
   for i = 1:3
      if imag(ZtempV(i))==0
         zV(j) = ZtempV(i);
         j = j + 1;
      end
   end

   ZV = max(zV);

   for i = 1:3
    alpha_prime_V(i)=(ulambda/Av+(1-ulambda)/Am)*ln_gamma_total_V(i)+(1-
    ulambda)/Am*(log(bV/bi(i))+bi(i)/bV-1) + ai(i)/bi(i)/R/T;
    phiV(i)= exp( bi(i)/bV*(ZV-1) - log(ZV-BV) - alpha_prime_V(1)/2.828*log((ZV+2.414*BV)/(ZV-
    0.414*BV)) );
   end
```

% LIQUID CALCULATION

% the same calculation procedure as the vapor phase can be applied to obtain the fugacity coefficient in the liquid phase

```
   g1new = phiL(1)/phiV(1); g2new = phiL(2)/phiV(2); g3new = phiL(3)/phiV(3);
```

```
    x2 = (1+(g1new-g3new)*x(3)-g1new)/(g2new-g1new);
end
```

A.3.3. Matlab Code of Ternary SLE

```
function [x3] = LCVM_solidliquid_ternary_corrected(x1)

R = 8.31451;
%  1 = CO2 2 = Ethyl lactate 3 = Sclareol

Tc(1) = 304.2; wi(1) = 0.225; Pc(1) = 7.3815e6;
Tc(2) = 588; wi(2) = 0.6; Pc(2) = 3.86e6;
Tc(3) = 845.5; wi(3) = 1.023; Pc(3) = 1.58e6;

T =273.15+25; PB = 600*6894.757; R = 8.31451; z =10;

x(3) = 0.0000001;
x3 = 0.01;
%Arbitrary value of 4000 Pa = 0.04 bar for triple point pressure
%Arbitrary value of 300 ml/mol for solid molar volume
%deltaCp term is neglected

% Sclareol physical properties
Ptp = 1e4; v3s = .300e-3; DeltaH_fus = 26225; Ttp = 376.46; DeltaCp = 0.0;

for i = 1:3
    K(i) = 0.37464 + 1.5422*wi(i) - 0.26992*wi(i)^2;
    alfa(i) = ( 1 + K(i)*( 1 - sqrt(T/Tc(i)) ) )^2;
    ai(i) = 0.45724*R^2*Tc(i)^2/Pc(i)*alfa(i);
    bi(i) = 0.07780*R*Tc(i)/Pc(i);
end

while abs(x(3)-x3) > 10^(-10)
    x(3) = x3
    x(1) = x1;
    x(2) = 1-x(1)-x(3);

% LIQUID CALCULATION
% the same calculation procedure as the vapor phase described in section 4.3.2 can be applied to obtain the fugacity coefficient in the liquid phase

% SOLID CALCULATION at the triple point pressure
    %species 3
    Apure = ai(3)*Ptp/(R^2*T^2);
    Bpure = bi(3)*Ptp/R/T;

    %   S(1)*X^N + ... + S(N)*X +S(N+1)
    %   Peng Robinson coefficients of the cubic eq.
    S(1) = 1;
    S(2) = Bpure - 1;
    S(3) = Apure - 3*Bpure^2 - 2*Bpure;
```

```
    S(4) = Bpure^3 + Bpure^2 - Apure*Bpure;
    %   Solve for the roots.
    Ztemppure = roots(S);
    %   I will consider only the smallest value.
    j = 1;
    for i = 1:3
       if imag(Ztemppure(i))==0
          zpure(j) = Ztemppure(i);
          j = j + 1;
       end
    end

    Z = min(zpure);
    phi_pure=exp(Z-1-log(Z-Bpure)-Apure/(2*sqrt(2)*Bpure)*log((Z+2.414*Bpure)/(Z-0.414*Bpure)) );
    f_pure = phi_pure * Ptp;
    fS=f_pure*exp( DeltaH_fus/R*(1/Ttp-1/T) + v3s*(PB-Ptp)/R/T - DeltaCp/R*(log(Ttp/T)-Ttp/T+1) );
    fL(3) = PB * phiL(3);
    x3 = fS/ fL(3);
end
```

A.3.4. Matlab Code of Ternary SVLE

```
function [x3] = SVLE_CES_corrected(PB)

T = 25+273.15;
R = 8.31451;
%  1 = CO2 2 = Ethyl lactate 3 = Sclareol

Tc(1) = 304.2; wi(1) = 0.225; Pc(1) = 7.3815e6;
Tc(2) = 588; wi(2) = 0.6; Pc(2) = 3.86e6;
Tc(3) = 845.5; wi(3) = 1.023; Pc(3) = 1.58e6;

%Arbitrary value of 10000 Pa = 0.1 bar for triple point pressure
%Arbitrary value of 300 ml/mol for solid molar volume
%deltaCp term is neglected

% Sclareol physical properties
Ptp = 1e4; v3s = .300e-3; DeltaH_fus = 26225; Ttp = 376.46; DeltaCp = 0.0;

for i = 1:3
   K(i) = 0.37464 + 1.5422*wi(i) - 0.26992*wi(i)^2;
   alfa(i) = ( 1 + K(i)*( 1 - sqrt(T/Tc(i)) ) )^2;
   ai(i) = 0.45724*R^2*Tc(i)^2/Pc(i)*alfa(i);
   bi(i) = 0.07780*R*Tc(i)/Pc(i);
end

x(3) = 0.0000001;
x3 = 0.01;

g1new = 50;
```

```
Ethyllactate_sat=40;
g2new = Ethyllactate_sat/PB;
Sclareol_sat = 4;
g3new = Sclareol_sat/PB;

while abs(x(3)-x3) > 10^(-6)
   x(3) = x3;
   x(2) = (1+(g1new-g3new)*x(3)-g1new)/(g2new-g1new);
   x(1) = 1-x(3)-x(2);

   y1 = g1new*x(1); y2 = g2new*x(2); y3 = g3new*x(3);
   m = y1 + y2 + y3;
   y(1) = y1/m; y(2) = y2/m; y(3) = y3/m;

% VAPOR CALCULATION
% to calculate fugacity coefficients in the vapor phase

% LIQUID CALCULATION
% to calculate fugacity coefficients in the liquid phase

   g1new = phiL(1)/phiV(1);
   g2new = phiL(2)/phiV(2);
   g3new = phiL(3)/phiV(3);

% SOLID CALCULATION at the triple point pressure
   fL(3) = PB * phiL(3);
   x3 = fS/ fL(3);
   x2 = (1+(g1new-g3new)*x3-g1new)/(g2new-g1new);
   x1 = 1-x3-x2;
end
```

A.4. Physical Properties of Components used in Validating the Thermodynamic Codes

Table A-1 and Table A-2 list the physical properties of several components, which were used in the PR-LCVM calculation to validate the binary VLE code and the ternary SVLE code.

Table A-1. Physical properties of components used in the calculation to validate the binary VLE code. The data are obtained from DIPPR database or elsewhere as noted.

	Propane	Butyl Propanoate	Ethanol	Ethyl Acetate	Ethyl Hexanoate
Tc (K)	369.8	610[a]	514	523.3	611.6
Pc (MPa)	4.25	2.55[a]	6.14	3.88	2.55
ω	0.152	0.547[a]	0.644	0.366	0.555

[a] Joback method [4]

Table A-2. Physical properties of components used in the calculation to validate the ternary SVLE code. The data are obtained from DIPPR database.

	Acetone	Ethyl Acetate	Cholesterol	Tetradecanoic Acid
Tc (K)	508.2	523.3	959	765
Pc (MPa)	4.7	3.88	1.25	1.7
ω	0.307	0.366	0.948	0.943
ΔH_{fus} (KJ/mol)	-	-	39.1	45.1
T_m (K)	-	-	421.65	327.37
v_s (l/mol)	-	-	0.338	0.224
P_{tp} (bar)	-	-	0.752	0.0396
ΔC_p (J/mol K)	-	-	218.84	-

A.5. Sclareol Boiling Point and Critical Temperature Values obtained from Several Sources

Table A-3 summarizes the sclareol boiling point values obtained from several sources. Table A-4 summarizes the critical temperature values of sclareol calculated from several group contribution methods. Some methods, such as Lydersen, Ambrose, and Klincewicz & Reid, require the solute boiling point to calculate for the critical temperature. The sclareol boiling point values selected for the sclareol critical temperature calculations are 852.1 K and 671.45 K, which is the average of the boiling point range obtained from SciFinder Scholar.

Table A-3. Sclareol boiling point from various sources.

P (mmHg)	Tb (K)	Sources
19	491.15	Advanced Biotech
19	491.15-493.15	Sigma Aldrich
760	613.15	J.J Reynolds Tobacco Company
760	656.45-686.45	SciFinder Scholar
760	852.1	www.gpengineeringsoft.com/pages/pdtphysprops.html (This software uses Joback/Lydersen)

Table A-4. Sclareol critical temperature values and their calculation methods [4-14].

Tb (K)	Tc (K)	Method
671.45	845.5	http://pirika.com/chem/TCPEE/criP/ourCP.htm (This software uses Joback)
not required	836.6	Fedors
671.45 852.1	830.5 1053.9	Lydersen
671.45 852.1	831.2 1054.8	Ambrose
671.45 852.1	856.4 1136.4	Klincewicz & Reid
852.28	1058.6	Joback & Reid
852.28	1058.6	Modified Joback
624.4	813.7	Constantinou & Gani
506.5	761.9	Morejon & Fontdevilla
826.9	1027	Stein & Brown

A.6. References

1. Huron, M. and J. Vidal, New mixing rules in simple equations of state for representing vapor-liquid equilibria of strongly nonideal mixtures. Fluid Phase Equilibria, 1979. **3**(4): p. 255-271.

2. Michelsen, M., *A modified Huron-Vidal mixing rule for cubic equations of state.* Fluid Phase Equilibria, 1990. **60**: p. 213-219.

3. Boukouvalas, C., et al., *Prediction of vapor-liquid equilibrium with the LCVM model: A linear combination of the vidal and michelsen mixing rules coupled with the original UNIFAC and the t-mPR equation of state.* Fluid Phase Equilibria, 1994. **92**: p. 75-106.

4. Joback, K. and R. Reid, *Estimation of pure-component properties from group-contributions.* Chemical Engineering Communications, 1987. **57**(1): p. 233-243.

5. Fedors, R.F., *A relationship between chemical structure and the critical temperature.* Chemical Engineering Communications, 1982. **16**(1): p. 149 - 151.

6. Daubert, T., *Chemical engineering thermodynamics*. 1985: McGraw-Hill.

7. Reid, R., J. Prausnitz, and B. Poling, *The properties of gases and liquids.* McGraw-Hill Book Co, 1973. **80**: p. 320.

8. Ambrose, D., *Correlation and estimation of vapour-liquid critical properties.* 1979: National Physical Library.

9. Ambrose, D., *Correlation of the boiling points of alkanols.* 1976.

10. Klincewicz, K. and R. Reid, *Estimation of critical properties with group contribution methods.* AIChE journal, 1984. **30**(1): p. 137-142.

11. Devotta, S. and V. Pendyala, *Modified joback group contribution method for normal boiling point of aliphatic halogenated compounds.* Industrial & Engineering Chemistry Research, 1992. **31**(8): p. 2042-2046.

12. Constantinou, L. and R. Gani, *New group contribution method for estimating properties of pure compounds.* AIChE Journal, 1994. **40**(10): p. 1697-1710.

13. Marrero-Morejon, J. and E. Pardillo-Fontdevila, *Estimation of pure compound properties using group-interaction contributions.* AIChE Journal, 1999. **45**(3): p. 615-621.

14. Stein, S. and R. Brown, *Estimation of normal boiling points from group contributions.* Journal of Chemical Information and Computer Sciences, 1994. **34**(3): p. 581-587.

B. Experimental Ternary Phase Behavior of the Sclareol-Ethyl Lactate-CO_2 System

B.1. High Pressure View Cell

The phase observation experiments were performed in the high-pressure cylindrical cell. The scion image software was used to capture the image of the view cell and then calculated the corresponding liquid level. In order to know the fluid volume before and after addition of carbon dioxide, an equation based on the dimensions of the view cell relating the liquid level and the fluid volume was derived as the following. Figure B-1 shows the schematic diagram of the view cell.

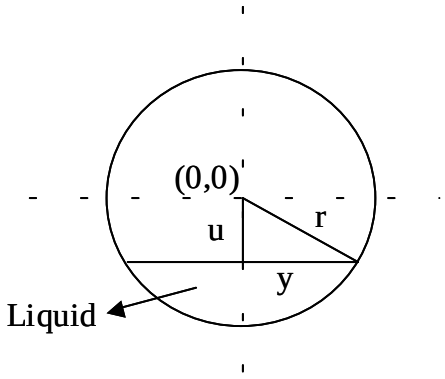

Figure B-1. Schematic diagram of the high-pressure view cell**.**

If the length of the cylinder is *L*, the cross-sectional area of the cylindrical cell, *A*, is given in Equation (B.1).

$$A = 2\sqrt{r^2 - u^2}L \tag{B.1}$$

Integrating the cross-sectional area with respect to *u* will then provide the equation for volume [1].

$$V = \int 2L\sqrt{r^2 - u^2}\,du \tag{B.2}$$

$$V(u) = 2L\left[\frac{u\sqrt{r^2 - u^2}}{2} + \frac{r^2}{2}\sin^{-1}\left(\frac{u}{r}\right)\right] \text{ ; for } u = -r \text{ to } r \tag{B.3}$$

If we shift the coordinate as is shown in Figure B-2, subsequent steps to modify Equation (B.3) are described as follows.

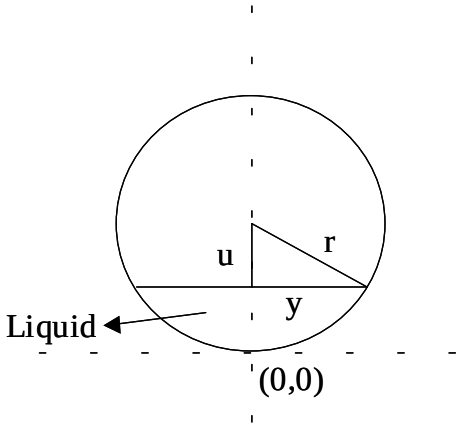

Figure B-2. Schematic diagram of the high-pressure view cell with a modified coordinate.

$$x = u + r \tag{B.4}$$

$$V(x) = V(u) - V(u = -r) \tag{B.5}$$

$$V(x) = 2L\left[\frac{u\sqrt{r^2 - u^2}}{2} + \frac{r^2}{2}\sin^{-1}\left(\frac{u}{r}\right) - \frac{r^2}{2}\sin^{-1}(-1)\right] \tag{B.6}$$

Substitute Equation (B.4) into (B.6) and $\sin^{-1}(-1) = -\frac{p}{2}$:

$$V(x) = 2L\left[\frac{(x-r)\sqrt{r^2-(x-r)^2}}{2} + \frac{r^2}{2}\sin^{-1}\left(\frac{x-r}{r}\right) + \frac{p.r^2}{4}\right] \quad \text{(B.7)}$$

B.2. Sclareol Solubility in Carbon Dioxide

Figure B-3 illustrates the sclareol solubility in CO_2 obtained experimentally and predicted using PR-LCVM at 298.15, 308.15 K and various pressures. The experimental procedure to determine the solubility of sclareol in CO_2 was described in chapter 3.

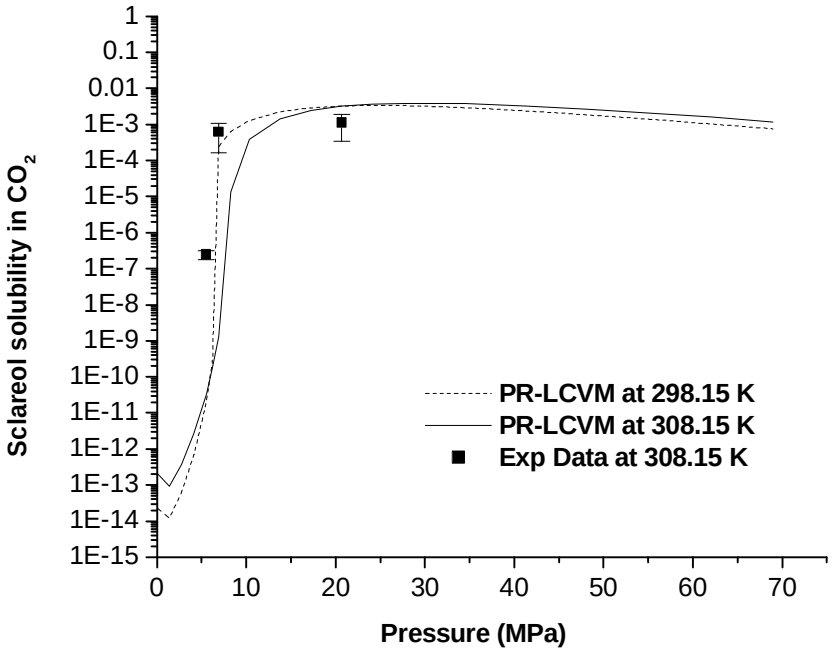

Figure B-3. Solubility of sclareol in carbon dioxide in terms of weight fraction obtained experimentally and predicted using PR-LCVM at 298.15, 308.15 K, and various pressures.

B.3. References

1. Murray, R., *Mathematical handbook of formulas and tables.* Spiegel-Schaum's Outline Series, 1968.

C. Extraction of Sclareol from Clary Sage using Mixtures of Ethyl Lactate and Carbon Dioxide

C.1. Summary of Experimental Conditions and Results for Various Pressures and Ethyl Lactate Compositions (w_{EL}^*): 6.89 MPa, w_{EL}^* = 0-0.9

6.89 MPa, w_{EL}^* = 0.9

Experimental Conditions

Mass of baled sage	33.6	g
Mass of EL	260.5	g
Mass of CO_2	30.10	g
Volume of CO_2+EL mixture around system	88.25	mL

Experimental Results

1st sampling:					
Volume of mixture sampled	87.9	mL	Sclareol Conc. in extract	11.67	g/L
Mass of mixture	95.26	g	Sclareol mass in extract	937.48	mg
Mass of EL	85.38	g	% Sclareol in extract by weight	37.02	%
Mass of CO_2	9.88	g	Expected sclareol mass	1095.36	mg
Calculated volume of EL	81.94	mL	% Sclareol yield	85.59	%
Volume of extract from exp	80.3	mL			
Sampling flow rate	0.6	mL/min			
Sampling time	2.44	hrs			
2nd sampling:					
Volume of mixture sampled	91.53	mL	Sclareol Conc. in extract	0.63	g/L
Mass of mixture	99.03	g	Sclareol mass in extract	54.49	mg
Mass of EL	89.09	g	% Sclareol in extract by weight	9.94	%
Mass of CO_2	9.94	g	Expected sclareol mass	1095.36	mg
Calculated volume of EL	85.50	mL	% Sclareol yield	90.56	%
Volume of extract from exp	86.65	mL			
Sampling flow rate	0.6	mL/min			
Sampling time	2.54	hrs			
Depressurization:					
Sclareol Conc.	2.253	g/L	Total mass of sclareol	1071.73	mg
Sclareol mass	79.77	mg	Expected sclareol mass	1095.36	mg
Volume collected	~35.4	mL	% Sclareol yield	97.84	%
			% Sclareol purity	22.97	%

6.89 MPa, w_{EL}^{*} = 0.57

Experimental Conditions

Mass of baled sage	33.5	g
Mass of EL	104.2	g
Mass of CO_2	71.85	g
Volume of CO_2+EL mixture around system	84.38	mL

Experimental Results

1st sampling:					
Volume of mixture sampled	88.44	mL	Sclareol Conc. in extract	16.22	g/L
Mass of mixture	95.01	g	Sclareol mass in extract	829.85	mg
Mass of EL	55.61	g	% Sclareol in extract by weight	54.27	%
Mass of CO_2	39.40	g	Expected sclareol mass	1092.10	mg
Calculated volume of EL	53.37	mL	% Sclareol yield	75.99	%
Volume of extract from exp	51.25	mL			
Sampling flow rate	0.5-0.7	mL/min			
Sampling time	2.5	hrs			
2nd sampling:					
Volume of mixture sampled	106.12	mL	Sclareol Conc. in extract	2.40	g/L
Mass of mixture	113.46	g	Sclareol mass in extract	146.64	mg
Mass of EL	62.80	g	% Sclareol in extract by weight	30.69	%
Mass of CO_2	50.66	g	Expected sclareol mass	1092.10	mg
Calculated volume of EL	60.27	mL	% Sclareol yield	89.41	%
Volume of extract from exp	61	mL			
Sampling flow rate	0.5-0.7	mL/min			
Sampling time	2.95	hrs			
Depressurization:					
Sclareol Conc.	0.007	g/L	Total mass of sclareol	976.58	mg
Sclareol mass	0.09	mg	Expected sclareol mass	1092.10	mg
Volume collected	~12.5	mL	% Sclareol yield	89.42	%
			% Sclareol purity	41.45	%

6.89 MPa, w_{EL}^{*} = 0.35

Experimental Conditions		
Mass of baled sage	33.4	g
Mass of EL	52.1	g
Mass of CO_2	107.02	g
Volume of CO_2+EL mixture around system	85.7	mL

Experimental Results

1st sampling:					
Volume of mixture sampled	88.47	mL	Sclareol Conc. in extract	26.75	g/L
Mass of mixture	91.83	g	Sclareol mass in extract	759.74	mg
Mass of EL	31.23	g	% Sclareol in extract by weight	57.72	%
Mass of CO_2	60.60	g	Expected sclareol mass	1088.84	mg
Calculated volume of EL	29.97	mL	% Sclareol yield	69.78	%
Volume of extract from exp	28.4	mL			
Sampling flow rate	0.5-0.7	mL/min			
Sampling time	2.5	hrs			
2nd sampling:					
Volume of mixture sampled	99.96	mL	Sclareol Conc. in extract	3.12	g/L
Mass of mixture	103.52	g	Sclareol mass in extract	97.43	mg
Mass of EL	37.77	g	% Sclareol in extract by weight	33.83	%
Mass of CO_2	65.75	g	Expected sclareol mass	1088.84	mg
Calculated volume of EL	36.24	mL	% Sclareol yield	78.72	%
Volume of extract from exp	31.25	mL			
Sampling flow rate	0.5-0.7	mL/min			
Sampling time	2.78	hrs			
Depressurization:					
Sclareol Conc.	2.20	g/L	Total mass of sclareol	879.16	mg
Sclareol mass	21.99	mg	Expected sclareol mass	1088.84	mg
Volume collected	~10	mL	% Sclareol yield	80.74	%
			% Sclareol purity	45.2	%

6.89 MPa, w_{EL}^{*} = 0.19

Experimental Conditions		
Mass of baled sage	33.8	g
Mass of EL	52.1	g
Mass of CO_2	228.48	g
Volume of CO_2+EL mixture around system	91.06	mL

Experimental Results

1st sampling:					
Volume of mixture sampled	91.02	mL	Sclareol Conc. in extract	45.58	g/L
Mass of mixture	87.76	g	Sclareol mass in extract	804.45	mg
Mass of EL	16.34	g	% Sclareol in extract by weight	63.24	%
Mass of CO_2	71.42	g	Expected sclareol mass	1101.88	mg
Calculated volume of EL	15.68	mL	% Sclareol yield	73.01	%
Volume of extract from exp	17.65	mL			
Sampling flow rate	0.5	mL/min			
Sampling time	3.03	hrs			
2nd sampling:					
Volume of mixture sampled	100.23	mL	Sclareol Conc. in extract	5.63	g/L
Mass of mixture	94.49	g	Sclareol mass in extract	91.48	mg
Mass of EL	16.94	g	% Sclareol in extract by weight	37.86	%
Mass of CO_2	77.55	g	Expected sclareol mass	1101.88	mg
Calculated volume of EL	16.25	mL	% Sclareol yield	81.31	%
Volume of extract from exp	16.25	mL			
Sampling flow rate	0.5	mL/min			
Sampling time	3.34	hrs			
Depressurization:					
Sclareol Conc.	6.747	g/L	Total mass of sclareol	933.04	mg
Sclareol mass	37.11	mg	Expected sclareol mass	1101.88	mg
Volume collected	~5.5	mL	% Sclareol yield	84.68	%
			% Sclareol purity	51.07	%

6.89 MPa, w_{EL}^{*} = 0.1

Experimental Conditions

Mass of baled sage	33.7	g
Mass of EL	39.075	g
Mass of CO_2	331.51	g
Volume of CO_2+EL mixture around system	87	mL

Experimental Results

1st sampling:					
Volume of mixture sampled	88.55	mL	Sclareol Conc. in extract	71.96	g/L
Mass of mixture	78.40	g	Sclareol mass in extract	482.14	mg
Mass of EL	8.27	g	% Sclareol in extract by weight	65.11	%
Mass of CO_2	70.13	g	Expected sclareol mass	1098.62	mg
Calculated volume of EL	7.94	mL	% Sclareol yield	43.89	%
Volume of extract from exp	6.7	mL			
Sampling flow rate	0.5	mL/min			
Sampling time	2.95	hrs			
2nd sampling:					
Volume of mixture sampled	100.32	mL	Sclareol Conc. in extract	66.33	g/L
Mass of mixture	90.04	g	Sclareol mass in extract	460.97	mg
Mass of EL	10.06	g	% Sclareol in extract by weight	73.04	%
Mass of CO_2	79.98	g	Expected sclareol mass	1098.62	mg
Calculated volume of EL	9.66	mL	% Sclareol yield	85.85	%
Volume of extract from exp	6.95	mL			
Sampling flow rate	0.5	mL/min			
Sampling time	3.34	hrs			
Depressurization:					
Sclareol Conc.	28.259	g/L	Total mass of sclareol	1054.74	mg
Sclareol mass	111.62	mg	Expected sclareol mass	1098.62	mg
Volume collected	~3.95	mL	% Sclareol yield	96.01	%
			% Sclareol purity	69.15	%

6.89 MPa, w_{EL}^{*} = 0.09

Experimental Conditions

Mass of baled sage	33.8	g
Mass of EL	26.05	g
Mass of CO_2	267.55	g
Volume of CO_2+EL mixture around system	89	mL

Experimental Results

1st sampling:					
Volume of mixture sampled	92.65	mL	Sclareol Conc. in extract	82.66	g/L
Mass of mixture	82.53	g	Sclareol mass in extract	657.11	mg
Mass of EL	7.41	g	% Sclareol in extract by weight	65.36	%
Mass of CO_2	75.13	g	Expected sclareol mass	1101.88	mg
Calculated volume of EL	7.11	mL	% Sclareol yield	59.64	%
Volume of extract from exp	7.95	mL			
Sampling flow rate	0.5	mL/min			
Sampling time	3.09	hrs			
2nd sampling:					
Volume of mixture sampled	100.3	mL	Sclareol Conc. in extract	55.09	g/L
Mass of mixture	87.02	g	Sclareol mass in extract	366.35	mg
Mass of EL	7.44	g	% Sclareol in extract by weight	65.35	%
Mass of CO_2	79.58	g	Expected sclareol mass	1101.88	mg
Calculated volume of EL	7.14	mL	% Sclareol yield	92.88	%
Volume of extract from exp	6.65	mL			
Sampling flow rate	0.5	mL/min			
Sampling time	3.34	hrs			
Depressurization:					
Sclareol Conc.	20.280	g/L	Total mass of sclareol	1061.99	mg
Sclareol mass	38.53	mg	Expected sclareol mass	1101.88	mg
Volume collected	~1.9	mL	% Sclareol yield	96.38	%
			% Sclareol purity	65.36	%

6.89 MPa, w_{EL}^{*} = 0.06

Experimental Conditions		
Mass of baled sage	33.5	g
Mass of EL	18.756	g
Mass of CO_2	309.46	g
Volume of CO_2+EL mixture around system	91	mL

Experimental Results

1st sampling:					
Volume of mixture sampled	88.6	mL	Sclareol Conc. in extract	81.87	g/L
Mass of mixture	73.91	g	Sclareol mass in extract	245.62	mg
Mass of EL	4.02	g	% Sclareol in extract by weight	52.44	%
Mass of CO_2	69.90	g	Expected sclareol mass	1092.10	mg
Calculated volume of EL	3.86	mL	% Sclareol yield	22.49	%
Volume of extract from exp	3	mL			
Sampling flow rate	0.5	mL/min			
Sampling time	2.95	hrs			
2nd sampling:					
Volume of mixture sampled	100.64	mL	Sclareol Conc. in extract	81.61	g/L
Mass of mixture	84.40	g	Sclareol mass in extract	338.68	mg
Mass of EL	5.44	g	% Sclareol in extract by weight	56.76	%
Mass of CO_2	78.96	g	Expected sclareol mass	1092.10	mg
Calculated volume of EL	5.22	mL	% Sclareol yield	53.50	%
Volume of extract from exp	4.15	mL			
Sampling flow rate	0.5	mL/min			
Sampling time	3.35	hrs			
Depressurization:					
Sclareol Conc.	80.116	g/L	Total mass of sclareol	688.46	mg
Sclareol mass	104.15	mg	Expected sclareol mass	1092.10	mg
Volume collected	~1.3	mL	% Sclareol yield	63.04	%
			% Sclareol purity	54.94	%

6.89 MPa, w_{EL}^{*} = 0.04

Experimental Conditions

Mass of baled sage	33.8	g
Mass of EL	12.504	g
Mass of CO_2	301.58	g
Volume of CO_2+EL mixture around system	90.34	mL

Experimental Results

1st sampling:					
Volume of mixture sampled	90.61	mL	Sclareol Conc. in extract	69.58	g/L
Mass of mixture	72.83	g	Sclareol mass in extract	243.54	mg
Mass of EL	2.40	g	% Sclareol in extract by weight	51.71	%
Mass of CO_2	70.43	g	Expected sclareol mass	1101.88	mg
Calculated volume of EL	2.30	mL	% Sclareol yield	22.10	%
Volume of extract from exp	3.5	mL			
Sampling flow rate	0.5	mL/min			
Sampling time	4.56	hrs			
2nd sampling:					
Volume of mixture sampled	81.89	mL	Sclareol Conc. in extract	85.36	g/L
Mass of mixture	68.86	g	Sclareol mass in extract	209.13	mg
Mass of EL	2.96	g	% Sclareol in extract by weight	55.60	%
Mass of CO_2	65.90	g	Expected sclareol mass	1101.88	mg
Calculated volume of EL	2.84	mL	% Sclareol yield	41.08	%
Volume of extract from exp	2.45	mL			
Sampling flow rate	0.5	mL/min			
Sampling time	2.73	hrs			
Depressurization:					
Sclareol Conc.	62.995	g/L	Total mass of sclareol	509.37	mg
Sclareol mass	56.70	mg	Expected sclareol mass	1101.88	mg
Volume collected	~0.9	mL	% Sclareol yield	46.23	%
			% Sclareol purity	53.31	%

6.89 MPa, w_{EL}^{*} = 0

Experimental Conditions

Mass of baled sage	33.6	g
Mass of EL	0	g
Mass of CO_2	235.91	g
Volume of CO_2+EL mixture around system	89.41	mL

Experimental Results

1st sampling:					
Volume of mixture sampled	89.6	mL			
Mass of mixture	71.54	g	Sclareol mass	52.78	mg
Mass of EL	0.00	g	% Sclareol in extract by weight	48.76	%
Mass of CO_2	71.54	g	Expected sclareol mass	1095.36	mg
Calculated volume of EL	0.00	mL	% Sclareol yield	4.82	%
Sampled into EL	4	mL			
Sampling flow rate	0.6	mL/min			
Sampling time	2.49	hrs			
2nd sampling:					
Volume of mixture sampled	100.33	mL			
Mass of mixture	78.99	g	Sclareol mass	92.35	mg
Mass of EL	0.00	g	% Sclareol in extract by weight	44.57	%
Mass of CO_2	78.99	g	Expected sclareol mass	1095.36	mg
Calculated volume of EL	0.00	mL	% Sclareol yield	13.25	%
Sampled into EL	2	mL			
Sampling flow rate	0.6	mL/min			
Sampling time	2.79	hrs			
Depressurization:					
Sclareol Conc.	5.097	g/L	Total mass of sclareol	170.61	mg
Sclareol mass	25.48	mg	Expected sclareol mass	1095.36	mg
Sampled into EL	5	mL	% Sclareol yield	15.58	%
			% Sclareol purity	47.36	%

6.89 MPa, w_{EL}^{*} = 0

Experimental Conditions

Mass of baled sage	33.5	g
Mass of EL	0	g
Mass of CO_2	289.71	g
Volume of CO_2+EL mixture around system	89	mL

Experimental Results

1st sampling:					
Volume of mixture sampled	89.12	mL			
Mass of mixture	72.06	g	Sclareol mass	28.81	mg
Mass of EL	0.00	g	% Sclareol in extract by weight	40.53	%
Mass of CO_2	72.06	g	Expected sclareol mass	1092.10	mg
Calculated volume of EL	0.00	mL	% Sclareol yield	2.64	%
Sampled into EL	4	mL			
Sampling flow rate	0.6	mL/min			
Sampling time	2.48	hrs			
2nd sampling:					
Volume of mixture sampled	100.17	mL			
Mass of mixture	80.56	g	Sclareol mass	101.74	mg
Mass of EL	0.00	g	% Sclareol in extract by weight	44.27	%
Mass of CO_2	80.56	g	Expected sclareol mass	1092.10	mg
Calculated volume of EL	0.00	mL	% Sclareol yield	11.95	%
Sampled into EL	2	mL			
Sampling flow rate	0.6	mL/min			
Sampling time	2.78	hrs			
Depressurization:					
Sclareol Conc.	14.826	g/L	Total mass of sclareol	160.20	mg
Sclareol mass	29.65	mg	Expected sclareol mass	1092.10	mg
Sampled into EL	2	mL	% Sclareol yield	14.67	%
			% Sclareol purity	41.78	%

C.2. Experimental Conditions: 10.34 MPa, w_{EL}^{*} = 0.3-0.9

10.34 MPa, w_{EL}^{*} = 0.88

Experimental Conditions

Mass of baled sage	33.8	g
Mass of EL	260.5	g
Mass of CO_2	34.16	g
Volume of CO_2+EL mixture around system	81.08	mL

Experimental Results

1st sampling:					
Volume of mixture sampled	86.19	mL	Sclareol Conc. in extract	11.38	g/L
Mass of mixture	93.51	g	Sclareol mass in extract	888.59	mg
Mass of EL	82.67	g	% Sclareol in extract by weight	51.29	%
Mass of CO_2	10.84	g	Expected sclareol mass	1101.88	mg
Calculated volume of EL	79.34	mL	% Sclareol yield	80.64	%
Volume of extract from exp	78.1	mL			
Sampling flow rate	1	mL/min			
Sampling time	1.44	hrs			
2nd sampling:					
Volume of mixture sampled	93.5	mL	Sclareol Conc. in extract	0.51	g/L
Mass of mixture	101.59	g	Sclareol mass in extract	45.06	mg
Mass of EL	89.82	g	% Sclareol in extract by weight	17.84	%
Mass of CO_2	11.77	g	Expected sclareol mass	1101.88	mg
Calculated volume of EL	86.20	mL	% Sclareol yield	84.73	%
Volume of extract from exp	89.2	mL			
Sampling flow rate	1	mL/min			
Sampling time	1.56	hrs			
Depressurization:					
Sclareol Conc.	0.534	g/L	Total mass of sclareol	949.58	mg
Sclareol mass	15.93	mg	Expected sclareol mass	1101.88	mg
Volume collected	~29.85	mL	% Sclareol yield	86.18	%
			% Sclareol purity	33.45	%

10.34 MPa, w_{EL}^{*} = 0.54

Experimental Conditions

Mass of baled sage	33.2	g
Mass of EL	208.4	g
Mass of CO_2	174.42	g
Volume of CO_2+EL mixture around system	85.04	mL

Experimental Results

1st sampling:					
Volume of mixture sampled	88.29	mL	Sclareol Conc. in extract	17.76	g/L
Mass of mixture	95.05	g	Sclareol mass in extract	892.56	mg
Mass of EL	52.06	g	% Sclareol in extract by weight	52.67	%
Mass of CO_2	43.00	g	Expected sclareol mass	1082.32	mg
Calculated volume of EL	49.96	mL	% Sclareol yield	82.47	%
Volume of extract from exp	50.25	mL			
Sampling flow rate	0.5-0.7	mL/min			
Sampling time	2.45	hrs			
2nd sampling:					
Volume of mixture sampled	100	mL	Sclareol Conc. in extract	2.04	g/L
Mass of mixture	107.72	g	Sclareol mass in extract	114.67	mg
Mass of EL	58.26	g	% Sclareol in extract by weight	29.03	%
Mass of CO_2	49.46	g	Expected sclareol mass	1082.32	mg
Calculated volume of EL	55.91	mL	% Sclareol yield	93.06	%
Volume of extract from exp	56.35	mL			
Sampling flow rate	0.5-0.7	mL/min			
Sampling time	2.78	hrs			
Depressurization:					
Sclareol Conc.	0.382	g/L	Total mass of sclareol	1012.95	mg
Sclareol mass	5.72	mg	Expected sclareol mass	1082.32	mg
Volume collected	~15	mL	% Sclareol yield	93.59	%
			% Sclareol purity	40.18	%

10.34 MPa, w_{EL}^{*} = 0.29

Experimental Conditions

Mass of baled sage	33.8	g
Mass of EL	95.864	g
Mass of CO_2	237.20	g
Volume of CO_2+EL mixture around system	87.13	mL

Experimental Results

1st sampling:					
Volume of mixture sampled	88.21	mL	Sclareol Conc. in extract	37.19	g/L
Mass of mixture	90.34	g	Sclareol mass in extract	887.92	mg
Mass of EL	26.38	g	% Sclareol in extract by weight	60.07	%
Mass of CO_2	63.96	g	Expected sclareol mass	1101.88	mg
Calculated volume of EL	25.32	mL	% Sclareol yield	80.58	%
Volume of extract from exp	23.875	mL			
Sampling flow rate	0.5-0.7	mL/min			
Sampling time	2.45	hrs			
2nd sampling:					
Volume of mixture sampled	101.97	mL	Sclareol Conc. in extract	1.91	g/L
Mass of mixture	104.07	g	Sclareol mass in extract	53.95	mg
Mass of EL	28.39	g	% Sclareol in extract by weight	23.21	%
Mass of CO_2	75.68	g	Expected sclareol mass	1101.88	mg
Calculated volume of EL	27.25	mL	% Sclareol yield	85.48	%
Volume of extract from exp	28.25	mL			
Sampling flow rate	0.5-0.7	mL/min			
Sampling time	2.83	hrs			
Depressurization:					
Sclareol Conc.	0.530	g/L	Total mass of sclareol	946.38	mg
Sclareol mass	4.51	mg	Expected sclareol mass	1101.88	mg
Volume collected	~8.5	mL	% Sclareol yield	85.89	%
			% Sclareol purity	40.09	%

C.3. Experimental Conditions: 5.52 MPa, w_{EL}^{*} = 0.35-0.9

5.52 MPa, w_{EL}^{*} = 0.89

Experimental Conditions

Mass of baled sage	33.7	g
Mass of EL	260.5	g
Mass of CO_2	32.87	g
Volume of CO_2+EL mixture around system	87.49	mL

Experimental Results

1st sampling:					
Volume of mixture sampled	87.94	mL	Sclareol Conc. in extract	10.05	g/L
Mass of mixture	95.02	g	Sclareol mass in extract	857.60	mg
Mass of EL	84.35	g	% Sclareol in extract by weight	36.50	%
Mass of CO_2	10.67	g	Expected sclareol mass	1098.62	mg
Calculated volume of EL	80.95	mL	% Sclareol yield	78.06	%
Volume of extract from exp	85.3	mL			
Sampling flow rate	1	mL/min			
Sampling time	1.47	hrs			
2nd sampling:					
Volume of mixture sampled	94.82	mL	Sclareol Conc. in extract	0.60	g/L
Mass of mixture	102.60	g	Sclareol mass in extract	53.28	mg
Mass of EL	91.40	g	% Sclareol in extract by weight	4.91	%
Mass of CO_2	11.21	g	Expected sclareol mass	1098.62	mg
Calculated volume of EL	87.71	mL	% Sclareol yield	82.91	%
Volume of extract from exp	88.35	mL			
Sampling flow rate	1	mL/min			
Sampling time	1.58	hrs			
Depressurization:					
Sclareol Conc.	1.552	g/L	Total mass of sclareol	962.42	mg
Sclareol mass	51.54	mg	Expected sclareol mass	1098.62	mg
Volume collected	~33.2	mL	% Sclareol yield	87.60	%
			% Sclareol purity	20.42	%

5.52 MPa, w_{EL}^{*} = 0.56

Experimental Conditions

Mass of baled sage	33.8	g
Mass of EL	208.4	g
Mass of CO_2	161.02	g
Volume of CO_2+EL mixture around system	82.5	mL

Experimental Results

1st sampling:					
Volume of mixture sampled	89.09	mL	Sclareol Conc. in extract	14.05	g/L
Mass of mixture	95.24	g	Sclareol mass in extract	871.76	mg
Mass of EL	53.19	g	% Sclareol in extract by weight	50.22	%
Mass of CO_2	42.06	g	Expected sclareol mass	1101.88	mg
Calculated volume of EL	51.04	mL	% Sclareol yield	79.12	%
Volume of extract from exp	62.025	mL			
Sampling flow rate	0.5-0.7	mL/min			
Sampling time	2.47	hrs			
2nd sampling:					
Volume of mixture sampled	102.75	mL	Sclareol Conc. in extract	1.36	g/L
Mass of mixture	109.69	g	Sclareol mass in extract	78.25	mg
Mass of EL	60.15	g	% Sclareol in extract by weight	14.26	%
Mass of CO_2	49.53	g	Expected sclareol mass	1101.88	mg
Calculated volume of EL	57.73	mL	% Sclareol yield	86.22	%
Volume of extract from exp	57.5	mL			
Sampling flow rate	0.5-0.7	mL/min			
Sampling time	2.85	hrs			
Depressurization:					
Sclareol Conc.	0.660	g/L	Total mass of sclareol	959.44	mg
Sclareol mass	9.43	mg	Expected sclareol mass	1101.88	mg
Volume collected	~14.3	mL	% Sclareol yield	87.07	%
			% Sclareol purity	32.92	%

5.52 MPa, w_{EL}^{*} = 0.35

Experimental Conditions

Mass of baled sage	33.8	g
Mass of EL	125.04	g
Mass of CO_2	229.98	g
Volume of CO_2+EL mixture around system	81.85	mL

Experimental Results

1st sampling:					
Volume of mixture sampled	88.57	mL	Sclareol Conc. in extract	25.96	g/L
Mass of mixture	91.12	g	Sclareol mass in extract	802.12	mg
Mass of EL	32.62	g	% Sclareol in extract by weight	61.89	%
Mass of CO_2	58.50	g	Expected sclareol mass	1101.88	mg
Calculated volume of EL	31.30	mL	% Sclareol yield	72.80	%
Volume of extract from exp	30.9	mL			
Sampling flow rate	0.5-0.7	mL/min			
Sampling time	2.46	hrs			
2nd sampling:					
Volume of mixture sampled	101.74	mL	Sclareol Conc. in extract	6.36	g/L
Mass of mixture	103.97	g	Sclareol mass in extract	227.25	mg
Mass of EL	35.89	g	% Sclareol in extract by weight	40.26	%
Mass of CO_2	68.08	g	Expected sclareol mass	1101.88	mg
Calculated volume of EL	34.44	mL	% Sclareol yield	93.42	%
Volume of extract from exp	35.75	mL			
Sampling flow rate	0.5-0.7	mL/min			
Sampling time	2.83	hrs			
Depressurization:					
Sclareol Conc.	0.649	g/L	Total mass of sclareol	1035.93	mg
Sclareol mass	6.57	mg	Expected sclareol mass	1101.88	mg
Volume collected	~10.125	mL	% Sclareol yield	94.01	%
			% Sclareol purity	50.29	%

D. Purification and Recovery of Sclareol from a Dense CO_2-Ethyl Lactate Extract

D.1. Other Methods to Purify the Ethyl Lactate and CO_2 Extract

D.1.1. Liquid-Liquid Extraction using Aqueous Ammonium Sulfate Solution

The addition of a given ammonium sulfate concentration to the mixture of water and ethyl lactate would completely separate the two liquids. An experiment to see the effect of addition of aqueous salt solution into the plant extract (6.89 MPa, w_{EL}^{*} = 0.35) was performed. First, approximately 4.5 g of salt was added to a vial containing 8 mL of water, and the mixture was mixed up until a homogenous solution formed. Subsequently, this mixture was added to the plant extract in the separatory funnel. The solution was mixed up for 15 minutes and let to stand at RT for 1 day. The separation between the aqueous salt layer (bottom) and the extract (top) is shown in Figure D-1.

The sclareol concentration in the top and the bottom layer of the solution was determined by gas chromatography. The GC results showed that the sclareol concentration before addition of the aqueous salt and the sclareol concentration in the top layer solution (after addition of aqueous salt) are relatively the same, respectively, 28.99 and 28.32 g/L. In addition, there wasn't any significant change in the color of the bottom layer (aqueous salt solution). This is an indication that the aqueous salt solution is not able to extract neither the plant pigments nor sclareol from the CO_2+EL extract.

Figure D-1. Liquid-liquid extraction using aqueous salt solution.

D.1.2. Liquid-Liquid Extraction using Hexane

Hexane was applied to the CO_2+EL extract in order to extract some non-polar impurities and plant pigments. Small amount of water (~ 0.2 mL) was added to the 1 mL extract (6.89 MPa, w_{EL}^{*} = 0.35) to make the extract immiscible with hexane. Hexane (2 mL) was then added to the aqueous extract, and the mixture was shaken for 15 minutes and let to stand at RT for 1 day. The separation between the hexane layer (top) and the aqueous ethyl lactate layer (bottom) is shown in Figure D-2.

The sclareol concentration in the top and the bottom layer of the solution was determined by gas chromatography. The GC results showed that 27.8 % of sclareol was dissolved in the hexane layer. The color of the extract changed from a dark green to a brownish green while the hexane layer changed from a clear to a greenish solution. The % sclareol purity in the bottom and top layer was determined to be relatively the same. It is thus

concluded from the experiment that hexane is not able to selectively extract the impurities from the CO_2+EL extract.

Figure D-2. Liquid-liquid extraction using hexane.

D.2. Solubility of Sclareol in Ethyl Lactate at Low Temperature

The information on the sclareol solubility in ethyl lactate at low temperature is essential in an attempt for searching out method to recover sclareol from the CO_2+EL extract. If a solution in equilibrium between the solid and the liquid phase is altered in such a way that the amount of the dissolved solids exceeds the equilibrium concentration, the system will seek to attain equilibrium by getting rid of this excess solids concentration. The resulting process is called crystallization from solutions and the concentration-gradient driving force is called supersaturation [1]. For example, cooling a solution with dissolved solids will generally precipitate some of the dissolved solids due to the decrease in the solid solubility at lower temperatures.

The experimental procedure to determine the sclareol solubility in ethyl lactate at low temperature is as follows. A known amount of sclareol was dissolved in a known amount of ethyl lactate. The mixture was stirred in the oven at 308.15 $\pm$ 0.5 K for 2 hours or until homogenous. The solution was then cooled down to a desired temperature and stirred for 4 hours. Subsequently, the solution was filtered and the sclareol concentration in the filtered solution was analyzed by gas chromatography. The experiments were performed at 262.15 $\pm$ 0.5 and 275.15 $\pm$ 0.5 K with a control experiment at 298.15 $\pm$ 0.5 K. For each temperature, several solutions with various initial concentrations of sclareol in ethyl lactate were prepared. The results are summarized in Figure D-3. As shown in this figure, ethyl lactate is capable to dissolve a relatively high concentration of sclareol at very low temperatures. The solubility values at these low temperatures are close to those at room temperature. This experiment concludes that cooling the plant extract to recover/precipitate sclareol is not a good method.

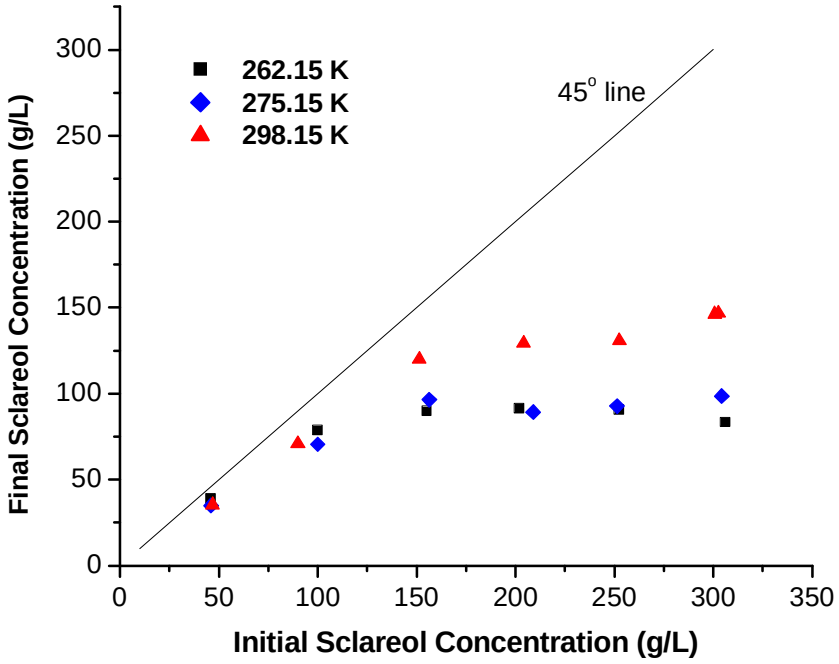

Figure D-3. Solubility of sclareol at low temperatures.

D.3. Addition of Water to the Ethyl Lactate and CO_2 Extract to Precipitate Sclareol

This section describes the recovery process of sclareol from the CO_2+EL extract using water as the antisolvent. The experiments were performed for the extracts obtained at 6.89 MPa and w_{EL}^{*} = 0.1, 0.35. In this precipitation experiment, the extracts were not initially purified with the activated carbon. Water was added to the extract until achieving the desired concentration, ~ 78 % (w/w) of water, which was selected based on the solubility data of sclareol in the mixture of ethyl lactate and water. Once water was added, the solution became cloudy. The mixture was then placed in the refrigerator (278.15 $\pm$ 1 K) overnight to enhance sclareol precipitation. For w_{EL}^{*} = 0.1, the solution separated into the oil phase (top), the solid precipitate phase, and water-ethyl lactate phase. The solid precipitate phase contained some

particles floating around the solution, and was separated from the solution via a vacuum filtration. The oil phase, on the other hand, resembled a thin sheet floating on top of the mixture, and could be easily separated with a spatula.

The concentration of sclareol in both the oil and solid precipitate phases was determined in terms of weight fraction, after dried in the oven for 2-3 days at 318.15 $\pm$ 1 K. A known weight of precipitates was dissolved in a known volume of ethyl lactate, and the amount of sclareol in the solution was quantified by GC analysis. The amount of the non-precipitated sclareol and impurities was calculated by analyzing the sclareol purity and the sclareol concentration in the water-ethyl lactate phase. The mass of the oil and the solid precipitate phases as well as the distribution of the phase-separated sclareol in each phase was determined from the mass balance calculation. The same analysis was performed for the extract with w_{EL}^{*} = 0.35. The pictures of the precipitation experiments were described in Figure D-4 and Figure D-5. The results were summarized in Table D-1.

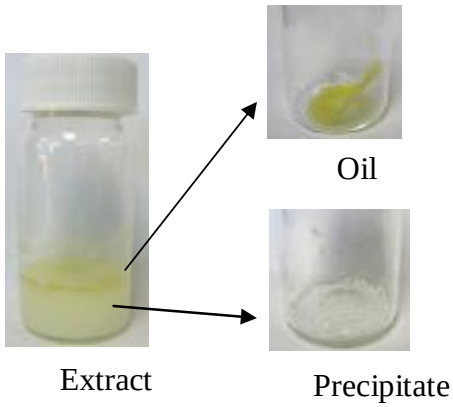

Figure D-4. Picture of the water addition to the extract (w_{EL}^{*} = 0.1, P = 6.89 MPa) experiment.

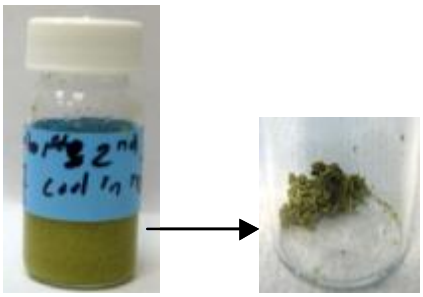

Extract after Water is added

Solid Precipitate Phase

Figure D-5. Picture of the water addition to the extract (w_{EL}^{*} = 0.35, P = 6.89 MPa) experiment.

Table D-1. Results summary of sclareol precipitation by addition of water experiment (80 % water by volume).

	Extract ω_{EL}^{*} = 0.1	Extract ω_{EL}^{*} = 0.35
Sclareol concentration (g/L)	83.45	28.99
Sclareol purity %(w/w)	69.15	57.72
% Sclareol phase separates/precipitates	99.8	99.31
Sclareol purity in the solid precipitate phase %(w/w)	78.12	65.98
Sclareol purity in the oil phase %(w/w)	61.34	-
Fraction of sclareol in the solid precipitate phase %(w/w)	47.42	100
Fraction of sclareol in the oil phase %(w/w)	52.58	-

It is shown from Table D-1 that the addition of water into the extract resulted in nearly complete phase separation of sclareol. For w_{EL}^{*} = 0.35, the oil phase was not observed. The % sclareol purity in the precipitates was higher than the purity of the extract before water was added. This is an indication that some impurities remained dissolved in the solution. For w_{EL}^{*} = 0.1, the oil phase was clearly observed, and nearly complete phase separation of sclareol occurred. The % sclareol purity in the solid precipitate phase was higher than in the oil phase. Additionally, the distribution of sclareol in both phases was calculated to be nearly equal. In conclusion, the addition of water directly into the extract, without being initially

purified with activated carbon, did not produce sclareol with significantly higher purity than the original solution.

Other experiments were to see the effect of changing the concentration of water. The experiment was performed for the extract with w_{EL}^{*} = 0.1 and two different concentrations of water (33 % and 50 % water by volume). Water was added to the extract until achieving the desired concentration. The mixture was then placed in the refrigerator (278.15 $\pm$ 1 K) overnight to enhance sclareol precipitation. The solution separated into two distinct layers, and we defined them as top and bottom layer. The top layer was more viscous than the bottom layer, as described in Figure D-6. The sclareol purity in the top and the bottom layer was then determined in terms of weight fraction. The distribution of the sclareol in the top and the bottom layer was determined from the mass balance calculation. As shown in Figure D-6, the separation of layer was not as apparent when 33 % water by volume was added. Thus, the analysis was not performed on this solution. The results for the experiment with 50 % water by volume are summarized in Table D-2.

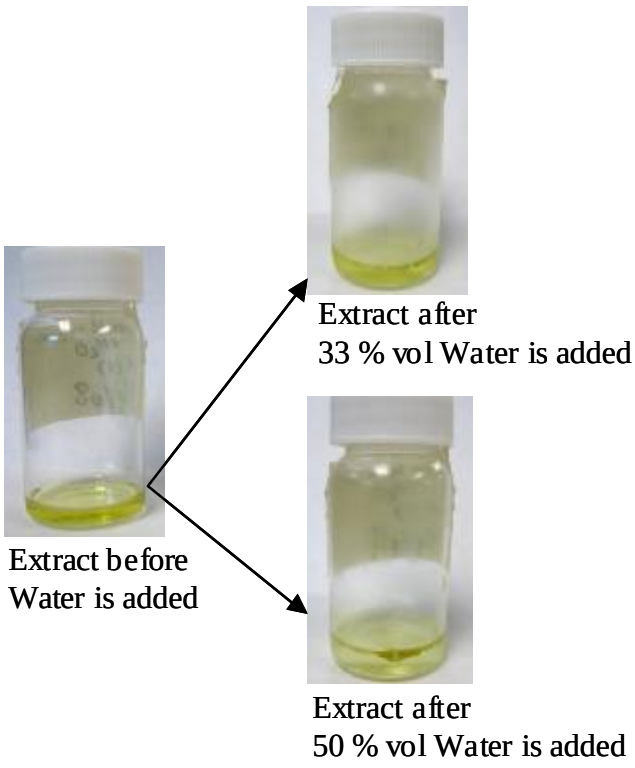

Figure D-6. Picture of the water addition to the extract (w_{EL}^{*} = 0.1, P = 6.89 MPa) experiment.

Table D-2. Results summary of sclareol precipitation by addition of water experiment (50 % water by volume). .

	Extract ω_{EL}^{*} = 0.1 with 50 % water by volume
Sclareol concentration (g/L)	83.45
Sclareol purity %(w/w)	69.15
Sclareol purity in the solid precipitate phase %(w/w)	75
Sclareol purity in the oil phase %(w/w)	54
Fraction of sclareol in the solid precipitate phase %(w/w)	42.5
Fraction of sclareol in the oil phase %(w/w)	57.5

It is shown from Table D-2 that the % sclareol purity in the bottom layer was higher than in the top part. In addition, the bottom layer contained slightly greater amount of sclareol. To conclude from this experiment, varying the amount of water did not considerably increase the purity of the sclareol-rich solution (bottom layer).

Another experiment was to observe the effect of applying centrifugation after the extract was mixed with a certain amount of water. The centrifugation was expected to enhance the separation of the precipitated sclareol from the precipitated impurities. The extract (w_{EL}^{*} = 0.09-0.1, 6.89 MPa) was first purified with activated carbon. A certain activated carbon concentration (~ 60 g/L) was added to 2 mL extract, which was kept in an oven maintained at a fixed temperature (323.15 $\pm$ 1 K). The solution was stirred for 1.5 hours, and subsequently the solution was filtered into a 20 mL centrifugation bottle. The volume of the collected extract was measured, and the amount of sclareol in the collected extract was quantified by GC analysis. The purity of sclareol in the collected extract in terms of weight fraction was also determined. Water was then added to the extract until achieving a mixture with 78 % (w/w) of water. Centrifugation was then applied to the mixture at RT for 1 hour with a rotating speed of 15000 rpm (20000 rcf). After centrifugation, the oil phase stick on the side wall of the centrifuge bottle, and were collected by scraping them with a spatula. The solid precipitate phase floated around the water-ethyl lactate phase, and was separated from the liquid phase via a vacuum filtration. The sclareol purity in both phases was then determined in terms of weight fraction. The distribution of the sclareol in each phase was determined from the mass balance calculation. The results for the centrifugation experiment are summarized in Table D-3. It can be concluded from the results that centrifugation did not improve the separation of sclareol from the impurities. As a result of centrifugation, the mass of the solid precipitate phase, which contains 92 % (w/w) of sclareol, is much less than the oil phase. The experiments with the same conditions without centrifugation, on the other

hand, would result in a higher amount of the solid precipitate phase (precipitates with a higher percentage of sclareol), as described in Chapter 5.

Table D-3. Results summary of sclareol precipitation by addition of water and centrifugation experiment.

	Extract ω_{EL}^{*} = 0.09
Sclareol concentration before activated carbon (g/L)	67.9
Sclareol purity before activated carbon %(w/w)	60
Sclareol concentration after activated carbon (g/L)	66
Sclareol purity after activated carbon %(w/w)	71.4
% Sclareol phase separates	99.8
Sclareol purity in the solid precipitate phase %(w/w)	92
Sclareol purity in the oil phase %(w/w)	74.4
Fraction of sclareol in the solid precipitate phase %(w/w)	18.6
Fraction of sclareol in the oil phase %(w/w)	81.4

D.4. Separation of Water from Ethyl Lactate by Addition of Ammonium Sulfate

After the plant extract was purified with the activated carbon, a certain concentration of water was added to the extract in order to precipitate sclareol. After the precipitated sclareol was collected from the solution, the remaining solution was a mixture of ethyl lactate and water with some dissolved substances. In order to make the process industrially attractive, a method to separate ethyl lactate and water must be developed so that ethyl lactate can be recycled for the extraction process whereas water is recycled for the liquid antisolvent process. The distillation process of the water-ethyl lactate system simulated using Aspen Plus is presented in Chapter 5. In this section, another separation method called salting out is presented.

The separation of an organic phase from an aqueous phase by the addition of a salt has been known for nearly a century [2]. This method is commonly used by biochemists in the

purification of proteins, which are highly charged, by controlling the salt concentration, pH, or temperature [2-4]. Weak intermolecular forces (e.g. hydrogen bonds) between organic molecules or non-electrolytes and water are easily disrupted by the hydration of electrolytes. For example, potassium carbonate was added to the mixture of water and ethanol, which are miscible in all proportions, to separate the two liquids [2].

In the experiment to separate ethyl lactate and water, 3 different concentrations of ammonium sulfate were added to the mixture containing 80 % of water by volume. The solution was mixed up until the salt was completely dissolved. The solution was let to sit at RT for 1 day and the formation of phases was observed. The results are summarized in Table D-4.

Table D-4. Summary of the experiments to separate water and ethyl lactate using ammonium sulfate.

Sol	H_20 (mL)	EL (mL)	$(NH4)_2SO_4$ (g)	after shaking for 2 min **Observation**	after a day **Observation**
1	8	2	0.5198	no separation occurs	no separation occurs
2	8	2	2.001	separation occurs; bottom layer is cloudy	separation occurs; bottom layer is clear
3	8	2	4.5064	separation occurs; bottom layer is clear	separation occurs; bottom layer is clear

As shown, separation occurred for solution 2 and 3. It was presumed that the bottom layer was the aqueous salt solution while the top part contained ethyl lactate-rich solution. For solution 2 and 3, the volume of the top layer was measured. The top layer of solution 2 contained less than 2 mL while the top layer of solution 3 contained more or less 2 mL. Based on this result, it is certain that more than 2 g of ammonium sulfate is needed to completely separate ethyl lactate and water. Further analysis must be performed to find the

exact amount of ammonium sulfate needed to achieve a complete separation between ethyl lactate and water at a certain mixture composition. One quick analysis is by measuring the pH and the volume of each layer as salt is added.

D.5. Activated Carbon Regeneration

Activated carbon is a microcrystalline, non-graphitic form of carbon, which has been processed to develop an internal porosity. The pore sizes of the activated carbon can be controlled in distribution by the choice of the carbon feedstock and the mode of operation. The activation process at temperatures of 573.15-773.15 K, usually performed in oxygen (air), provide carbons with properties of an acidic surface oxide nature and therefore primarily adsorb bases. At temperatures of 1073.15-1173.15 K, usually with steam, CO_2, or ammonia, provide carbons with basic surface oxide properties and preferentially adsorb more acidic components. Amphoteric material is usually prepared at temperature activation of 773.15-1073.15 K. The activation process may also be accomplished at very high temperature, such as 1273.15 K, and by chemically assisted and unassisted means. The chemical agents include zinc chloride, phosphoric acid, potassium hydroxide, and simple steam activation of the carbonized char. Steam activation is the most commonly employed. The residual chemical activators and inherent metals in the carbons are removed by washing them with acid and water.

Several methods to regenerate spent carbon have been developed over the past several years, including thermal, chemical, and steam methods [6]. For thermal regeneration, one method that has been developed through the pilot-plant stage is the fluidized-bed regeneration. It utilizes a fluidized-bed of coarse, inert particles, which maintain a constant-

temperature zone. The spent activated carbon is fed into the bottom of the coarse, inert, bed and carried through the bed by the action of the fluidizing gas. The carbon is then recovered from the effluent gas stream with cyclone collectors or some other collection device. The efficiency of the process depends on the temperature, retention time, and the composition of the gas (or the controlled atmosphere). The process is typically performed at temperatures range of 773.15-1073.15 K.

In the typical regeneration process by chemical method, the spent carbon is treated with a solution of certain chemicals, which vary according to the adsorbed materials. For example, in regeneration of chromium-impregnated carbon, the caustic (NaOH) solution is passed over the spent carbon to remove the adsorbed chromium. Water is then run through the carbon to rinse away any residual caustic. Subsequently, acid is passed through the carbon to restore the pH necessary for the best adsorption capability, and again water to wash away any residual acid. For the treatment with steam, the spent carbon is first dispersed in water to form an aqueous solution. The suspension is sent to the atomizing spray nozzle and mixed with the steam. The mixture is then passed through the heated reactor vessel. In this zone, the aqueous phase of the carbon slurry is converted to steam and the carbon and steam mixture is heated to the reactivation temperature of at least about 873.15 K. The carbon is recovered from the stream by a suitable filter.

D.6. References

1. Schweitzer, P., *Handbook of separation techniques for chemical engineering*. 1988, Mc Graw-Hill, New York, USA.

2. Shakhashiri, B., *Chemical demonstrations: a handbook for teachers of chemistry*. 1983: University of Wisconsin Press.

3. Lehninger, A., D. Nelson, and M. Cox, *Principles of biochemistry*. New York, 1993: p. 12.

4. Kaegi, J. and A. Schaeffer, *Biochemistry of metallothionein.* Biochemistry, 1988. **27**(23): p. 8509-8515.

5. Roy, G., *Activated carbon applications in the food and pharmaceutical industries*. 1995: CRC Press.

6. Cheremisinoff, P. and F. Ellerbusch, *Carbon adsorption handbook.* Ann Arbor Science Publishers Inc. Ann Arbor, Mich.,(04: 07 CHE), 1978: p. 1063.